FRIEDRICH-ALEXANDER
UNIVERSITÄT
ERLANGEN-NÜRNBERG

TECHNISCHE FAKULTÄT

Department of Materials Science

Glass and Ceramics

ANNUAL REPORT 2012

Preface

The Institute of Glass and Ceramics centres on research and teaching in the fields of processing, microstructure, properties as well as application of glasses, ceramics and composites. In the 2012 report a comprehensive overview on the main activities will be presented.

In the field of engineering ceramics (Peter Greil) research work centred on fundamental aspects of crack healing and processing and properties of lightweight cellular materials. Cellular piezoelectric PZT structures with auxetic behaviour were processed. Research facilities on a new approach for digital rapid prototyping based on high precision *pick-and-placer* technology were installed (see survey on selected research projects).

In the area of functional ceramics (Andreas Roosen) current research addresses colloidal processing of nano-sized powders for tape casting, multilayer processing and printing technologies for the manufacture of optical and electronic parts. Printing was extended to inkjet and rotational printing. The investigation of anisotropic shrinkage due to particle orientation during tape casting was extended to verify the influence of pore orientation. Lamination and co-firing techniques of different green tapes for microelectronic and refractory applications were developed.

Research activities in the glass group (Lothar Wondraczek) centred on optical properties of novel glass systems. A DFG priority program 1594 on "*Topological engineering of ultra strong glasses*" was launched in 2012. The scientific vision of the priority programme is a significant breakthrough in the understanding of the mechanical properties of disordered solids, going beyond empirical or semi-empirical approaches. Glasses with GPa strength by demonstrating defect-tolerant materials and toughening strategies based on ab initio understanding of the interplay between stress fields and topological features in the bulk and on surfaces will be explored. Lothar Wondraczek accepted a call from Friedrich Schiller University of Jena to be appointed as Director of Otto Schott Institute for Glass Research by 1 August 2012.

New research funds were acquired from DFG and industries. International cooperation with Nagoya Institute of Technology (NITech) was intensified by mutual exchanges of students and faculties. A group of 30 students of ENSCI Limoges visited our laboratories for excursion. Furthermore, a number of foreign guests were visiting our laboratories for carrying out research work. Members of the Institute of Glass and Ceramics were involved in the organisation of the annual conference of the German Ceramic Society (DKG) in Nuremberg with more than 280 attendees. In the field of ceramics processing the institute in co-operation with the German Ceramic Society organized a very successful conference on "Joining of Ceramics", which was held in the Town Hall of Erlangen attracting 110 participants from industry and academia. The 5th Advanced Training Course on Tape Casting and Ceramic Multilayer Technology was held at the Institute in February 2012 in cooperation with the German Ceramic Society.

We would like to thank all members and friends of the Institute of Glass and Ceramics for their continuing support and cooperation.

Peter Greil and Andreas Roosen

OUTLINE

1. INSTITUTE OF GLASS AND CERAMICS 5

Staff 5

Graduates 8

Visiting Students and Scientists 12

Teaching 14

Laboratories 16

2. RESEARCH 20

Survey 20

Selected Research Highlights 23

3. PUBLICATIONS 36

Papers 36

Proceedings 86

Books 86

4. CONFERENCES, WORKSHOPS, LECTURES, AWARDS 87

Conferences and Workshops Organised by Members of the Institute 87

Invited Lectures 90

Awards 92

5. ADDRESS AND MAP 94

Department of Materials Science - Glass and Ceramics 94

Institute of Advanced Materials and Processes (ZMP) 95

Pratum Fürth 96

6. IMPRESSUM 97

1. INSTITUTE OF GLASS AND CERAMICS

Staff

Faculties

Prof. Dr. Peter Greil	Head of Institute
Prof. Dr. Andreas Roosen	Functional Ceramics
Prof. Dr. Lothar Wondraczek[1]	Glass
Priv.-Doz. Dr. Nahum Travitzky	Ceramics Processing

Administration

Karin Bichler	Candice Iwai
Ursula Klarmann	Evelyne Penert-Müller

Senior Research Staff

Dr.-Ing. Ulrike Deisinger	Ceramic Multilayer Processing
Dr.-Ing. Tobias Fey	Cellular Ceramics and Simulation

Research Staff

Advanced Engineering Ceramics and Rapid Prototyping

M.Sc. Alexander Bonet	M.Sc. Benjamin Dermeik
M.Sc. Ina Filbert	Dipl.-Ing. Lorenz Schlier
Dipl.-Ing. (FH) Tobias Schlordt	

[1] now with Friedrich-Schiller-University of Jena

Functional Ceramics

Dipl.-Ing. Michael Beck

Dipl.-Ing. (FH) Ingo Götschel[2]

Dipl.-Ing. Daniel Jakobsen

M.Sc. Torsten Schüler[2]

M.Sc. Moritz Wegener

M.Sc. Zongwen Fu

M.Eng. Michael Hambuch

Dipl.-Ing. Nadja Kölpin[2]

Dipl.-Ing. Alfons Stiegelschmitt

Cellular Ceramics and Simulation

Dr. rer. nat. Andrea Dakkouri-Baldauf

Dipl.-Ing. Michael Götz[2]

Dr. rer. nat. Sreejith Krishnan

Dipl.-Ing. Bodo Zierath

Dr. Guo Ping Bei

Dr. Young Jae Kang[2]

Dipl.-Ing. Joana Pedimonte

Glass

Dipl.-Ing. Ning Da[2]

Dipl.-Ing. (FH) Robert Meszaros[2]

M.Sc. Karsten Nielsen[1]

M.Sc. Weijuan Zhang[2]

M.Sc. Guojun Gao

Dr. Doris Möncke[1]

Dr. Sergey Sirotkin

Dipl.-Ing. Anja Winterstein[1]

Technical Staff

Sabine Brungs

Dipl.-Ing. Helmut Hädrich

Timotheus Barreto-Nunes

Peter Reinhardt

Eva Springer

Hana Strelec

Evelyn Gruber

Beate Müller

Heike Reinfelder[3]

Alena Schenkel-Rybar

Dipl.-Ing. Alfons Stiegelschmitt

Andreas Thomsen

[1] now with Friedrich-Schiller-University of Jena [2] now in industry [3] now at IPAT, FAU

Our team at the annual football championship of the Department of Materials Science and Engineering

Graduates

Bachelor Thesis

Rudolf Borchardt

Enhancing the efficiency of biomassreactors by means of solar spectral conversion

Tobias Früh

Manufacturing of biomimetic composite tapes via tape casting

Stefan Gruner

Sintering of Cu-exudating borosilicate glasses

Jonas Herbst

Formation of metallic nanoparticles in ionic glasses

Stefan Pfeiffer

Influence of Al_2O_3-Fasern fibers on microstructure and properties of paper-derived Al_2O_3-substrates

Frank Schinzel

Tape cast glass-ceramic composites and characterization of thermo-mechanical properties for high temperature applications

Johanna Schmidt

Manufacturing of hierarchical Al_2O_3 foams

Stanislaus Schwanke

Robocasting of hollow filaments

Benjamin Seemann

Formation and characterization of spectral conversion foils for biomass reactors

Daniel Subatzus

Multilayer processing for ceramic bioreactors

Clemens Vennebusch

Tape casting of optically transparent spinel

Diploma Thesis

Christoph Baumgärtner

Formation and characterization of the microstructure of nano-porous anodic layers on titanium substrate

Daniel Jakobsen

Microstructure evolution during sintering of piezoceramics

René Kaiser

Discrete-element modelling of 3D printing process

Bodo Zierath

Residual stress strengthening of Al_2O_3

Master Thesis

Ina Filbert

Surface modification of polymer-derived ceramics

Zongwen Fu

3D printing of silicon-based ceramics

Dominik Orzol

Deposition of highly efficient antireflective coatings on solar glass

Li Wang

Co-firing of metallized magneto-ceramics

Moritz Wegener

Processing of nano-sized powders in a stirred media ball mill for tape casting of transparent doped yttria alumina garnets

Rong Zhao

Properties of multilayer glass/silicone composite structures

Ph.D. Thesis

Lars Müller

Copper deposition on silicon nitride ceramics for joining

Daniel Galsterer

Porous silicon carbide for exhaust gas purification

Dr. Daniel Galsterer after successful Ph.D. examination

Cora Schillig

Joining of ceramic components of solid oxide fuel cells with glasses and glass-ceramics

Dr. Cora Schillig after successful Ph.D. examination

Visiting Students and Scientists

Dr. Steferson Luiz Stares (January 2011 - February 2013)

Federal University of Santa Catarina, Florianópolis, Santa Catarina, Brazil

Dr. Janaína Accordi Junkes (April 2011 - March 2012)

Federal University of Santa Catarina, Florianópolis, Santa Catarina, Brazil

Kotaro Hattori (November 2011 - January 2012)

Nagoya Institute of Technology, Nagoya, Japan

Kensuke Kato (September 2012 - November 2012)

Nagoya Institute of Technology, Nagoya, Japan

Prof. Dr. Xiaowei Yin (October 2012 - November 2012**)**

Northwestern Polytechnical University, Xi'an, Shaanxi, China

Naoki Kato (October 2012 - December 2012)

Nagoya Institute of Technology, Nagoya, Japan

Veronica Moreno (November 2012)

Federal University of Santa Catarina, Florianópolis, Santa Catarina, Brazil

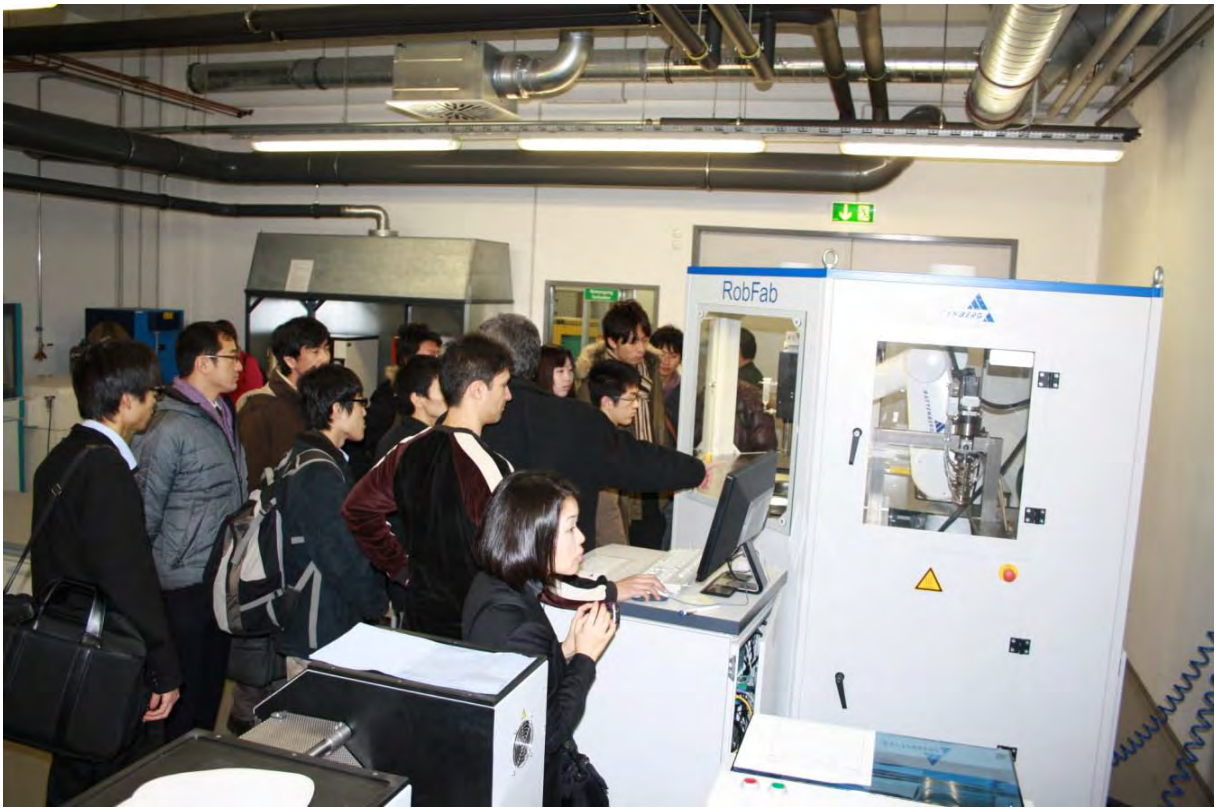

Visit of a Japanese delegation of the Nagoya Institute of Technology (NITech), Nagoya, Japan; in front of the Institute of Advanced Materials and Processes (ZMP), Fürth, Germany, (March 2012)

Teaching

The Department of Materials Science and Engineering offers a Bachelor and a Master programme. The bachelor course is a three years programme (six semesters) which qualifies for the master programme (three semesters).

The curriculum consists of the "*Grundstudium*" during the first 2 years, devoted to the fundamental scientific education. It introduces the student very early into materials science and engineering concepts by offering courses on materials structures, properties, thermodynamics, kinetics, chemistry, processing, product manufacturing, analysis and testing as well as practical training. Examinations follow immediately after each semester.

The subsequent advanced programme in the 5th and 6th semester broadly deepens the entire field of materials science and engineering. Courses on economics, management and other soft skills are obligatory. This period ends with a Bachelor Thesis of nine weeks duration. Additionally, the student has to perform an industrial internship of 12 weeks.

The Master programme in the 7th and 8th semester is devoted to specialisation in a selected "*Kernfach*" (core discipline), including corresponding seminars. The student has to select an additional "*Technisches Schwerpunktfach*" (special technical discipline) which offers the possibility of specialisation. Finally, the programme is completed by a Master Thesis of six months.

In addition to this Materials Science and Engineering programme, the Institute of Glass and Ceramics is involved in the new programme “Nanotechnology” of the Department of Materials Science and Engineering. We also contribute to Bachelor programmes “Energy Technology”, “Medical Technology” and the Elite course “Advanced Materials and Processes”.

Courses offered by the faculties of the Glass and Ceramics Institute

1. Semester

- Introduction to Inorganic Non-metallic Materials, P. Greil

3. Semester

- Materials Characterisation and Testing, A. Roosen

4. Semester

- Solid-state Kinetics, L. Wondraczek

5. Semester

- Processing and Applications of Glasses, P. Greil
- Processing and Applications of Ceramics, A. Roosen

Major Courses 7. and 8. Semester

- Biomimetic Engineering Materials and Processes, C. Zollfrank
- Ceramic Materials in Medicine, P. Greil
- Computational Calculation of Crack Probabilities, T. Fey
- Electroceramics I + II, A. Roosen
- Engineering Ceramics, P. Greil
- Innovative Processing Techniques for Advanced Ceramic Materials, P. Greil
- Mechanical Testing, T. Fey
- Non-destructive Testing, T. Fey
- Physics and Chemistry of Glasses and Ceramics: I. Thermodynamics of Condensed Systems, P. Greil
- Powder Synthesis and Processing, A. Roosen
- Rapid Prototyping, N. Travitzky
- Silicate Ceramics: From Natural Raw Materials to Modern Applications, N. Travitzky
- Stresses and Mechanical Strength, T. Fey

Laboratories

Technical hall (600 m²): equipped with facilities for advanced processing, shaping, melting and sintering as well as molding of glass, ceramics and composites

Main Equipment

Laboratories

- Biomaterials laboratory
- Ceramography workshop
- Functional ceramics laboratory
- Glass laboratories
- Mechanical testing laboratory
- Multilayer laboratory
- Polymer processing laboratory
- Powder characterization laboratory
- Processing workshop
- Rapid Prototyping laboratory
- SEM/AFM laboratory
- Simulation laboratory
- Technical hall
- X-ray charcterisation laboratory

Analysis

Thermal analysis

- 3-dimensional optical dilatometer
- Push rod dilatometers (up to 1800 °C)
- Thermal analysis (DTA/TGA/DSC/TMA)
- Thermal conductivity device
- Viscometry (beam bending)

Powder characterisation

- ESA acoustophoretic analyser (Zeta-meter)
- Dynamic light scattering particle size analyser
- Gas absorption analyser (BET)
- Laser scattering particle size analyser
- X-ray diffractometers (high-temperature)

Optical analysis

- FT-IR spectrometer
- High-resolution fluorescence spectrometer (Fluorolog-3, Horiba Jobin Yvon)
- Light Microscopes (digital, polarization, in-situ hot stage)
- Scanning electron microscope (variable pressure, ESEM and high temperature with EDX)
- UV-VIS-NIR spectrometers

Mechanical testing

- High precision mechanical testing with optical tracking system (EXAKT)
- Impulse Excitation Measurement (buzz-o-sonic)
- Micro hardness tester
- Servo hydraulic mechanical testing systems (also high temp.)
- Single fibre tensile testing machine
- Viscosimeter and elevated-temperature viscosimeter

Structural analysis

- 2D laser scanning microscope (UBM)
- 3D Laser scanner
- Atomic force microscope (AFM)
- Electron paramagnetic resonance spectroscopy
- He-pycnometer
- High accuracy weighing scales
- Laser-Flash LFA 457
- Mercury porosimeter
- Micro-CT Sky scan 1172
- Microwave and ultrasonic devices for non-destructive testing
- Raman-microscope with two excitation lasers

Chemical analysis

- High-pressure liquid chromatograph
- ICP-OES (Spectro Analytical Instruments)

Processing

Powder and slurry processing

- Attrition mills
- Agitator bead mill
- Disc mill
- Intensive mixers (Eirich, powder and inert gas/slurry)
- Jaw crusher
- Overhead mixer
- Pick and Placer
- Planetary ball mills
- Planetary centrifugal mixer (Thinky)
- Rotary evaporators
- Sieve shakers
- Single ball mill
- Thermo kneader
- Three-roll mill
- Tumbling mixers
- Ultrasonic homogenizer

Shaping

- 3D printers
- Advanced screen printing device
- Calender
- CNC High speed milling machine
- Cold isostatic press
- Electrospinning machine
- Flaring cup wheel grinding machine
- Fused deposition modelling device (FDM)
- High precision cutting device
- Hot cutting device
- Laminated object manufacturing devices (LOM)
- Lamination presses
- Langmuir–Blodgett trough
- Lapping and polishing machines
- Low-pressure injection moulding machine
- Precision diamond saws
- PVD coaters
- Robot-controlled device
- Roller coater
- Sheet former
- Spin coater
- Tape caster
- Textile weaving machine
- Twin screw extruder
- Ultrasonic drill
- Vacuum infiltration device

Heat treatment

- Autoclave
- Dryers
- Furnaces (air, N_2, Ar, Vac, High-Vac, forming gas) up to 2500 °C for sintering, glass melting, infiltration, debindering, pyrolysis
- Gradient furnace
- High-temperature spray furnace

2. RESEARCH

Survey

Research centres on basic aspects of ceramics, glasses and composites. Materials for applications in microelectronics, optics, energy, automotive, environmental, chemical technologies and medicine were investigated. Research was carried out in close cooperation with partners from national and international universities and industries.

Research Projects (in alphabetical order)	Funding	Principal Investigator
Accelerated glass durability testing	EnCN	Prof. Wondraczek
Bioactive ceramic cages	IN	Prof. Greil / Dr. Fey
Bismuth activated glasses with IR luminescence for broad band amplifier applications in laser technology	DFG	Prof. Wondraczek
Cellular ceramics for heat absorbers	EnCN	Prof. Greil
Deformation and sintering behaviour of preceramic papers	DFG	PD Dr. Travitzky
Disperse systems for electronic manufacturing	DFG	Prof. Roosen
Eu^{2+} doped glasses with broad band luminescence behaviour	DFG	Prof. Wondraczek
Experimental study and simulation of anisotropic effects in cast green tapes	DFG	Prof. Roosen
Flexible manufacturing of preceramic paper based refractory components	DFG	Prof. Greil
Glass melt filled photonic fibers	DFG	Prof. Wondraczek
Hierarchical cellular ceramics and composites	DFG	Prof. Greil
High temperature stable ignition components based on defined 2D and 3D SiSiC structures	AiF	PD Dr. Travitzky

Research Projects (in alphabetical order)	Funding	Principal Investigator
Highly resistant multilayer systems	BFS	Prof. Wondraczek
Lightweight cellular ceramics	EC	Prof. Greil
Lightweight ceramics	AiF	PD Dr. Travitzky
Long time stability of glasses	BFS	Prof. Wondraczek
Manufacturing of multilayer refractories by tape casting	DFG	Prof. Roosen
Manufacturing of transparent ceramic substrates	BMBF	Prof. Roosen
Mechanochemical properties of nitridated glasses	DFG	Prof. Wondraczek
New glasses for photonic crystal fibers	EC	Prof. Wondraczek
Polymer derived ceramics for bearing applications	IN	PD Dr. Travitzky
Relaxation behaviour of compressed inorganic glasses	DFG	Prof. Wondraczek
Robocasting of macrocellular ceramic 3D-lattice structures with hollow filaments	DFG	PD Dr. Travitzky
Self healing MAX phase ceramics	DFG	Prof. Greil
Stable and metastable multi phase systems at high temperatures	DFG	Prof. Greil
Structured carbon based catalyst support structures for CO hydration	DFG	Dr. Fey
Tape on Ceramic Technology	BMBF	Prof. Roosen
Transparent glass foams	EC	Prof. Wondraczek

Projects of Prof. Wondraczek were transferred to University of Jena or finished.

Funding organisations:

AiF: Industrial Research Cooperation

BFS: Bavarian Science Foundation

BMBF: Federal Ministry of Education and Research

DFG: German Science Foundation

EC: Cluster of Excellence (“Engineering of Advanced Materials”)

EnCN: Energy Campus Nuremberg

IN: Industry

Prof. Dr. Peter Greil congratulates Dipl.-Ing. Helmut Hädrich
for 40 years of service (July 2012)

Selected Research Highlights

Photoelastic imaging of residual stress distribution in epoxy interface layers of ceramics with periodic building-bloc structure

Tobias Fey, Michael Götz, Peter Greil

Distribution of residual stresses generated by thermal expansion misfit in the epoxy interface bonding of two-dimensional alumina building bloc layers was analyzed by photoelastic measurements. Building blocs of sintered alumina with cubic shape and equal size of 1.34 mm were arranged into 2D layers of tetragonal and monoclinic unit cell geometries. Interface bonding was achieved by infiltration of an optically transparent epoxy resin with a layer thickness varying from 145 to 580 µm.

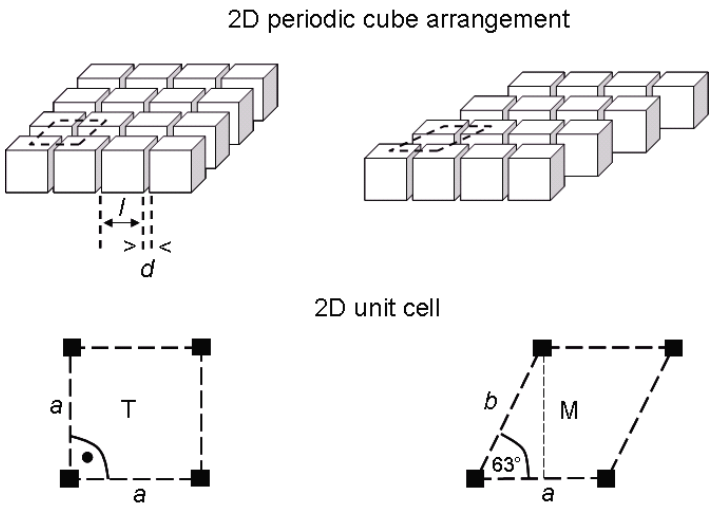

2D periodic building bloc layer structures prepared from alumina building blocs.

Lines of equal maximum shear stress (is chromatics) were recorded by photoelastic imaging applying circular polarized monochromatic light (dark field mode). The specimen plate of 25 x 25 mm^2 in size was placed between two $\lambda/4$ wave plates and crossed polarizer and analyzer.

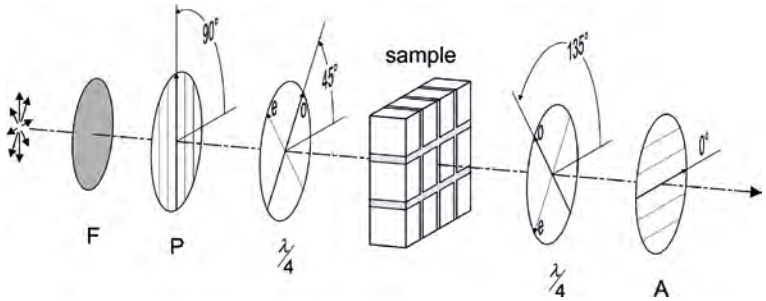

Path of light in the optical experiment setup for photoelastic imaging.

In a dark field (circular polariscope) the intensity of the transmitted light varies as

$$I = I_0 \sin^2 \pi \frac{Cd(\sigma_{11} - \sigma_{22})}{\lambda}$$

I_0 is the intensity ahead of the polarisator, C is the stress-optical constant derived from stress optical measurements of pure epoxy resin sample, d is the specimen thickness and σ_{11} - σ_{22} is the difference between the principal stresses in a plane normal to the light propagation direction. Though, sin^2 is a multivalued function, only first order fringes were imaged since retardation δ << wave length λ. Con-tour lines of equal intensity (isochromatics) correspond to the trajectories of equal $(\sigma_{11} - \sigma_{22})$. In interface bonding area where $(\sigma_{11} - \sigma_{22}) = 0$ e.g. hydrostatic residual stress, $I \rightarrow 0$ (darkness). The following figure shows the photo-elastic birefringence patterns of first order taken from the region where the interface bonding layer of thickness t = 290 µm connects four (tetragonal) or three (monoclinic) individual alumina cubes, respectively. Dark contrast in the centre of the bonding layer indicates an isotropic state of residual (hydrostatic) stress. Near to the alumina surface, however, birefringence photoelastic intensity increases which may be attributed to an increasing difference in principal stress components e.g. anisotropic state of stress. The maxima of photoelastic intensity can be observed in the bonding polymer layer close to the building bloc edges.

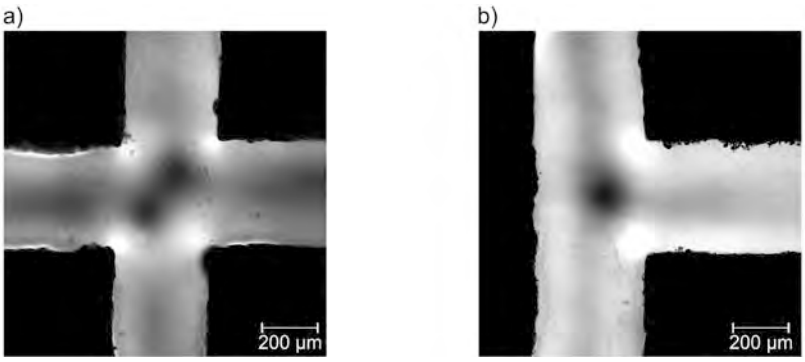

Photoelastic imaging of stress distribution in the polymer bonding layer of periodic alumina composites.

The photoelastic fringe patterns were simulated by plotting the differences of principal components of the stress tensor $\boldsymbol{\sigma_{ii}}$ which correspond to Tresca´s shear stress,

$$\sigma_{tresca} = 2\tau_{\max} = \max\left(|\sigma_{11} - \sigma_{22}|, |\sigma_{22} - \sigma_{33}|, |\sigma_{33} - \sigma_{11}|\right)$$

τ_{max} is the maximum shear stress. The calculations of stress tensor were carried out in plane-stress mode. At locations where shear stress vanishes $\tau_{xy} \rightarrow 0$ and $\sigma_{Tresca} \rightarrow 0$ no birefringent patterns can be observed and the state of stress corresponds to a mean hydrostatic stress. FE calculation of Tresca´s shear stress distribution in the interface bonding layer confirmed a non-isostatic state of stress

in the interface bon-ding layer with high stress anisotropy close to the building bloc surfaces and maximum Tresca stresses up to 33 MPa close to the edges.

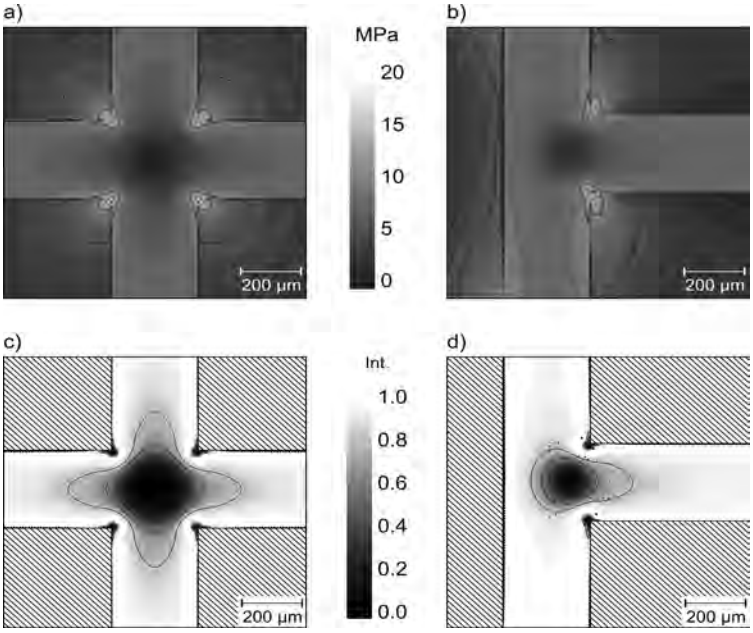

Tresca stress distribution (a, b) and corresponding simulated photoelastic intensity distribution (c, d) for tetragonal (a, c) and monoclinic (b, d) geometry.

Crack healing ceramics of MAX phase composites

Joana Pedimonte, Guoping Bei, Tobias Fey, Peter Greil

Ceramic materials that are able to repair flaws and cracks and recover initial properties constitute a vital field of materials science that gained in significance recently. Rough guidelines for acceleration of crack healing reaction were derived from crack healing kinetics as expressed by the relations derived for pore perturbation and sintering and for an environmental oxidation reaction. Microstructure modifications should envisage grain boundaries with enhanced diffusivity, reduction of grain size (e.g. nanoscale powders with high surface energy), and dispersion of repair fillers that are able to stimulate healing reaction at lower activation energy (chemical (catalysis) or mechanical activation (e.g. accumulated lattice strain energy)).

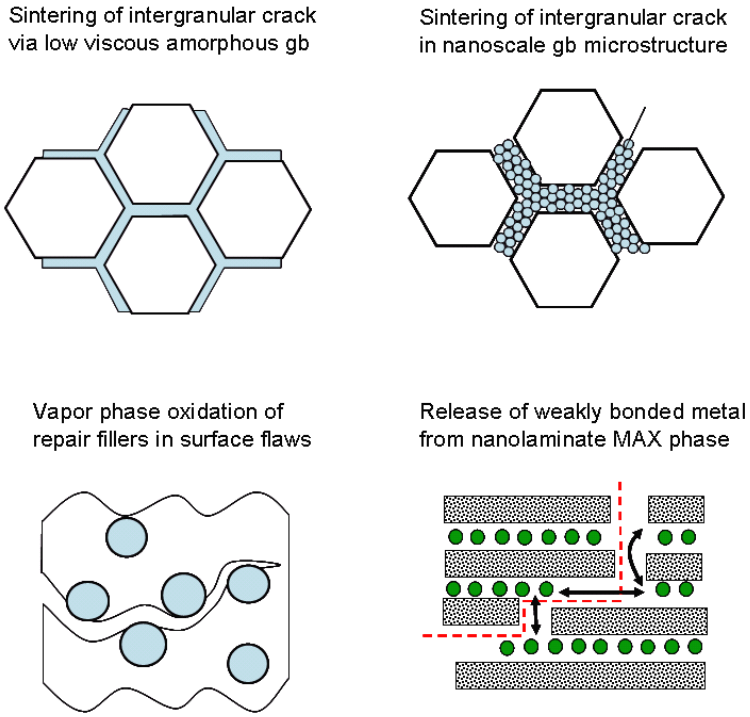

Microstructures providing enhancement of material transport and repair filler reactivity.

For the oxidation of MAX phases $M_{n+1}AX_n$ with M = Ti, V, ..., A = Al, Si, ..., X = C, N and n = 1 - 6, weak bonding between M-A and preferred oxidation of A is the main mechanism. The formation temperature of A containing oxides was found to depend on the bonding strength and stability of MAX phases. While oxidation temperatures of 1100 – 1200 °C were reported for preferred oxidation of Al forming hard, strong and protective Al_2O_3 layer on Ti_3AlC_2 and Ti_2AlC lower oxidation temperatures < 1000 °C might be expected by substituting with an A-element of lower bonding energy than Al. MAX phase based composite materials with low melting metals like Sn, In, or Pb on the A position might be of great interest to serve as repair filler requiring significantly lower healing temperatures to trigger oxidation healing reaction compared to common engineering ceramic materials. For example, substitution of A element Al (cohesive energy $E_c \approx 10.4$ eV and mi-

gration energy (0001) $E_m \approx 0.82$ eV) by Sn ($E_B \approx 8.1$ eV and $E_m \approx 0.66$ eV) in Ti_2AC was shown to decrease the temperature for A-element oxidation

$$2\ Al + 3/2\ O_2 \rightarrow Al_2O_3 \qquad \Delta G_{740°C} = -1356\ kJ/mol$$

$$Sn + O_2 \rightarrow SnO_2 \qquad \Delta G_{500°C} = -415\ kJ/mol$$

measured by DTA and XRD from approximately 740 °C to 500 °C, Fig. 8. At these temperatures crack filling with the oxide reaction products was observed by SEM whereas oxidation of Ti requires significantly higher temperatures. Though a lower cohesive energy corresponds to a reduced thermal stability of the MAX phase surface coating of activated repair fillers may avoid decomposition during consolidation offering a high potential for development of repair filler loaded composite ceramics with enhanced crack healing ability at temperatures below 1000 °C.

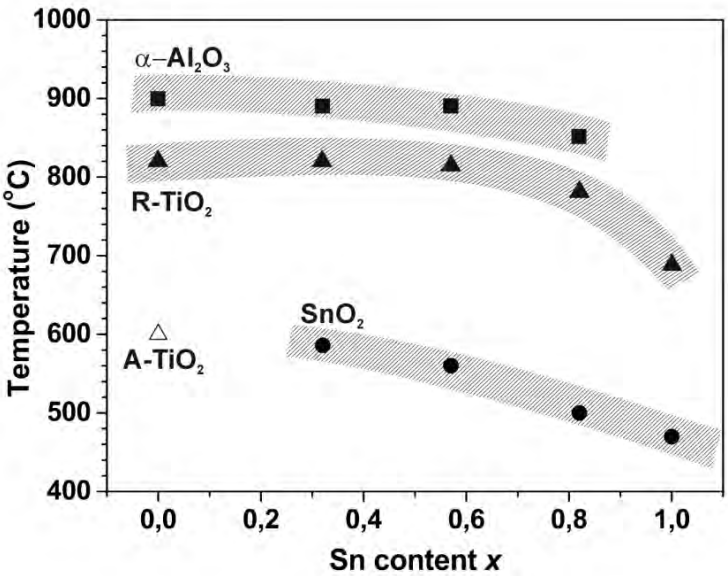

Reduction of oxidation temperature for M and A elements of M_2AC phase with M = Ti and A = Al and Sn.

P. Greil, Generic principles of crack-healing ceramics – Review, *J. Adv. Ceram*. 1 (2012) 249-267

G.P. Bei, J. Pedimonte, T: Fey, P. Greil, Oxidation Behaviour of MAX Phase $Ti_2Al_{(1-x)}Sn_xC$ solid solution, submitted (2013)

Crack healing in polymer derived ceramics

Lorenz Schlier, Nahum Travitzky, Peter Greil

Nitridation crack healing in polymer derived SiOC ceramics may yield improved mechanical properties of extrusion formed filler loaded polysiloxane polymer systems. While nitridation of Si-O-C based ceramic residue requires temperatures exceeding 1200 °C significantly lower reaction temperatures below 1000 °C may be achieved in the presence of catalytically active metal silicide fillers ($MeSi_2$ with Me = Fe, Cr, V). For example, polysiloxanes filled with carbide and metal silicide fillers (Fe-Si-Cr) exhibit crack healing in nitrogen atmosphere by formation of metal nitride reaction products which exhibit a pronounced volume expansion effect. Simultaneously, the repair filler triggers nitridation of the Si-O-C matrix as a heterogeneous catalyst at temperatures as low as 800 °C with Si_2N_2O and Si_3N_4 filling the crack space

$$2\ SiO\ (g) + C\ (s) + N_2\ (g) \rightarrow Si_2N_2O\ (s) + CO\ (g) \qquad \Delta G_{800°C} = -437\ kJ/mol$$

$$3\ SiO\ (g) + 3\ C\ (s) + 2\ N_2\ (g) \rightarrow Si_3N_4\ (s) + 3\ CO\ (g) \qquad \Delta G_{800°C} = -428\ kJ/mol$$

High mobility of vapour phase reactants SiO (g) and N_2 (g) facilitates long range transport and nitride and oxinitride reaction products may fill open pores and cracks. Compared to the low level of fracture toughness of 1 – 2 $MPam^{1/2}$ associated with the porous and amorphous microstructure of the polymer derived ceramic residue, formation of dense crystalline oxinitride/nitride surface layers may attain significantly higher toughness ranging from 3 (Si_2N_2O) to > 6 $MPam^{1/2}$ (Si_3N_4).

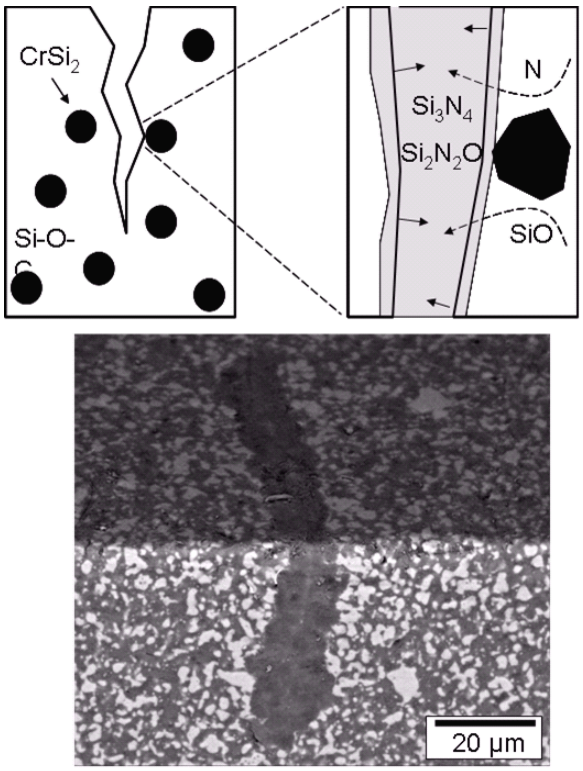

Repair filler catalyzed nitridation crack healing in polymer-derived Si-O-C ceramics.

Moreover, the catalytic fillers dispersed in the Si-O-C may undergo nitridation reaction, as for example,

$$3\ CrSi_2 + 11/2\ N_2 \rightarrow 3\ CrN + 2\ Si_3N_4 \qquad \Delta G_{800°C} = -607\ kJ/mol$$

which ultimately may give rise for a pronounced volume expansion factor. Penetration of nitrogen causes effective reduction of porosity at least near the surface which gave rise for a pronounced improvement of fracture strength (σ_{heal}/σ_0) ≈ 1.5. Since surface nitridation treatment may effectively trigger healing of open cracks without forming low viscous oxide products (silica and silicates) we can expect improved wear stability at elevated temperatures.

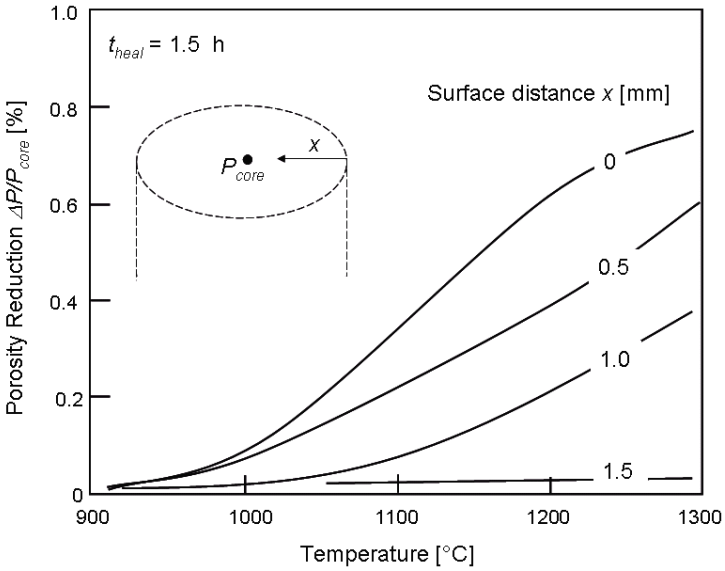

Crack healing by catalyzed ($CrSi_2$) nitridation of polymer derived Si-O-C ceramic.

The bending strength measured on samples after nitridation treatment and without surface finishing reaches values up to 400 MPa (1300 °C). Filling of pores and healing of cracks accessible to the nitrogen atmosphere by Si_2N_2O and Si_3N_4 reaction products may be considered as a potential mechanism for reduction of defect size as well as enhancement of fracture toughness giving rise for the improvement of fracture stress by approximately + 35 %.

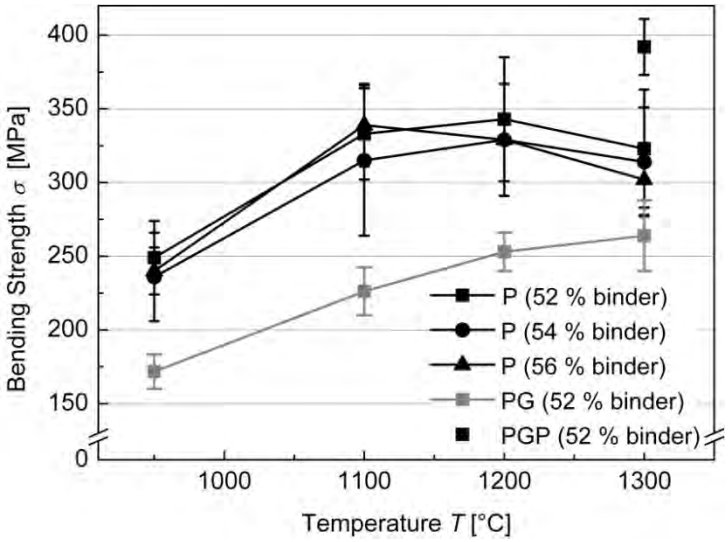

Bending strength measured after pyrolysis at 950 °C (Ar) and subsequent annealing in N_2-atmosphere for 2 h at various temperatures (P), after removing the reaction layer by grinding (PG) and after subsequent reannealing at the same temperature (PGP) for different binder contents and post treatments after pyrolysis.

P. Greil, Advancements in Polymer-Filler Derived Ceramics, *J. Kor.Ceram.Soc*. 49 (2012) 279-286

L. Schlier, N. Travitzky, J. Gegner, P. Greil, Surface strengthening of extrusion formed polymer/filler derived ceramic composites, *J. Ceram. Sci. Techn*. 3 (2012) 181-188

Robocasting of Alumina Lattice Truss Structures

Tobias Schlordt, Felix Keppner, Nahum Travitzky, Peter Greil

Robocasting of aqueous colloidal α-Al_2O_3 gels for manufacturing of cellular ceramics with periodical lattice truss structures was investigated. Three dimensional alumina grids with periodical lattice structure were manufactured on a six-axis robotic system equipped with a single screw micro-extruder (RobFab, Battenberg ROBOTIC GmbH & Co. KG, Marburg, Germany). 1. Real time tactile and optical sensor control operating at a frequency of 200 Hz allows deposition of a continuous filament with a lateral resolution < 50 µm at a line deposition velocity of 35 mm/s. Temperature and relative humidity in the fabrication chamber (400 x 400 x 400 mm^3) were kept constant at 20 °C and 22 %, respectively. A stainless steel nozzle (Model Number 100792, UES AG, Krefeld, Germany) with a circular hole having a diameter of 500 µm was applied.

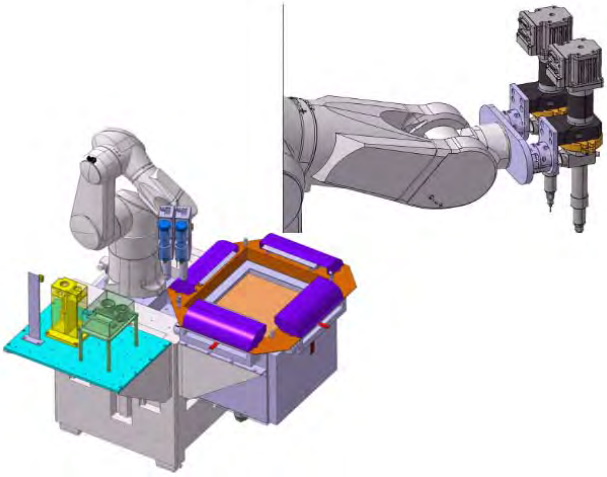

Scheme of six-axis high precision robotic system applied for robocasting.

Coagulation of gels loaded with 48 vol% α-Al_2O_3 was induced by adding NH_4Ac. The gels exhibit shear-thinning behavior, shear elastic moduli ranging from 6.7 to 390 kPa and yield-stresses from 25 to 570 Pa. Though the reference viscosity η at 0 g/l NH_4Ac was shifted to values more than one order of magnitude higher by addition of 50 g/l NH_4Ac, shear thinning behavior remained unaffected and the coagulated alumina gel achieved adequate rheological behavior required for the robocasting process,

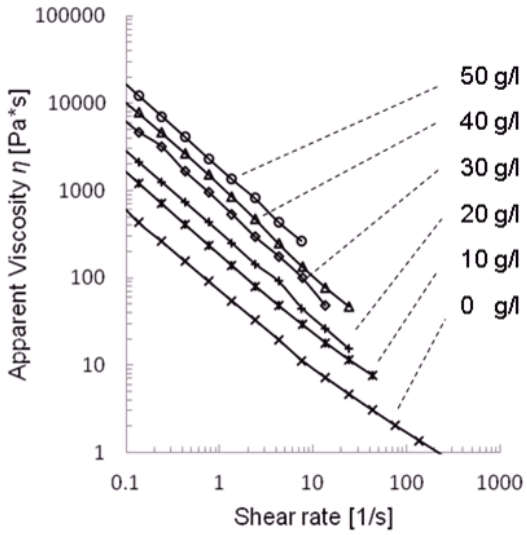

Viscosity over shear rate (a) and shear elastic modulus over shear stress (b) measurements on colloidal alumina gels loaded with different content of NH_4Ac coagulant.

Three dimensional lattice truss structure of sintered alumina with dimensions of 32 x 32 x 3 mm^3 were prepared by continuous filament writing of the alumina gel coagulated with 50 g/l NH_4Ac. The lattice structure consists of alternating layers formed by a linear array of circular rods aligned parallel with a distance of 1 mm and an angle of 90° between alternating layers. Thus, macroscopic cell patterns with tetragonal symmetry and a cell size of 1 x 1 mm^2 were formed with continuous as well as porous walls (free spanning ligaments). A micro-extrusion nozzle of circular geometry and a diameter of 500 µm was applied which after sintering at 1650 °C for 2h resulted in a filament diameter of approximately 400 µm.

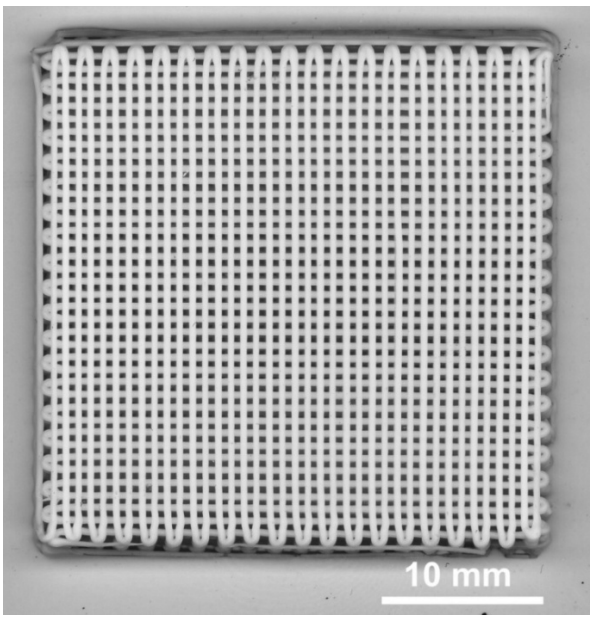

Sintered alumina lattice truss structure of tetragonal cell geometry fabricated from colloidal alumina gel with a coagulant content of 50 g/l NH_4Ac applying an extrusion speed of 35 mm/s.

Fabrication of lattice truss structures with the ligaments connected to form continuous walls as well as spanning lattice structures with free spanning strut ligaments requires control of ligament deflection during the continuous writing process. Based on beam theory viscous flow ligament deflection driven by gravitation was analyzed and processing parameters to avoid deflection were derived.

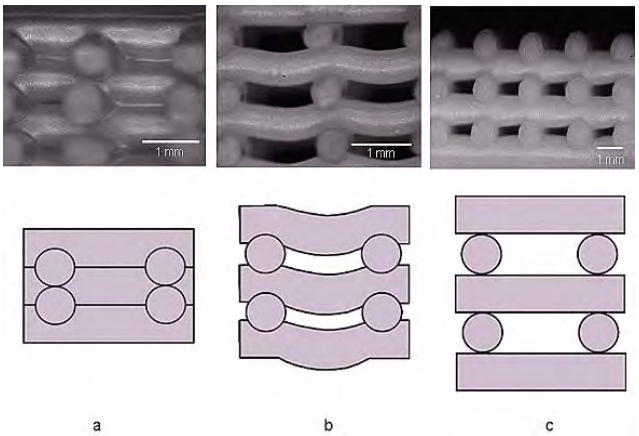

Wall structures of sintered alumina lattice truss structures perpendicular to the deposition plane of robocasting applying a constant deposition rate of 35 mm/s: a) continuous wall ($d_z = \phi/2$; 30 g/l NH_4Ac); b) porous wall with spanning but deflected ligaments ($d_z = \phi$, 30 g/l NH_4Ac); c) porous wall with almost undeflected ligaments ($d_z = \phi$, 50 g/l NH_4Ac).

T. Schlordt, F. Keppner, N. Travitzky, P. Greil, Robocasting of Alumina Lattice Truss Structures, J. Ceram. Sci. Techn. 3 (2012) 81-88

Anisotropic shrinkage of cast green tapes

Zongwen Fu, Andreas Roosen

During tape casting the slurry is exposed to shearing stresses below the doctor blade. The effective shear rate depends on the casting speed v_{draw} and on the gap-height h between the moving carrier film and the fixed doctor blade. In this velocity profile the ceramic particles perform a continuous rotation of time dependent speed. This is described by the Jeffery´s orbit:

$$\Phi(t) = \arctan\left(r \tan \frac{\dot{\gamma} \cdot t}{r + \frac{1}{r}} \right)$$

with Φ: orientation angle, t: time, γ: shear rate, r: aspect ratio. For non-equiaxed particles, an unbalanced rotation occurs leading to an average orientation of the particles in casting direction. Investigations of the morphology of ceramic powders by means of a flow particle image analyzer (Malvern Instruments, Worcestershire, U.K.) show that particles exhibit a strong deviation from the spherical shape. This particle orientation causes inhomogeneous particle packing, which was determined quantitatively; it is the cause for the anisotropic shrinkage behaviour of green tapes. With x as casting direction and z as thickness direction, the relation between the tape shrinkage ε in the three dimensions is $\varepsilon_z > \varepsilon_y > \varepsilon_x$. The coefficient of anisotropy shrinkage K is defined as

$$K = 1 - (\varepsilon_x / \varepsilon_y).$$

The particle shape has a strong effect on the K-factor. Tapes from nearly spherical powders exhibit low K-values < 2, whereas platelet shaped powders showed K-values of app. 13. Anisotropic shrinkage impedes miniaturization of multilayer structures, because after co-firing the structures of different layers should have an overlap of at least 50 % to guarantee interconnectivity. Because these structures are in the range of 50 µm, a position accuracy of ± 25 µm is needed. If K is too big or the structures are too fine, these requirements cannot be met.

To understand why particle orientation causes an anisotropic shrinkage, sintering models had been reviewed. Basically, two mechanisms are important for densification; on the one hand, grain growth is controlled by geometric factors of particles including contact points and areas. On the other hand, pore elimination is controlled by geometric factors of the pores and pore coordination number. Therefore, the pore orientation was described quantitatively, too. This required the deve-

lopment of a suitable method. By measuring the pore space N in the three axes, a pore orientation factor S was defined as

$$S = 1 - (N_x/N_y)$$

If S is > 0, the pores are aligned in x-direction, S < 0 describes pore alignment in y-direction. Fig. 1 shows the results of a green tape which was processed with a platelet shaped powder. Future research focuses on implementing the data of the oriented microstructure analysis into sintering models to explain anisotropic shrinkage.

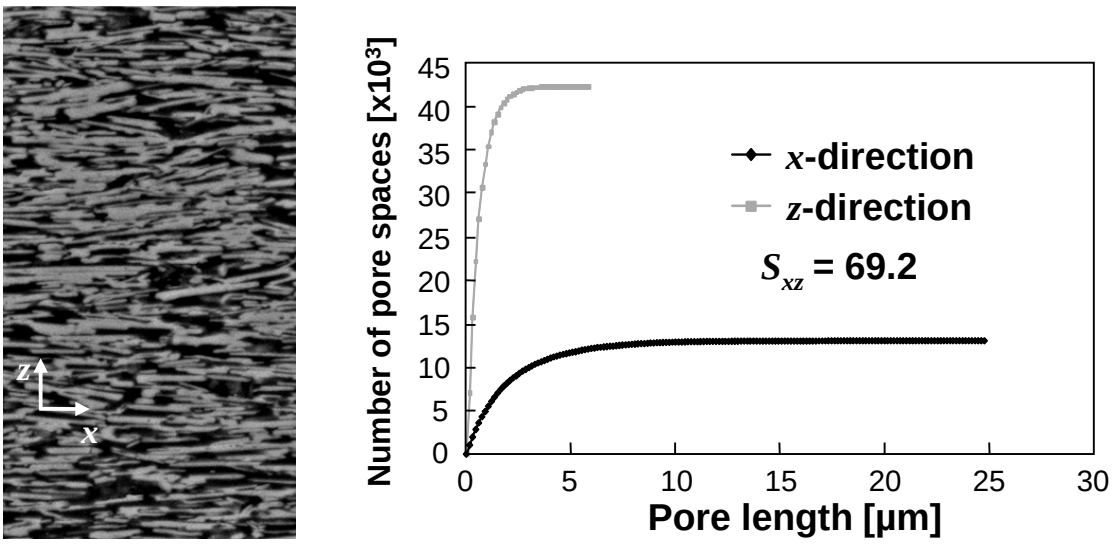

Fig. 1: Cast green tape of platelet powder and the corresponding pore analysis.

Casting of ultrathin and ultrathick green tapes

Moritz Wegener, Daniel Jakobsen, Andreas Roosen

Typically tape casting is used to manufacture green tapes in the thickness range of 10 to 1000 µm. The thickness of cast green tapes d_{Tape} depends primarily on the casting height h, the casting speed v, the hydrostatic pressure ΔP, the design of the casting head, and the consistency of the slurry as described in the following equation (Chou, Ko, Yan, J. Am. Cer. Soc., 1987):

$$d_{Tape} = \frac{\alpha \cdot \beta}{2} \frac{\rho_{Slurry}}{\rho_{Tape}} h \cdot (1 + \frac{h^2 \Delta P}{6 \eta v l})$$

with l: length of doctor blade, α: correction factor for side flow, β: correction factor for weight loss during drying, ρ_{Slurry}: density of slurry, ρ_{Tape}: density of green tape, η: viscosity. In multilayer technology and for printed electronics, there is a demand to cast green tapes exhibiting thicknesses < 1 µm. In contrast, for advanced refractory multilayer composites with improved thermo-shock and corrosion properties, thick tapes in the range of 5 mm and above are of interest. On both research topics the group of functional ceramics is focussing.

For thin layers with thicknesses < 1 µm, nano-sized powders have to be used which requires improved deagglomeration techniques and specific requirements for the dispersing agents and a decrease in solid loading of the slurry. In addition, the doctor-blade technique is not suitable to cast layers of constant thickness in this thickness range; therefore, casting was done by means of a profile rod (Fig. 1). With this technique, starting from well-dispersed slurries, layers of down to 250 nm could be cast continuously which are suitable for lamination. The application of these layers in printed field effect transistors and other applications is under investigation.

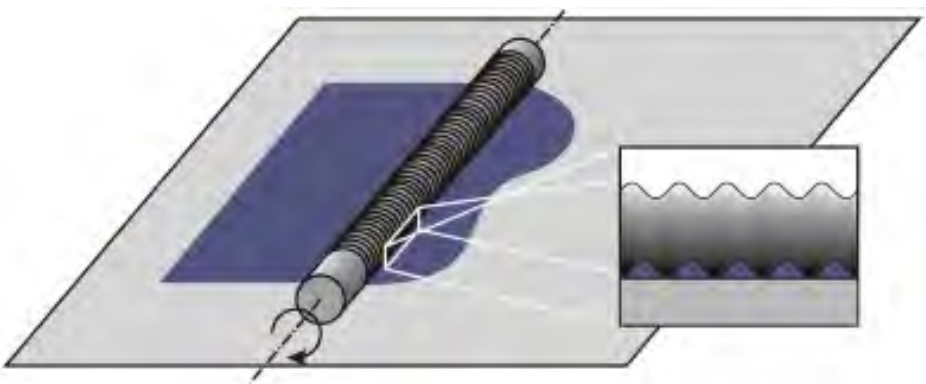

Fig. 1: Principle of profile rod technique (Straue, Prado, Polster, Roosen: J. Am. Cer. Soc., 2011)

The manufacture of thick green tapes for refractory multilayer applications with thicknesses > 1 mm requires the use of coarse particles up to 1 mm diameter. For such powders the deagglomeration process can be performed in mixing devices, because attractive forces are not dominant. The slurry should exhibit high solid loadings to reduce undesired side flow and segregation effects as well as to accelerate drying. Such tapes can be laminated, too (Fig. 2). The manufacture of multilayer composites with optimized layer design is in progress.

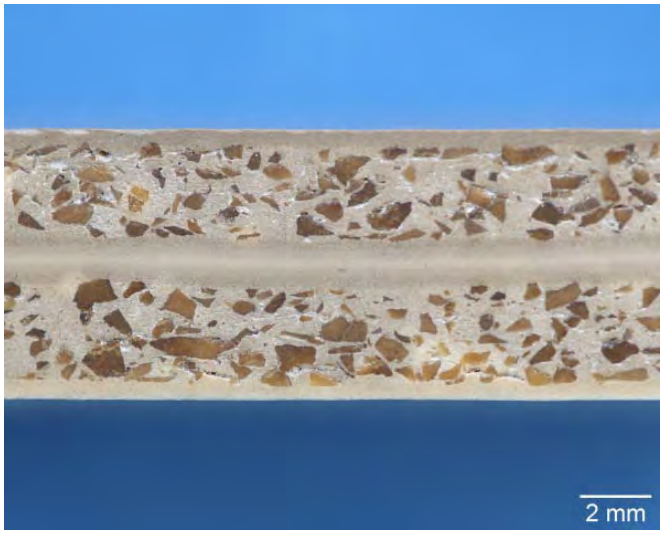

Fig. 2: Fired MgO multilayer structure: Two porous and coarse-grained tapes are joined with dense and fine-grained layers.

3. PUBLICATIONS

Papers

(in alphabetical order)

01/12 F. Angeli, O. Villain, S. Schuller, T. Charpentier, D. de Ligny, L. Bressel, L. Wondraczek

Effect of temperature and thermal history on borosilicate glass structure

PHYSICAL REVIEW B, Vol. 85, Issue: 5, Article Number 054110 (2012)

DOI: 10.1103/physRevB.85.054110

02/12 M. Batentschuk, R. Geisler, J. Hum, F. Iqbal, F. Meister, A. Osvet, A. Stiegelschmitt, A. Winnacker

Eu^{2+} and Eu^{3+} based "concentrated phosphors" as converters for UV LED light: two approaches and two new examples

Appl. Phys. B 106 (2012) 211–221

DOI: 10.1007/s00340-011-4735-5

03/12 R. Bathelt, T. Soller, K. Benkert, C. Schuh, A. Roosen

Neodymium doping of KNNLT

Journal of the European Ceramic Society 32 (2012) 3767-3772

DOI: 10.1016/j.jeuceramsoc.2012.05.025

04/12 R. Cao, M. Peng, L. Wondraczek, J. Qiu

Superbroad near-to-mid-infrared luminescence from Bi_5^{3+} in $Bi_5(AlCl_4)_3$

OPTTICS EXPRESS, Vol. 20, Nr. 3, 2562-2571(2012)

DOI: 10.1364/OE.20.002562

05/12 B. Ceron-Nicolat, F. Wolff, A. Dakkouri-Baldauf, T. Fey, H. Münstedt, P. Greil

Graded Cellular Ceramics from Continuous Foam Extrusion

Advanced Engineering Materials 14(2012) 12, 1097-1103

DOI: 10.1002/adem.201200039

06/12 J. Cypris, L. Schlier, N. Travitzky, P. Greil, M. Weclas

Heat release process in three-dimensional macro-cellular SiC reactor under Diesel engine-like conditions

Fuel 102(2012) 115-128

DOI: 10.1016/j.fuel.2012.05.038

07/12 R. Detsch, O. Guillon, L. Wondraczek, A. Boccaccini

Initial Attachment of rMSC and MG-63 Cells on Patterned Bioglass® Substrates

Advanced Engineering Materials Vol.14 (2012) 38-44

DOI: 10.1002/adem.201180068

08/12 G. Gao, M. Peng, L. Wondraczek

Temperature dependence and quantum efficiency of ultrabroad NIR photoluminescence from Ni^{2+} centers in nanocrystalline Ba-Al titanate glass ceramics

OPTICS LETTERS, Vol. 37, Issue: 7, 1166-1168 (2012)

DOI: 10.1364/OL.37.001166

09/12 G. Gao, S. Reibstein, E. Spiecker, M. Peng, L. Wondraczek

Broadband NIR photoluminescense from Ni^{2+}-doped nanocrystalline Ba-Al titanate glass ceramics

J. Mater. Chem., 2012, 22, 2582-2588

DOI: 10.1039/c1jm14292e

10/12 J.L. Garden, H. Guillou, J. Richard, L. Wondraczek

Non-equilibrium configurational Prigogine-Defay ratio

Journal of Non-Equilibrium Thermodynamics, Vol. 37, Issue: 2, 143-177 (2012)

DOI: 10.1515/jnetdy-2011-0036

11/12 J.L. Garden, H. Guillou, R. Richard, L. Wondraczek

Affinity and its derivatives in the glass transition process

Journal of Chemical Physics, Vol. 137, Issue: 2, Nr. 024505

DOI: 10.1063/1.4733333

12/12 I. Götschel, Y. Hayashi, K. Kakimoto, A. Roosen

Tape Casting of Al_2O_3, MgO, and $MgAl_2O_4$ for the Manufacture of Multilayer Composites for Refractory Applications

Int. J. Appl. Ceram. Technol. 9 [2] 329-340 (2012)

DOI: 10.1111/j.1744-7402.2011.02664.x

13/12 I. Götschel, A. Roosen

Corrosion Resistance of Dense and Porous Tape-cast Oxide Refractories against CaO-Fe_2O_3 SiO_2 Slag

Refractories WORLDFORUM, 4 (2012) [1], 137-142

14/12 M. Götz, T. Fey, P. Greil

Vibration Assisted Self-Assembly Processing of Ceramic Based-Composites with Modular Meta-Structure

J. Am. Ceram. Soc. 95 [1] 95-101 (2012)

DOI: 10.1111/j.1551-2916.2011.04844.x

15/12 P. Greil

Advancements in Polymer-Filler Derived Ceramics

Journal of Korean Ceramic Society, Vol. 49, Nr. 4, pp. 279-286 (2012)

DOI: 10.4191/kcers.2012.49.4.279

16/12 P. Greil

Generic principles of crack-healing ceramics

Journal of Advanced Ceramics 2012, 1[4], 249-267

DOI: 10.1007/s40145-012-0020-2

17/12 M. Grosser, M. Münch, H. Seidel, C. Bienert, A. Roosen, U. Schmid

The impact of substrate properties and thermal annealing on tantalum nitride thin films

Applied Surface Science 258 (2012) 2894-2900

DOI: 10.1016/j.apsusc.2011.11.003

18/12 B. Gutbrod, N. Travitzky, A. Richter, M. Göbbels, P. Greil

Slag Corrosion of Preceramic Paper Derived Multilayer Oxide Refractory

Refractories Worldforum 4 (2012) [4] 103-109

19/12 C. Heiss, N. Travitzky, P. Greil

Manufacturing of silicon carbide knit fabrics

Adv. Eng. Mat., 14 (3), 2012, 162-165

DOI: 10.1002/adem.201100192

20/12 N. Jordanov, L. Wondraczek, I. Gutzow

Thermodynamic properties of vitreous electrodes in a Ni/NiP glass-crystal Galvanic cell

Journal of Non-Crystalline Solids xxx (2012) xxx-xxx (published online 2012)

DOI: 10.1016/j.jnoncrysol.2012.10.028

21/12 N. Jordanov, L. Wondraczek, I. Gutzow

Thermodynamic properties of amorphous solids: The electrochemical approach

Journal of Non-Crystalline Solids 358 (2012) 1239-1256

DOI: 10.1016/j.jnoncrysol.2012.02.031

22/12 Y.-J. Kang, T. Fey, P. Greil

Synthesis of Ti_2SnC MAX Phase by Mechanical Activation and Melt Infiltration

Advanced Engineering Materials (2012) 14 Nr. 1-2, 85-91

DOI: 10.1002/adem.201100186

23/12 S. Karlsson, B. Jonson, L. Wondraczek

Copper, silver, rubidium and caesium ion exchange in soda-lime-silica float glass by direct deposition and in line melting of salt pastes

Glass Technol.: Eur. J. Glass Sci. Technol. A ***53****, 1-7 (2012)*

24/12 K. Kioka, T. Honma, K. Oh-ishi, S. Reibstein, N. Da, L. Wondraczek, T. Komatsu

Effect of Al_2O_3 addition on the formation of perovskite-type $NaNbO_3$ nanocrystals in silicate-based glasses

Journal of Non-Crystalline Solids 358 (2012) 1523–1529

DOI: 10.1016/j.jnoncrysol.2012.04.011

25/12 C. Kluthe, B. Dermeik, W. Kollenberg, P. Greil, N. Travitzky

Processing, Microstructure and Properties of Paper-Derived Porous Al_2O_3 Substrates

J. Ceram. Sci. Tech., 03, [3] 111-118 (2012)

DOI: 10.4416/JCST2012-00008

26/12 N. Kölpin, M. Wegener, E. Teuber, S. Polster, L. Frey, A. Roosen

Conceptional design of nano-particulate ITO inks for inkjet printing of electron devices

J. Mater. Sci. (2013) 48:1623-1631 (published online 2012)

DOI: 10.1007/s10853-012-6919-8

27/12 R. Meszaros, B. Merle, M. Wild, K. Durst, M. Göken, L. Wondraczek

Effect of thermal annealing on the mechanical properties of low-emissivity physical vapor deposited multilayer-coatings for architectural applications

Thin Solid Films 520 (2012) 7130–7135

DOI: 10.1016/j.tsf.2012.07.086

28/12 O. Montedo, D. Hotza, A. Novaes de Oliveira, R. Meszaros, N. Travitzky, P. Greil

Crystallisation Kinetics of a β-Spodumene-Based Glass Ceramic

Advances in Materials Science and Engineering (2012); Article ID 52428, 8 pages

DOI: 10.1155/2012/525428

29/12 K.H. Nielsen, M.M. Smedskjaer, M. Peng, Y.Z. Yue, L. Wondraczek

Surface-luminescence from thermally reduced bismuth-doped sodium aluminosilicate glasses

Journal of Non-Crystalline Solids 358 (2012) 3193-3199

DOI: 10.1016/j.jnoncrysol.2012.09.021

30/12 S. Reibstein, N. Da, J.-P. Simon, E. Spiecker, L. Wondraczek

Phase separation and crystal precipitation in supercooled sulphophosphate ionic melts

Phys. Chem. Glasses: Eur. J. Glass Sci. Technol. B53, 61-67 (2012)

31/12 L. Schlier, N. Travitzky, J. Gegner, P. Greil

Surface strengthening of extrusion formed polymer/filler derived ceramic composites

J. Ceram. Sci. Tech., 03 [04], 2012, 181-188

DOI: 10.4416/JCST2012-00018

32/12 T. Schlordt, F. Keppner, N. Travitzky, P. Greil

Robocasting of Alumina Lattice Truss Structures

J. Ceram. Sci. Tech., 03 [2] 81-88 (2012)

DOI: 10.4416/JCST2012-00003

33/12 M.A. Schmidt, D.Y. Lei, L. Wondraczek, V. Nazabal, S.A. Maier

Hybrid nanoparticle-microcavity-based plasmonic nanosensors with improved detection resolution and extended remote-sensing ability

Nat Commun. 2012;3:1108

DOI: 10.1038/ncomms2109

34/12 S. Sirotkin, R. Meszaros, L. Wondraczek

Chemical Stability of ZnO-Na_2O-SO_3-P_2O_5 Glasses

International Journal of Applied Glass Science 3 [1] 44-52 (2012)

DOI: 10.1111/j.2041-1294.2011.00076.x

35/12 N. Straue, M. Rauscher, M. Dressler, A. Roosen

A Tape Casting of ITO Green Tapes for Flexible Electroluminescent Lamps

J. Am. Ceram. Soc. 95 [2] 684-689 (2012)

DOI: 10.1111/j.1551-2916.2011.04836.x

36/12 S. Striepe, N. Da, J. Deubener, L. Wondraczek

Micromechanical properties of Na, Zn-sulfophosphate glasses

Journal of Non Crystalline Solids, Vol. 358, Issue: 6-7, 1032-1037(2012)

DOI: 10.1016/j.jnoncrysol.2012.01.045

37/12 L.A. Strobel, S.N. Rath, A.K. Maier, J.P. Beier, A. Arkudas, P. Greil, R.E. Horch, U. Kneser

Induction of bone formation in biphasic calcium phosphate scaffolds by bone morphogenetic protein-2 and primary osteoblasts

J Tissue Eng Regen Med (2012)

DOI: 10.1002/term.1511

38/12 N. Travitzky

Processing of ceramic-metal composites

Advances in Applied Ceramics, Volume 111, Numbers 5-6, August 2012, pp. 286-300(15)

DOI: 10.1179/1743676111Y.0000000073

39/12 A. Winkel, R. Meszaros, S. Reinsch, R. Müller, N. Travitzky, T. Fey, P. Greil, L. Wondraczek

Sintering of 3D-Printed Glass/HAp Composites

J. Am. Ceram. Soc., ***95 [11]*** *3387-3393 (2012)*

DOI: 10.1111/j.1551-2916.2012.05368.x

40/12 A. Winterstein, S. Manning, H. Ebendorff-Heidepriem, L. Wondraczek

Luminescence from bismuth-germanate glasses and its manipulation through oxidants

Optical Materials Express, Vol. 2, Issue 10, pp. 1320-1328 (2012)

DOI: 10.1364/OME.2.001320

41/12 F. Wolff, B. Ceron Nicolat, T. Fey, P. Greil, H. Münstedt

Extrusion Foaming of a Preceramic Silicone Resin with a Variety of Profiles and Morphologies

Advanced Engineering Materials 2012, 14 Nr. 12, 1110-1115

DOI: 10.1002/adem.201100351

42/12 D.C. Yu, S. Ye, M.Y. Peng, Q.Y. Zhang, L. Wondraczek

Sequential three-step three-photon near-infrared quantum splitting in β-$NaYF_4$:Tm^{3+}

Appl. Phys. Lett. ***100****, 191911 (2012)*

DOI: 10.1063/1.4714505

43/12 W.J. Zhang, Q.J. Chen, J.P. Zhang, Q. Qian, Q.Y. Zhang, L. Wondraczek

Enhanced NIR emission from nanocrystalline LaF_3:Ho^{3+} germanate glass ceramics for E-band optical amplification

Journal of Alloys and Compounds, Volume 541, issue (November 15, 2012), pp. 323-327

DOI: 10.1016/j.jallcom.2012.06.092

PHYSICAL REVIEW B 85, 054110 (2012)

Effect of temperature and thermal history on borosilicate glass structure

Frédéric Angeli,[1,*] Olivier Villain,[2] Sophie Schuller,[3] Thibault Charpentier,[2] Dominique de Ligny,[4] Lena Bressel,[4] and Lothar Wondraczek[5]

[1]*CEA, DEN, Laboratoire d'étude du Comportement à Long Terme, 30207 Bagnols-sur-Cèze, France*
[2]*CEA, IRAMIS, Laboratoire de Structure et Dynamique par Résonance Magnétique, UMR CEA/CNRS 3299, 91191 Gif-sur-Yvette, France*
[3]*CEA, DEN, Laboratoire d'étude et Développement des Matrices de Confinement, 30207 Bagnols-sur-Cèze, France*
[4]*Université de Lyon, Université Lyon 1, CNRS, UMR5620, Laboratoire de Physico-Chimie des Matériaux Luminescents, F-69622 Villeurbanne, France*
[5]*Department of Material Science, Glass and Ceramics-WW3, University of Erlangen-Nuremberg, 91058 Erlangen, Germany*

(Received 28 September 2011; published 14 February 2012)

The influence of the temperature and quenching rate on the structure of a borosilicate glass was studied by high-resolution solid-state ^{11}B, ^{23}Na, ^{29}Si nuclear magnetic resonance (NMR) and high-temperature Raman spectroscopy. Data were obtained for glass in the solid state after annealing and quenching at cooling rates covering four orders of magnitude as well as in the liquid state from Raman experiments and from calorimetry and rheological data. Nuclear magnetic resonance measurements were used to calibrate the Raman spectra in order to quantify the change in boron coordination with temperature. This result can then be used to determine the fictive temperature of the glass directly from the boron coordination. The fictive temperature, heat capacity, and configurational entropy are extracted from calorimetry and viscosity measurements. Changes in the boron coordination account for only 25% of the configurational heat capacity of the liquid. The structural parameters capable of accounting for the remaining quantity are discussed on the basis of structural data, both local (inhomogeneity of the sodium distribution) and medium-range (from NMR parameter distribution). It has thus been shown that, although the B-O-B angular distributions of the boroxol rings (and probably the Si-O-Si distributions) are not affected by temperature, a structural disorder is identified through the angular distributions of the bonds linking borate and silicate groups.

DOI: 10.1103/PhysRevB.85.054110 PACS number(s): 61.43.Fs, 76.60.−k, 82.80.Gk

I. INTRODUCTION

Sodium borosilicate glass is a simple system underlying many industrial applications, including a large part of the waste containment glasses developed for spent nuclear fuel.[1] To avoid the formation of heterogeneities that could be detrimental to the properties of the glass matrix (viscosity, resistance to self irradiation, chemical durability, etc.), it is important to follow the melt structural evolution with temperature. Structural transformations above the glass transition temperature (T_g) can provide a better understanding of the mechanisms responsible for the liquid instability (liquid-liquid phase separation and crystallization in particular) arising from the presence of low-solubility elements, such as the rare earth elements or molybdenum in nuclear glass.[2]

Above T_g, the melt is characterized by major variations of second-order thermodynamic properties, such as heat capacity, thermal expansion, and compressibility, which can be related to configurational[3] structural changes that are still poorly known. The heat capacity of the glass is associated with atomic displacements around its equilibrium position (vibrational contribution) below T_g. At T_g, an additional contribution attributed to the distribution of atom positions appears and substantially increases with the temperature. In borates, borosilicates, or aluminoborosilicates, a decrease in tetrahedral boron with increasing quenching rates is clearly observed by nuclear magnetic resonance (NMR),[4–10] neutron diffraction,[11–13] or Raman spectroscopy.[13–16] These changes in the coordination number can represent a significant contribution to the configurational heat capacity, especially in borate glass.[7,12,13] The decrease in tetrahedral boron entails an increase in nonbridging oxygens (NBOs) that was directly confirmed by ^{17}O magic-angle spinning (MAS) NMR.[6] In borosilicate glass, the configurational contribution related to the change in boron speciation is smaller,[17] and the other structural parameters involved are not clearly established.

Numerous structural data have been acquired for sodium borosilicate glass; changes in the polymerization of the silicate network and in the ratio between tri- and tetracoordinate boron are well known according to the amount of alkalis, which can act either as charge compensators for tetrahedral boron or as network modifiers near NBOs.[18–21] Quantitative monitoring of these structural transformations is more difficult in the melt than in the solid. Nevertheless, the room-temperature glass structure already provides valuable information because it is closely related to its thermal history through the configuration acquired by the liquid when quenched. The temperature at which the glass configuration would correspond to the equilibrium configuration of the supercooled liquid, known as the fictive temperature (T_f), can vary over a range of about 200 K and is inversely proportional to the quenching rate.[22] It can be specifically imposed by annealing the glass within a narrow temperature range for which the relaxation times are not too long. It can also be studied over a broader temperature range by quenching the material at different rates.

We propose in this paper to correlate the data obtained in the solid and liquid states by coupling structural and thermodynamic approaches. A sodium borosilicate glass containing cesium was used as a nuclear glass composition model.[1] It constitutes a basic system before subsequently adding low-solubility elements (rare earth elements and molybdenum). Various heat treatments were applied, from annealing to

Appl Phys B (2012) 106:211–221
DOI 10.1007/s00340-011-4735-5

Applied Physics B
Lasers and Optics

Eu^{2+} and Eu^{3+} based "concentrated phosphors" as converters for UV LED light: two approaches and two new examples

M. Batentschuk · R. Geisler · J. Hum · F. Iqbal · F. Meister · A. Osvet · A. Stiegelschmitt · A. Winnacker

Received: 22 March 2011 / Revised version: 28 June 2011 / Published online: 11 October 2011

Abstract The absolute majority of phosphors are composed of a host lattice and some percentage of an activator. At higher activator concentrations the concentration quenching occurs. However, there are phosphors in which only minor quenching of the emission occurs with increasing of the activator content. Based on the existence of two different valence states of the Eu ion (2+ and 3+), two approaches for the development of "concentrated phosphors", i.e. light emitting materials in which the activator ion is a main part of the crystal lattice, are discussed. In both approaches, reduced energy migration leading to the luminescence quenching is considered as a main condition to reach a high quantum efficiency of a concentrated phosphor. Two kinds of phosphors—Eu^{2+}-doped alumosilicate and Eu^{3+}-doped oxyfluoride—are used as an experimental basis for this discussion. Starting from the stoichiometric $Ca_{1-x}Eu_x^{2+}Al_2Si_2O_8$ anorthite and $Eu^{3+}OF$ oxyfluorides, the non-stoichiometric powders with $Eu_{0.92}^{2+}Al_{1.76}Si_{2.24}O_8$, $Eu^{3+}(O, F)_{2.35}$ and $Eu^{3+}(O, F)_{2.16}$ compositions were synthesized by a solid state reaction and investigated. It was shown that—in spite of the almost 100% Eu concentration—light converters with high quantum efficiency of more than 45% can be realized. A possible application of these materials as UV LED light converters for white light emitting diodes are discussed as well.

M. Batentschuk (✉) · R. Geisler · J. Hum · F. Iqbal · F. Meister · A. Osvet · A. Stiegelschmitt · A. Winnacker
Department of Materials Science, University of Erlangen-Nuremberg, Martensstr. 5/7, 91058 Erlangen, Germany
e-mail: mirobat@ww.uni-erlangen.de
Fax: +49-9131-8528495

1 Introduction

1.1 Motivation for the development of UV LED excitable concentrated phosphors

The absolute majority of phosphors are composed of a host lattice and an activator with a concentration of some per cent. At higher concentrations, the so called concentration quenching occurs, due to the migration of the excitation energy to "killer"-centres. However, for some applications such as laser materials and light converters in white light LEDs a strong absorption is required. For instance, due to the high absorption, the light scattering in the powder converters for white light LEDs can be reduced essentially leading to the increase of their light yield. The high absorption of the excitation light can be reached by the increase of the activator concentration over the optimal value. It is surprising, however that there are phosphors in which only minor quenching of the emission occurs with further increasing of the activator content. In the limit, the activator concentration can reach 100%, i.e. the emitting ions can occupy all sites of certain cation in the crystal lattice. Such compounds are often called "concentrated phosphors". Actually, the term "concentrated phosphor" makes sense already when the concentration of activator ions reaches the two-digit percentage, i.e. in the case when the activator is a one of the main components of the crystal lattice.

The ways to reach the high efficiency in the concentrated phosphors are in principle known: either a phosphor should be so pure and perfect that the excited state does not reach a "killer" state during its life time, or the energy migration between neighbouring activator ions should be inhibited [1]. In the first case, the purity and the perfection of the crystals should be so high that it is not acceptable for technical applications. Regarding the second one, the restriction of the

Available online at www.sciencedirect.com
SciVerse ScienceDirect
Journal of the European Ceramic Society 32 (2012) 3767–3772
www.elsevier.com/locate/jeurceramsoc

Original article

Neodymium doping of KNNLT

R. Bathelt [a,*], T. Soller [a], K. Benkert [a], C. Schuh [a], A. Roosen [b]

[a] Siemens AG, Otto-Hahn-Ring 6, 80200 München, Germany
[b] University of Erlangen-Nürnberg, Martensstraße 5, 91058 Erlangen, Germany

Received 31 October 2011; received in revised form 15 May 2012; accepted 16 May 2012
Available online 13 June 2012

Abstract

The effect of stoichiometric trivalent Neodymium doping on $(K_{0.46}Na_{0.54})_{0.97}Li_{0.03}Nb_{0.81}Ta_{0.19}$ (KNNLT) is examined up to an amount of 1 mol% Nd. The sensitivity of the properties of KNNLT on the Nd-content is well pronounced. The main effect is the lowering of the orthorhombic-tetragonal phase transition temperatures accompanied by an increase of the piezoelectric response at room temperature. At low doping levels the densification is promoted while it is impeded at high doping levels. The relationship between microstructure and the sharpness of the orthorhombic-tetragonal phase transition is reviewed.

Keywords: Piezo; Lead-free; KNN; Trivalent doping; Thermal properties

1. Introduction

During the last 50 years $Pb(Zr,Ti)O_3$ (PZT)- based piezoceramics have been the dominating material in piezoelectric actuation due to their high piezoelectric response, good reproducibility and their well-understood and economic manufacturing properties.

In a general attempt to remove hazardous substances from electronic equipment, the EU constituted a ban of several toxic substances and heavy metals in electronic materials.[1,2] Exceptions such as for piezoelectrics are timely limited and are regularly revised. In the course of searching for lead-free piezo materials, the material families that were discarded in favor of PZT in the 1960s moved back to the focus of attention. Especially undoped potassium sodium niobate-(KNN) based materials display high Curie temperatures and appealing piezoelectric properties if they are densified properly and the stoichiometry is well monitored.[3,4] However, maintaining stoichiometry and high density is a difficult task due to the volatility of alkaline constituents,[5] yet it can be accomplished in an economical way by proper doping. In 2004, Saito et al.[6] proposed a KNN-based system doped with Li, Ta and Sb, which combined high sintering density and an outstanding piezoelectric performance in comparison to other lead-free materials. The high piezoelectric response is based mainly on the orthorhombic-tetragonal polymorphic phase transition that was shifted close to room temperature. Another reason for the increased performance is attributed to antimony doping: This might be due to an improved densification behavior, as well as the high electronegativity of Sb. However, antimony is as toxic as lead.[7,8]

In this paper a high performing KNN-based piezoelectric material doped with non-toxic Nd is presented.[9] In the PZT system, Nd turned out to be a feasible donor dopant to improve the piezo constant and piezoelectric coupling, but so far, it was not used as a dopant in KNN. The base material for Nd-doping was a KNN material doped with 3 mol% lithium and 19 mol% tantalum (KNNL3T19).[10] Though of higher complexity than pure KNN, this material shows high reproducibility, good densification behavior of up to 96% theoretical density (%TD), a good performance with a piezo coefficient $d_{33}^* = 290$pm/V (at an electric field strength of 2 kV/mm), a permittivity value of 700 and a low loss factor tan δ of 3.5%.

2. Experimental procedure

Several Nd-doped KNN-based compositions of the general formula $[(K_{0.46}Na_{0.54})_{0.97}Li_{0.03}]_{(1-3x)}Nd_xV_A'_{(2x)}Nb_{0.81}Ta_{0.19}O_3$ (KNNLN$_x$T) with a Nd concentration x ranging up to 1 mol% were prepared. For powder synthesis, commercially

* Corresponding author.
E-mail address: robert.bathelt@gmx.de (R. Bathelt).

0955-2219/$ – see front matter © 2012 Elsevier Ltd. All rights reserved.
http://dx.doi.org/10.1016/j.jeurceramsoc.2012.05.025

Superbroad near-to-mid-infrared luminescence from Bi_5^{3+} in $Bi_5(AlCl_4)_3$

Renping Cao,[1,3] Mingying Peng,[1,3*] Lothar Wondraczek,[3,4] and Jianrong Qiu[1,5]

[1]*Institute of Optical Communication Materials and State Key Laboratory of Luminescent Materials and Devices, South China University of Technology, Guangzhou 510640, China*
[3] *Department of Materials Science, University of Erlangen-Nuremberg, Erlangen 91058, Germany,*
[*] *equal contribution to this work*
[4] *lothar.wondraczek@ww.uni-erlangen.de*
[5] *qjr@scut.edu*
[*] *pengmingying@scut.edu.cn*

Abstract: Superbroad near-to-mid infrared (NIR-MIR) photoluminescence was observed from $Bi_5(AlCl_4)_3$ at room temperature, spanning the spectral range of about 1000 to 4000 nm. On the basis of structural considerations and dynamic analyses, Bi_5^{3+} clusters were identified as the optically active species, inherently differing from the species which is typically believed to be active in NIR-emitting Bi-doped glasses. In comparison to most other NIR-luminescent Bi-doped materials, the MIR-part of the luminescence spectrum is still present at room temperature. Emission intensity and excited state lifetime were found to exhibit abnormal temperature dependence, where the former increases with temperature up to a critical value of about 150 K. This behavior is related to a temperature-dependent overlap between ground state and excited states. The observed stabilization of MIR photoemission at room temperature may be a starting point for the development of Bi-based NIR-MIR light sources with superbroad emission spectrum, where Bi_5^{3+} or similar polycationic species act as optical gain medium.

OCIS codes: (160.2750) Glass and other amorphous materials; (160.2540) Fluorescent and luminescent materials; (140.4480) Optical amplifiers; (060.4510) Optical communications.

References and links

1. I. Bufetov and E. Dianov, "Bi-doped fiber lasers," Laser Phys. Lett. 6(7), 487–504 (2009).
2. M. Peng, J. Qiu, D. Chen, X. Meng, I. Yang, X. Jiang, and C. Zhu, "Bismuth- and aluminum-codoped germanium oxide glasses for super-broadband optical amplification," Opt. Lett. 29(17), 1998–2000 (2004).
3. I. A. Bufetov, M. A. Melkumov, S. V. Firstov, A. V. Shubin, S. L. Semenov, V. V. Vel'miskin, A. E. Levchenko, E. G. Firstova, and E. M. Dianov, "Optical gain and laser generation in bismuth-doped silica fibers free of other dopants," Opt. Lett. 36(2), 166–168 (2011).
4. A. V. Kir'yanov, V. V. Dvoyrin, V. M. Mashinsky, N. N. Il'ichev, N. S. Korkova, and E. M. Dianov, "Influence of electron irradiation on optical properties of Bismuth doped silica fibers," Opt. Express 19(7), 6599–6608 (2011).
5. V. Dvoyrin, V. Mashinsky, and E. Dianov, "Efficient bismuth-Doped Fiber Lasers," IEEE J. Quantum Electron. 44(9), 834–840 (2008).
6. M. A. Hughes, T. Akada, T. Suzuki, Y. Ohishi, and D. W. Hewak, "Ultrabroad emission from a bismuth doped chalcogenide glass," Opt. Express 17(22), 19345–19355 (2009).
7. S. Zhou, H. Dong, H. Zeng, G. Feng, H. Yang, B. Zhu, and J. Qiu, "Broadband optical amplification in Bi-doped germanium silicate glass," Appl. Phys. Lett. 91(6), 061919 (2007).
8. I. Razdobreev and L. Bigot, "On the multiplicity of Bismuth active centres in germano-aluminosilicate preform," Opt. Mater. 33(6), 973–977 (2011).
9. M. Peng, J. Qiu, D. Chen, X. Meng, and C. Zhu, "Superbroadband 1310 nm emission from bismuth and tantalum codoped germanium oxide glasses," Opt. Lett. 30(18), 2433–2435 (2005).
10. M. Peng, J. Qiu, D. Chen, X. Meng, and C. Zhu, "Broadband infrared luminescence from Li_2O-Al_2O_3-ZnO-SiO_2 glasses doped with Bi_2O_3," Opt. Express 13(18), 6892–6898 (2005).
11. M. Peng and L. Wondraczek, "Bismuth-doped oxide glasses as potential solar spectral converters and concentrators," J. Mater. Chem. 19(5), 627–630 (2009).
12. M. Peng, C. Zollfrank, and L. Wondraczek, "Origin of broad NIR photoluminescence in bismuthate glass and Bi-doped glasses at room temperature," J. Phys. Condens. Matter 21(28), 285106 (2009).

#158398 - $15.00 USD Received 22 Nov 2011; revised 10 Jan 2012; accepted 10 Jan 2012; published 20 Jan 2012

ADVANCED ENGINEERING MATERIALS

COMMUNICATION

DOI: 10.1002/adem.201200039

Graded Cellular Ceramics from Continuous Foam Extrusion**

By *Bruno Ceron-Nicolat, Friedrich Wolff, Andrea Dakkouri-Baldauf, Tobias Fey,* Helmut Münstedt* and *Peter Greil*

Cylindrical SiOC foam filaments with a radial gradient in pore cell size were processed by continuous extrusion foaming of a methyl polysilsesquioxane. Upon leaving the extrusion nozzle foaming was initiated by pressure release which caused precipitation of supersaturated carbon dioxide from the polymer filament. Rapid cooling of the thin filaments generates a radial gradient of melt viscosity which gives rise for formation of closed cell morphology of isotropic pore cells in the core (diameter < 200 μm) and non-isotropic pore cells near the sur-face (shell; <20 μm). After pyrolysis at temperatures ranging from 800 to 1400 °C the stabilized polymer gradient foams were converted into closed cell SiOC ceramic gradient foams. XRD reveals the SiOC residue to be amorphous up to 1200 °C whereas crystallization of ß-SiC was observed at 1400 °C. A superior compressive strength of 9 MPa and a Youngs modulus of 7 GPa at a relative density of 0.18 were measured at an optimum pyrolysis temperature of 1000 °C.

Lightweight ceramic foams of low-fractional density <0.3 offer attractive material properties such as low-thermal conductivity, low-dielectric constant, and non-catastrophic localized fracture behavior compared to bulk materials of same composition.[1,2] Current and emerging fields of application for ceramic foams with open and closed cell microstructures include high-temperature melt and gas filtration,[3] acoustic and thermal insulation,[4,5] sorption and catalysis,[6] chemical energy storage,[7] and biomedical engineering.[8] A variety of processing routes was developed for processing of ceramic foams from solid, liquid, and vapor precursor systems.[9] Foaming and pyrolysis of Si-containing preceramic polymers such as poly-carbosilanes, -silazanes, and -siloxanes was reported to yield ceramic foams with compositions in the system Si–C–N–O.[10] Ceramic foams derived from preceramic polymers are distinguished by a wide range of pore cell sizes which may extend over several orders of magnitude from mm (macro-cellular)[11] down to μm (micro-cellular).[12] Furthermore, depending on the polymer melt rheology and cross-linking behavior cellular structures with mono- or multi-modal pore cell size distribution, uniform or graded distribution of pore cell size, and open- or closed pore cell shape were successfully demonstrated.[13–15]

Preceramic polymer derived ceramic foams were mainly produced by coating of porous template foam (e.g., shape replication or reticulation), sacrifice of a space holder particle, and gas blowing (expansion) methods.[1] Gas blowing refers to a thermodynamic instability which causes release of a gaseous blowing agent from the melt which can be either a dissolved gas such as carbon dioxide (physical blowing) or a volatile product of condensation cross-linking reaction such as alcohol or water (chemical blowing). While the foaming methods described above involved a batch process it may be of interest to produce low-density ceramic foam from preceramic polymer by a continuous extrusion process. Continuous extrusion coupled to simultaneous foaming by precipitation of dissolved carbon dioxide was recently reported to yield low-density (fractional density <0.27) silicone resin foams.[16] It is the aim of this work to characterize the microstructure and mechanical properties of SiOC ceramic foam filaments produced by continuous extrusion foaming and pyrolysis of a methyl polysilsesquioxane melt. Radial pore microstructure gradient of foam filaments pyrolyzed at temperatures

[*] *B. Ceron-Nicolat, Dr. A. Dakkouri-Baldauf, Dr. T. Fey, Prof. P. Greil*
Department of Materials Science – Glass and Ceramics, University of Erlangen-Nuernberg, Martensstrasse 5, D-91058 Erlangen, Germany
E-mail: tobias.fey@ww.uni-erlangen.de
F. Wolff, Prof. Dr. H. Münstedt
Department of Materials Science – Polymer Materials, University of Erlangen-Nuernberg, Martensstrasse 7, D-91058 Erlangen, Germany

[**] *The authors gratefully acknowledge the funding from DFG Cluster of Excellence "Engineering of Advanced Materials" at the University of Erlangen-Nuernberg.*

Fuel 102 (2012) 115–128

Contents lists available at SciVerse ScienceDirect

Fuel

journal homepage: www.elsevier.com/locate/fuel

Heat release process in three-dimensional macro-cellular SiC reactor under Diesel engine-like conditions

J. Cypris [b,1], L. Schlier [a], N. Travitzky [a], P. Greil [a], M. Weclas [b,*]

[a] University of Erlangen–Nuremberg, Department of Materials Science, Martensstr. 5, D-91058 Erlangen, Germany
[b] University of Applied Sciences Nuremberg, Department of Mechanical Engineering, Kesslerplatz 12, D-90489 Nuremberg, Germany

HIGHLIGHTS

- Combustion reactor heat capacity significantly influences the thermodynamics of the process.
- Low- and high-temperature oxidation in a porous reactor is much faster with shorter delay time.
- Combustion temperature and pressure peaks are significantly reduced in porous reactor.
- Qualitative similarity of heat release process under Diesel and in porous reactor conditions.

ARTICLE INFO

Article History:
Received 18 September 2010
Received in revised form 17 May 2012
Accepted 23 May 2012
Available online 6 June 2012

Keywords:
Combustion in porous reactors
Clean flameless combustion under pressure
Diesel injection
Three dimensional printing
Macro-cellular silicon carbide

ABSTRACT

A specially developed macro-cellular SiC non-foam reactor has been used for investigations into Diesel-fuel injection, mixture formation and the heat release process inside a porous structure under piston-engine conditions. The heat release process has been compared to a free Diesel combustion indicating a significant influence of the reactor heat capacity on the thermodynamics of the process. Generally, the low- and high-temperature oxidation processes in a porous reactor are much faster, because of shorter delay time as compared to a free non-premixed combustion. High heat capacity of the porous reactor as compared to the gas heat capacity results in significantly reduced combustion temperature and corresponding combustion pressure peaks. Foam reactors with low and high pore density have also been compared in this investigation. The mixture formation, heat transfer and heat release processes performed in a porous reactor are very complex and depend on a number of different parameters of the combustion reactor in question: reactor structure, its heat capacity, pore size, specific surface area and wall junction geometry. Distribution of characteristic regions plotted in p–T areas indicates qualitative similarity of heat release process as performed under Diesel-like and in porous reactor conditions.

1. Introduction

Fuel injection, mixture preparation, low- and high-temperature oxidation processes (including ignition) play a critical role in the control of an engine combustion process, especially in the case of a self-ignition process, and corresponding exhaust emissions. The low-temperature oxidation is usually treated as a two-stage process: cool and blue flames are followed by high-temperature oxidation. The time between the beginning of fuel injection and the rapid pressure increase corresponding to the high-temperature heat release process is considered as an ignition delay period. During this period a number of complex chemical and physical processes have to be performed. For example chemical reactions (so-called pre-ignition or low-temperature oxidation processes) are performed in order to prepare proper conditions for a thermal ignition (auto ignition) process in dependence on the temperature and pressure conditions. Physics of the process must consider a chain of such processes as the fuel supply process (injection), spray distribution in space, spray atomization, fuel vaporization and mixing with air. These processes are of high complexity especially in the case of Diesel-like engine conditions where the resulting mixture is highly non-homogeneous and time–space dependent. For a future clean engine (required homogeneous combustion) the chemistry of the pre-ignition processes as well as controlled auto ignition are the key factors for process realization under variable engine loads and rates. Further engine development requires the realization of a combustion process fulfilling the following conditions: lowest fuel consumption (minimum CO_2) and nearly-zero exhaust emissions level. Both requirements can only be satisfied by the realization of a homogeneous combustion process. This process is here defined

* Corresponding author. Tel.: +49 9115801898; fax: +49 9115805710.
E-mail address: miroslaw.weclas@ohm-hochschule.de (M. Weclas).
[1] Present address: Fraunhofer Institute for Building Physics, Stuttgart, Germany.

0016-2361/$ - see front matter © 2012 Elsevier Ltd. All rights reserved.
http://dx.doi.org/10.1016/j.fuel.2012.05.038

RESEARCH ARTICLE

ADVANCED BIOMATERIALS

DOI: 10.1002/adem.201180068

Initial Attatchment of rMSC and MG-63 Cells on Patterned Bioglass® Substrates**

By *Rainer Detsch, Olivier Guillon, Lothar Wondraczek* and *Aldo R. Boccaccini**

A soft lithography technique was used to introduce surface patterns on the surface of sintered bioactive glass substrates. Osteoblast-like MG-63 cells and rat mesenchymal stem cells (rMSC) seeded on micropatterned bioactive glass surfaces showed different behavior with rMSC exhibiting a better initial attachment than MG-63 cells. Both cytoskeleton formation and cell spreading of rMSC were supported by the bioactive surfaces. In addition, the structured surfaces seemed to guide MG-63 cells to a larger extent than rMSC. The in vitro results are important considering the continuous development of bone tissue scaffolds based on silicate bioactive glasses.

Tissue engineering aims to restore function to diseased or damaged tissue using combinations of functional cells, bioactive molecules, and biodegradable engineered scaffolds.[1,2] In bone tissue engineering, bioactive ceramics such as hydroxyapatite (HA), calcium phosphates, and bioactive silicate glasses are highly investigated because they are capable of reacting with physiological fluids forming strong bonds to bone tissue.[3] Silicate bioactive glasses, for example, 45S5 Bioglass®,[4] exhibit favorable characteristics for bone engineering applications considering that reactions on the material surface induce the release of critical concentrations of soluble Si, Ca, P, and Na ions, which can lead to upregulation of a family of genes in osteoblasts and thus to favorable intracellular and extracellular responses promoting rapid bone formation.[5–7] In addition, there is in vitro and in vivo evidence showing that bioactive glasses dissolution product can have a positive effect on angiogenesis in tissue engineering constructs.[8,9]

[*] *R. Detsch, Prof. A. R. Boccaccini*
Institute of Biomaterials, University of Erlangen-Nuremberg, 91058 Erlangen, Germany
E-mail: aldo.boccaccini@ww.uni-erlangen.de
O. Guillon
Ceramics Group, Materials Science, Technische Universität Darmstadt, 64287 Darmstadt, Germany
L. Wondraczek
Institute of Ceramics and Glasses, University of Erlangen-Nuremberg, 91058 Erlangen, Germany

[**] *The authors thank Dr. U. Deisinger, Institute of Glass and Ceramics, University of Erlangen-Nuremberg, for roughness measurements. Shuyong Cao and Britta Lilge, TU Darmstadt, are acknowledged for manufacturing patterned films.*

Bioglass® based glass-ceramic scaffolds fabricated by the foam replication method are attracting interest for bone engineering approaches due to their high biocompatibility and bioactivity coupled with adequate mechanical properties.[10,11]

However, the incorporation of specific surface topographic features or patterns when designing the scaffold surface architecture, in order to enhance the attachment and proliferation of cells, has not been investigated in these scaffolds.

Recent advances in sintering, patterning, and three-dimensional printing technologies of bioceramics and bioactive glasses[12–16] offer new opportunities to develop advanced biomaterials and the next generation of implantable devices and tissue scaffolds with desired tissue–implant interaction by incorporating engineered surface patterns. In the class of soft lithography techniques using an elastomer stamp,[17] micromolding in capillaries has proven to be an effective and simple method to pattern ceramic layers.[18,19] Using this technology, fabrication of line arrays with typical width between a few hundreds of nm to several hundreds of micrometers and the development of complex ceramic shapes is possible.[20] In this fabrication method, a drop of slurry or suspension infiltrates the voids left between a patterned mould and a substrate (channels). After drying, removal of the stamp and firing, stable functional patterns are produced.[21] When controlling the adhesion of the sintering layer to the substrate, it is also possible to fabricate free-standing foils.[22] In addition, by using larger amounts of slurry, ceramic layers or bodies with a structured surface at the micrometric scale can be obtained.[23] The method has been already applied to fabricate silica patterns on 3mol% Y_2O_3–ZrO_2 dense substrate for dental implants.[15] Combining sol–gel and soft lithography allowed the fabrication of micropillared silica surfaces with pillar

1166 OPTICS LETTERS / Vol. 37, No. 7 / April 1, 2012

Temperature dependence and quantum efficiency of ultrabroad NIR photoluminescence from Ni^{2+} centers in nanocrystalline Ba-Al titanate glass ceramics

Guojun Gao,[1] Mingying Peng,[2] and Lothar Wondraczek[1,*]

[1]Department of Materials Science, University of Erlangen-Nuremberg, Erlangen 91058, Germany

[2]Institute of Optical Communication Materials & State Key Laboratory of Luminescent Materials and Devices, South China University of Technology, Guangzhou 510641, China

*Corresponding author: lothar.wondraczek@ww.uni-erlangen.de

Received January 19, 2012; revised January 25, 2012; accepted January 25, 2012; posted January 27, 2012 (Doc. ID 161633); published March 23, 2012

Ultrabroad near-infrared (NIR) photoluminescence from Ni^{2+}-centers in nanocrystalline Ba-Al titanate glass ceramics was studied by temperature-dependent static and dynamic photoluminescence spectroscopy in the regime of 10 to 300 K. Photoluminescence covers the spectral range of about 1100 nm to >1600 nm with a typical bandwidth (FWHM) greater than 300 nm. For UV-LED excitation at 352 nm, an internal quantum efficiency of 65 % is obtained. The excited state lifetime τ at room temperature is 39 μs. The stimulated emission cross section σ_{em} is 8.5×10^{-20} cm², resulting in a practical figure of merit, $\sigma_{em} \cdot \tau$, of 3.3×10^{-24} cm² s at room temperature. These properties suggest suitability as a broadband gain medium for tunable lasers and optical amplifiers. © 2012 Optical Society of America

OCIS codes: 160.2540, 160.2750, 160.4670, 160.6990, 300.6280.

3d transition metal ions such as Ni^{2+}, Co^{2+}, and Cr^{4+} doped into inorganic matrices have been a subject of interest for many years due to their broadband near-infrared (NIR) photoluminescence (PL). In such materials, NIR PL arises from d-d transitions and is hence strongly dependent on ligand field and coordination [1–5]. While various efforts have been undertaken to make use of this property in next-generation broadband optical amplifiers for telecommunication and other applications, especially with Co^{2+} and Cr^{4+}, any breakthrough has so far been prevented by difficulties in stabilizing the specific valence and coordination state in a suitable matrix material [1,2]. From a practical point of view, Ni^{2+} species seem the most promising choice to approach this problem. In an inorganic matrix, they may be present in three different coordination states, tetrahedral (fourfold, $^{IV}Ni^{2+}$), trigonal (fivefold, $^{V}Ni^{2+}$) and octahedral (sixfold, $^{VI}Ni^{2+}$). Only $^{VI}Ni^{2+}$ has been known to provide efficient NIR emission [3–5]. Consequently, $^{VI}Ni^{2+}$-containing glass ceramics and single crystalline materials have drawn continuous attention over the last decade [3–5]. Of these two materials classes, glass ceramics, produced by controlled nucleation and crystallization of a suitable precursor glass, combine the advantages of glasses and crystalline materials: depending on viscosity and crystallization temperature of the precursor glass, they can be processed into optical fiber, and depending on the type of precipitated crystal species, high quantum efficiency (QE) can be obtained [6–8]. As a prerequisite, however, crystal precipitation must occur in sufficiently high number density to ensure very low crystallite size and, hence, high optical transparency. In this setting, the number of available matrix candidates has been limited to only a few systems, which typically rely on rare raw materials or exhibit major process limitations (such as high liquidus temperature and high dynamic fragility).

Recently, we reported on glasses of the type $30TiO_2$-$30BaO$-$30SiO_2$-$10Al_2O_3$ (TBSA, mol%) as a new matrix candidate [9]. In this system, nanocrystalline hollandite-type ($BaAl_2Ti_6O_{16}$, secondary $BaTiO_3$) Ba-Al titanates can be precipitated at high number density and crystal sizes of ~30 nm ± 10 nm. Upon crystallization, added Ni^{2+} species undergo a coordination change from fivefold to sixfold due to incorporation into the crystalline environment. This was demonstrated to result in an intense NIR PL emission band spanning the spectral range of 1.0 to 1.6 μm with a full width at half maximum (FWHM) of ~350 nm. Interestingly, it was shown that NIR PL can be induced with conventional near-UV (NUV) LEDs or other light sources and does not require laser excitation. In the present letter, we report on quantitative efficiency of photoemission from this material as a prerequisite for application as a gain medium in optical amplifiers. QE is obtained on the basis of low temperature static and dynamic PL spectroscopy, and stimulated emission cross section (σ_{em}) and figure of merit ($\sigma_{em}\tau$) are calculated.

A slab of ~50 g of TBSA precursor glass with a dopant concentration of 0.1 mol% (expressed as NiO) was prepared by conventional melting and quenching [9]. Melting was performed at 1550 °C for 2 hrs in alumina crucibles under ambient atmosphere. The melt was then poured into a preheated graphite mould and annealed for 2 h at 500 °C. Specimen of $15 \times 15 \times 2$ mm³ were cut from the obtained glass and polished to optical quality for spectroscopic analyses. Optimal conditions for transferring the precursor glass into a transparent nanocrystalline glass ceramic were found for annealing at 850 °C for 2 h (ambient atmosphere) [9].

Temperature-dependent analyses (10 to 300 K) were performed in a closed-cycle liquid helium cryostat. Static excitation and emission spectra were recorded through optical windows with a high-resolution spectrofluorometer (Edinburgh Instruments FLSP 920) equipped with a 450 W steady-state xenon lamp and a pulsed 60 W Xe flashlamp as excitation sources. Decay curves were obtained by time-correlated single photon counting (TCSPC). A nitrogen-cooled NIR photomultiplier tube

0146-9592/12/071166-03$15.00/0

View Article Online / Journal Homepage / Table of Contents for this issue
Dynamic Article Links

Journal of Materials Chemistry

Cite this: J. Mater. Chem., 2012, 22, 2582

www.rsc.org/materials

PAPER

Broadband NIR photoluminescence from Ni^{2+}-doped nanocrystalline Ba–Al titanate glass ceramics

Guojun Gao,[a] Sindy Reibstein,[a] Erdmann Spiecker,[b] Mingying Peng[c] and Lothar Wondraczek[*a]

Received 31st August 2011, Accepted 21st November 2011
DOI: 10.1039/c1jm14292e

Nanocrystalline Ba–Al titanate precipitates from supercooled TiO_2–BaO–SiO_2–Al_2O_3 melts by catalyzed volume nucleation in the presence of Ni^{2+}, forming a $BaAl_2Ti_6O_{16}$ hollandite-type lattice. Ni^{2+}-species are incorporated into the crystalline environment in octahedral coordination. Hollandite formation is accompanied by precipitation of tetrahedrally distorted $BaTiO_3$ as a secondary crystal phase, where crystal species and habitus can be clearly distinguished by dark-field transmission electron microscopy. Resulting photoluminescence due to spin-allowed relaxation of $^3T_{2g}(^3F)$ to $^3A_{2g}(^3F)$ in $^{VI}Ni^{2+}$ occurs from three distinct emission centers. It spans the spectral range of 1.0 to 1.6 μm and exhibits a lifetime of about 60 μs, which suggests applications in tunable lasers and broadband optical amplifiers. Besides red and IR laser excitation, NIR photoemission can be excited with conventional near UV light sources, *i.e.* in the spectral range of 350–420 nm. Decay kinetics as well as position and shape of the emission band can be adjusted by dopant concentration and synthesis conditions.

Introduction

Due to broad photoemission bands in the near infrared (NIR), 3d transition metal ions such as Ni^{2+}, Co^{2+} and Cr^{4+} are receiving significant and continuous attention for potential applications in tunable lasers and optical amplifiers.[1–6] However, the 3d electronic configuration is typically very sensitive to the ligand situation within the employed host material. That is, in oxide matrices, NIR luminescence is typically observed only when a specific coordination is provided, *e.g.* tetrahedral for Cr^{4+} and Co^{2+}, and octahedral for Ni^{2+}.[1–11] For Co^{2+}, reported NIR emission intensity is mostly very low which, at present, appears to rule out any concrete application.[12] Chromium ions usually partition in mixed valence, Cr^{3+}, Cr^{4+} and Cr^{6+}, but Cr^{3+} and Cr^{6+} can quench NIR luminescence from $^{IV}Cr^{4+}$. There is no practical way for avoiding the presence of Cr^{3+} and Cr^{6+} in most host candidates. In contrast, nickel ions which, in oxide hosts, typically reside solely as Ni^{2+} provide an interesting alternative. Consequently, the spectroscopic properties of Ni^{2+} doped glasses, glass ceramics and single crystals have attracted much attention over the last decade.[1–11,13–15] As mentioned before, the coordination state in which Ni^{2+} is incorporated into the host lattice is one of the key factors for achieving specific spectroscopic properties. The most frequently observed environments of Ni^{2+} in solid matrices are tetrahedral (fourfold coordination, $^{IV}Ni^{2+}$), trigonal bipyramidal (fivefold, $^{V}Ni^{2+}$) and octahedral (sixfold, $^{VI}Ni^{2+}$), respectively. In most oxide glasses, Ni^{2+} favors fivefold coordinated sites. For such $^{V}Ni^{2+}$ species, no or very weak NIR luminescence can be observed due to predominance of non-radiative relaxation. Significant radiative relaxation at room temperature and, hence, high NIR quantum efficiency are known only for $^{VI}Ni^{2+}$, *e.g.* in single-crystalline $LiGa_5O_8$: Ni^{2+}.[8] Major limitations of single-crystalline materials lie, however, in the complexity of their fabrication processes which may lead to low degrees of freedom in composition (dopant and co-dopant concentrations) as well as specimen shape (fiber, large-scale). In principle, this drawback can be overcome by fabricating a glass ceramic material, where a crystalline species is precipitated from a supercooled melt by controlled nucleation and crystallization.[16–19] In this way, conventional glass processing techniques (*e.g.*, melt casting, fiber drawing, extrusion, *etc.*) can be employed to obtain at least some of the properties of a crystalline host material. As a prerequisite, however, Ni^{2+} species must actually precipitate into the crystalline phase rather than remain in the residual glass phase.[8] Secondly, crystal growth must be limited to not more than several tens of nanometres in order to ensure optical transparency while, at the same time, a high crystallite volume fraction (crystallite number density) must be achieved. With these objectives, *e.g.*, NIR-luminescent nanocrystalline $LiGa_5O_8$: Ni^{2+} glass ceramics were prepared from Li_2O–Ga_2O_3–SiO_2 glasses by Suzuki *et al.*,[8] and β-Ga_2O_3 : Ni^{2+} glass ceramics from Na_2O–Al_2O_3–Ga_2O_3–SiO_2 glasses by Zhou *et al.*[10,20] In both materials, Ni^{2+} coordinates on octahedral sites, but besides

[a]*Institute of Glass and Ceramics, Department of Materials Science, University of Erlangen-Nuremberg, Martensstrasse 5, Erlangen, D-91058, Germany. E-mail: lothar.wondraczek@ww.uni-erlangen.de; Fax: +49 (0)9131 28311; Tel: +49 (0)9131 85 27553*
[b]*Center for Nanoanalysis and Electron Microscopy (CENEM), Department of Materials Science, University of Erlangen-Nuremberg, 91058, Germany*
[c]*Institute of Optical Communication Materials & State Key Laboratory of Luminescent Materials and Devices, South China University of Technology, Guangzhou, 510641, China*

J. Non-Equilib. Thermodyn. 37 (2012), 143–177
DOI 10.1515/jnetdy-2011-0035

Non-equilibrium configurational Prigogine–Defay ratio

Jean-Luc Garden, Hervé Guillou, Jacques Richard and Lothar Wondraczek

Communicated by Alexander Lion

Keywords. Prigogine–Defay ratio, non-equilibrium thermodynamics, affinity, glass transition.

Abstract

Classically, the Prigogine–Defay (PD) ratio involves differences in isobaric heat capacity, isothermal compressibility, and isobaric thermal expansion coefficient between a super-cooled liquid and the corresponding glass at the glass transition. However, determining such differences by extrapolation of coefficients that have been measured for super-cooled liquid and glassy state, respectively, poses the problem that it does not exactly take into account the non-equilibrium character of the glass transition. In this paper, we assess this question by taking into account the time dependence of configurational contributions to the three thermodynamic coefficients in the glass transition range upon varying temperature and/or pressure. Macroscopic non-equilibrium thermodynamics is applied to obtain a generalised form of the PD ratio. The classical PD ratio can then be taken as a particular case of this generalisation. Under some assumptions, the configurational PD ratio (CPD ratio) can be expressed in terms of fictive temperature and fictive pressure which, hence, provides another possibility to experimentally verify this formalism.

1 Introduction

Upon vitrification, some of the thermodynamic properties of a glass former undergo a pronounced change which can be measured experimentally. Classically, the Prigogine–Defay (PD) ratio is defined as the ratio of the

THE JOURNAL OF CHEMICAL PHYSICS 137, 024505 (2012)

Affinity and its derivatives in the glass transition process

J.-L. Garden,[1,a)] H. Guillou,[2,b)] J. Richard,[1] and L. Wondraczek[3]
[1]*Institut Néel, CNRS et UJF, 25 Avenue des Martyrs, 38042 Grenoble Cedex 09, France*
[2]*LIMMS/CNRS-IIS, Institute of Industrial Sciences, University of Tokyo, 4-6-1 Komaba, Meguro-ku, Tokyo 153-8505, Japan*
[3]*Departement of Materials Science, Chair of Glass and Ceramics, University of Erlangen-Nuernberg, 91058 Erlangen, Germany*

(Received 30 March 2012; accepted 19 June 2012; published online 12 July 2012)

The thermodynamic treatment of the glass transition remains an issue of intense debate. When associated with the formalism of non-equilibrium thermodynamics, the lattice-hole theory of liquids can provide new insight in this direction, as has been shown by Schmelzer and Gutzow [J. Chem. Phys. **125**, 184511 (2006)], by Möller *et al.* [J. Chem. Phys. **125**, 094505 (2006)], and more recently by Tropin *et al.* [J. Non-Cryst. Solids **357**, 1291 (2011); **357**, 1303 (2011)]. Here, we employ a similar approach. We include pressure as an additional variable, in order to account for the freezing-in of structural degrees of freedom upon pressure increase. Second, we demonstrate that important terms concerning first order derivatives of the affinity-driving-force with respect to temperature and pressure have been previously neglected. We show that these are of crucial importance in the approach. Macroscopic non-equilibrium thermodynamics is used to enlighten these contributions in the derivation of C_p, κ_T, and α_p. The coefficients are calculated as a function of pressure and temperature following different theoretical protocols, revealing classical aspects of vitrification and structural recovery processes. Finally, we demonstrate that a simple minimalist model such as the lattice-hole theory of liquids, when being associated with rigorous use of macroscopic non-equilibrium thermodynamics, is able to account for the primary features of the glass transition phenomenology. Notwithstanding its simplicity and its limits, this approach can be used as a very pedagogical tool to provide a physical understanding on the underlying thermodynamics which governs the glass transition process. © *2012 American Institute of Physics*. [http://dx.doi.org/10.1063/1.4733333]

I. INTRODUCTION

There are numerous approaches dealing with the glass transition process. Some are based on microscopic models, while others are mostly driven by macroscopic and phenomenological view-points. One of this approaches, is the thermodynamic of irreversible processes, or non-equilibrium thermodynamics. Within this latter approach, the notion of one or more structural order parameters is used to characterize the glassy state. Such structural order parameters ξ_i, have to be taken into account in addition to classical thermodynamic variables in order to describe the non-equilibrium aspect of the glass transition. The affinity A is the conjugated variable associated to the order parameter. It plays a fundamental role since it defines the driving force of the non-equilibrium process. The formalism of classical non-equilibrium thermodynamics has been developed by De Donder in a self-consistent manner.[1] The first attempts to apply this theory to glass science have been made by Prigogine and Defay,[2] and Davies and Jones.[3]

Non-equilibrium thermodynamics has been used all along the last century by different groups of researchers, and has seen renewed interest in the last few years.[4–15] As an example, Bouchbinder and Langer used the generalized non-equilibrium thermodynamics based on internal variables to investigate one of the most striking aspect of the glass transition, i.e., the Kovacs effect.[16] They provided fits of the numerical simulation curves obtained by Mossa and Sciortino on the Kovacs effect.[17] Among these recent works, Gutzow, Schmelzer, and co-workers have brought new aspects to the field.[18–24] Using the so-called lattice-hole theory of liquids, and an evolution equation for the order parameter as a function of temperature, they investigated the process of vitrification and structural recovery following defined temperature protocols.[18,19,23,24] Among other points, a new expression for the Prigogine-Defay ratio and a thermodynamic definition of the fictive temperature was provided.[18,24]

In this paper, we elaborate the same approach towards a more complete and rigorous treatment of the glass transition. First, we include pressure as an additional variable into the expression of the relaxation time to account for vitrification by pressure perturbation in analogy to temperature changes. Second, we demonstrate that the total derivatives of the affinity with respect to pressure and temperature are of crucial importance for the consistency of the approach. We show that to neglect them leads to incoherences such as discussed later.

The paper is organized as follows: In the Sec. II, the lattice-hole theory of liquids is recalled. The configurational Gibbs free energy is written as a function of pressure p, temperature T, order parameter ξ, and phenomenological parameters. Next, we illustrate how to extract the values of the phe-

a)Electronic mail: jean-luc.garden@grenoble.cnrs.fr.
b)Permanent address: Institut Néel, CNRS et UJF, 25 Avenue des Martyrs, 38042 Grenoble Cedex 09, France.

Int. J. Appl. Ceram. Technol., 9 [2] 329–340 (2012)
DOI:10.1111/j.1744-7402.2011.02664.x

International Journal of
Applied Ceramic TECHNOLOGY
Ceramic Product Development and Commercialization

Tape Casting of Al_2O_3, MgO, and $MgAl_2O_4$ for the Manufacture of Multilayer Composites for Refractory Applications

Ingo Götschel*

Department of Material Science and Engineering, Institute of Glass and Ceramics, University of Erlangen-Nuremberg, 91058 Erlangen, Germany

Yusuke Hayashi and Ken-ichi Kakimoto

Electroceramics Laboratory, Department of Materials Science and Engineering, Nagoya Institute of Technology, 466-8555 Nagoya, Japan

Andreas Roosen

Department of Material Science and Engineering, Institute of Glass and Ceramics, University of Erlangen-Nuremberg, 91058 Erlangen, Germany

The ceramic multilayer technique, which is based on tape-cast green sheets, has the potential to generate advanced composite materials. In this work, high-purity refractory oxides like α-alumina, magnesia, and magnesium aluminate spinel were used for tape casting and multilayer processing. Highly porous Al_2O_3 and $MgAl_2O_4$ tapes were obtained with 16–36% open porosity and pore sizes < 10 μm. Subsequently, increasing the grain sizes up to 1 mm led to multimodal slurries that yielded casting tapes of 3–5 mm thickness. Multilayer composites of different combination were prepared from these tapes by lamination and cofiring.

Introduction

Standard refractory products for steel casting and secondary industry are preshaped bricks, castables, and

*ingo.goetschel@ww.uni-erlangen.de

PAPERS

Corrosion Resistance of Dense and Porous Tape-cast Oxide Refractories against $CaO-Fe_2O_3-SiO_2$ Slag

I. Götschel, A. Roosen

Tape casting and lamination is the common technique to produce large volumes of advanced functional multilayer ceramics for industrial applications. Transferring this well-known process to refractories can lead to novel concepts combining improved materials properties like thermal shock and corrosion resistance. In this study the corrosion behaviour of sintered Al_2O_3, MgO, and $MgAl_2O_4$ carbon-free oxide refractory tapes to basic $CaO-Fe_2O_3-SiO_2$ (CFS) slag with additional MnO, P_2O_5 and MgO content was investigated by static sessile drop tests at 1390 °C in air. Penetration of the refractory by the slag, refractory dissolution and phase generation were investigated by SEM, EDS analysis and optical microscopy. The results pointed out that lower penetration of the slag can be attained by reducing open porosity to values below 15 % and pore sizes smaller than 20 µm, whereas chemical corrosion resistance is a consequence of the solubility of the used refractory oxides and its saturation in the liquid slag. This work investigates the main corrosion mechanism of tape-cast refractory microstructures as a basis for further development of multilayer refractories.

1 Introduction

Corrosion resistance is one of the main features, which refractory products must exhibit in industrial high temperature applications. In addition, the refractories must withstand high mechanical stresses caused by thermal shock and erosion. For steelmaking, rising steel qualities are making high demands on the corrosion behaviour of the used refractories at elevated temperatures and under severe conditions using corrosive additives like fluxes. The "clean-steel-technology" requires refractory products with low or zero carbon content, which means the traditionally used carbon bonded refractories have to be substituted without loosing durability and life-time, e.g., by the use of high purity alumina or spinel castables [1, 2]. High corrosion resistance combined with sufficient thermal shock resistance is also claimed for reliable functional components such as nozzles or slide gates. Therefore, new refractory concepts have to be developed to comply with these high demands in the future. The well-known multilayer technology has the great potential to create novel layered refractories combining corrosion and thermal shock resistance by the use of functional layers. Basic products for this technology are tape-cast ceramic green sheets. In industry, tape casting is the standard process for the manufacture of ceramic substrates and multilayer devices, e.g., capacitors, inductors, high integrated circuits and actuators [3]. Previous work was addressed to tape-cast carbon-free refractory oxide tapes of MgO, Al_2O_3 and $MgAl_2O_4$ of different microstructure for multilayer application by the use of sinter active powders and coarse fillers up to 1 mm [4]. The main focus of this study is to evaluate the basic corrosion mechanisms of these new refractory tapes. Refractory corrosion is often very complex and can be caused by different mechanisms like, e.g., penetration of the porous matrix, direct and indirect dissolution of the refractory components with or without precipitation of new phases or by oxido-reduction reactions [5, 6]. For the present laboratory investigation of the basic corrosion mechanisms of tape-cast microstructures a static corrosion test with a typical steel work slag was chosen, knowingly that the results can not be directly transferred to real applications because of the early saturation of the small amount of slag used and its change in composition.

2 Experimental Procedure

2.1 Evaluated compositions and preparation of the tapes

Ceramic green tapes of Al_2O_3, MgO and $MgAl_2O_4$ as well as two phase mixtures of them were prepared via tape casting of organic solvent based slurries containing fine ceramic powders and coarse aggregates with particle sizes up to 1 mm. The processing of the multimodal tape casting slurries was recently reported in more detail [4]. Four compositions exclusively composed of fine

Ingo Götschel, Andreas Roosen
University of Erlangen-Nuremberg
Department of Material Science, Glass and Ceramics
91058 Erlangen
Germany

Corresponding-Author: *Ingo Götschel*
E-mail:
ingo.goetschel@ww.uni-erlangen.de

Keywords: tape casting, refractory oxides, multilayer composites, slag corrosion

Received: 06.10.2011
Accepted: 24.10.2011

journal

J. Am. Ceram. Soc., 95 [1] 95–101 (2012)
DOI: 10.1111/j.1551-2916.2011.04844.x

Vibration Assisted Self-Assembly Processing of Ceramic-Based Composites with Modular Meta-Structure

Michael Götz, Tobias Fey,† and Peter Greil

Department of Materials Science (Glass and Ceramics), University of Erlangen-Nuremberg, D-91058, Erlangen, Germany

Modular structures of space-filling building blocks having dimension orders of magnitude larger (≈1000 μm) than the particle size (0.1–10 μm) may offer a high potential for near net shape manufacturing as well as toughening of brittle ceramic materials. We demonstrate vibration assisted periodic pattern formation of alumina cubes with an edge lengths of 1.3 mm. Two-dimensional and three-dimensional modular assembly structures of different unit cell symmetry were prepared. Unlike colloidal crystallization which suffers from a high degree of packing defects, vibration assisted gravitational assembly of space-filling building blocks offers a high potential for achieving periodic assembly structures with quasi-crystalline order, high packing densities and low defect content.

I. Introduction

CERAMICS with a three-dimensional (3-D) modular structure such as porous lattices or photonic crystals have found increasing interest in a variety of application fields including sensors, catalytic substrates, and tissue engineering scaffolds,[1] as well as for photonic and electromagnetic wave guides, circuits, filters, cavities, laser, antenna, and absorbers.[2] While the properties of an individual periodic element (thereafter called building block) are dominated by its microstructure (porosity, grain size, phase content, etc.), the behavior of the bulk material will strongly be influenced by the 3-D arrangement of the periodic elements (thereafter denoted meta-structure). Ceramic materials with a periodic meta-structure might offer exciting mechanical and other physical properties for engineering applications. For example, ceramics and ceramic-based composites with auxetic periodic meta-structures offer superior sound and shock absorption and thermal shock resistance,[3] or enhanced piezoelectric activity and sensitivity.[4] Interpenetrating phase composites (IPCs) in which a ceramic and a metal phase both exceed percolation threshold volume fractions and are topologically interconnected throughout the microstructure can combine a superior toughness with excellent creep resistance and high electrical as well as thermal conductivity.[5] The combination of a textured majority phase of reinforcing material with a minority (1–5 vol%) of soft, energy-dissipating, and crack-deflecting organic component is a common principle among mechanically robust materials such as mollusc shells, bones, teeth, and sponge spicules.[6–8] Nacre may serve as an example for natural nano-composite with its high toughness and a hierarchical brick mortar structure consisting of lamellar $CaCO_3$ aragonite layers (diameter 5–10 μm, thickness <250 nm) with a thin polymeric protein layer (<10 nm).[7,9] A tremendous improvement of toughness by mimicking the hierarchical microstructure of nacre could be demonstrated in various systems such as alumina/PMMA,[10] alumina/chitosan,[11] titania/PE,[12] hydroxyapatite/epoxy, and alumina/Al–Si.[13]

From a fundamental point of view the meta-structure level imposes scale- and geometry-dependent constraints on the electromagnetic wave interaction, which has become of particular interest for the development of novel photonic, magnetic and electromagnetic (EBG) band gap materials.[14] The EBG structures can be used to control and tailor optical processes such as emission and detection of electro-magnetic radiation and have tremendously gained in interest for EBG-based THz components, including sources, detectors, filters, waveguides, and artificial dielectrics.[15] The multiple-scattering nature of EBG-physics requires that the EBG structure for the frequency range of interest (100 GHz–10 THz) also requires that a corresponding wavelength range is 3 mm–30 μm. Thus, to produce useful bandgap structures in this wavelength range, there is a need for a novel fabrication technique that can provide feature sizes in the range 1 mm–10 μm.

Over the past decade, several reliable processing methods were developed to fabricate micron-scale materials and components from ceramic forming approaches as described in several excellent reviews.[16–19] Three-dimensional periodic microstructures with sub-millimeter feature size were fabricated by solid freeform fabrication techniques including fused deposition, printing, writing, casting, and stereolithographic techniques.[20,21] Pressing (e.g. tablet pressing), casting, and low pressure molding (extrusion) may be applied for shaping of micro-components with sizes exceeding 100 μm. Micro-components of smaller dimensions down to 10 μm can be processed by means of micro/nano-fabrication techniques including micro-molding, micro-embossing, LIGA, and lithography.[22–24] Periodic microstructures with submicron feature sizes are accessible by applying physical and chemical self-assembly principles as being used in colloid crystallization or biotemplating.[25,26] While self-assembly on the colloidal and molecular scales is dominated by specific molecular interaction, electrostatic, and van der Waals forces,[27] self-assembly on the level of discrete particles with features sizes exceeding 1–10 μm can readily be achieved by gravitation and external mechanical forces. Thus, dense packing structures (*fcc*) were achieved by slow sedimentation of colloidal particles in the so-called colloidal epitaxy process.[25] Applying one-dimensional vibration in the vertical direction was reported to induce particle rearrangement resulting in an increase of the packing density of a powder filled in a die from 0.6 (random close packing, *rcp*) to 0.64.[28,29] Even higher packing densities of 0.68 were achieved with two- and 3-D vibration which induced local crystallization of dense packing configuration *fcc* and *hcp*.[30,31]

The simplest way to completely fill a volume (e.g., packing factor → 1) is to use a space-filling polyhedron which has regular faces and congruent vertices. A space-filling polyhedron can be used to fill a volume without any overlap or

W.-C. Wei—contributing editor

Manuscript No. 29725. Received May 12, 2011; approved August 08, 2011.
Financial support from DFG Reinhart-Koselleck project (GR 961/32) is gratefully acknowledged.
†Author to whom correspondence should be addressed. e-mail: tobias.fey@ww.uni-erlangen.de

Journal of the Korean Ceramic Society
Vol. 49, No. 4, pp. 279~286, 2012.

http://dx.doi.org/10.4191/kcers.2012.49.4.279

Advancements in Polymer-Filler Derived Ceramics

Peter Greil†

University of Erlangen-Nuernberg, Department of Materials Science (Glass and Ceramics), Martensstr.5, D-91058 Erlangen, Germany

(Received May 22, 2012; Accepted June 21, 2012)

ABSTRACT

Microstructure tailoring of filler loaded preceramic polymer systems offers a high potential for property improvement of Si-based ceramics and composites. Advancements in manufacturing of bulk materials by controlling microstructure evolution during thermal induced polymer-ceramic transforma-tion and polymer-filler reactions will be presented. Rate controlled pyrolysis, multilayer gradient laminate design and surface modification by gas solid reaction are demonstrated to yield ceramic components of high fractional density and superior mechanical properties. Emerging fields of applications are presented.

Key words : Polymer-filler derived ceramics, Rate controlled pyrolysis, Surface modification

1. Introduction

Tailoring of composition and molecular structure combined with excellent plastic shaping technologies offers a great potential for development of advanced materials from organo-silicon based polymer precursor systems.[1] Polymer derived ceramics with compositions in the system Si-C-N-O (-M) with M = B, Al, Ti, Zr, etc. offer excellent thermal stability[2] as well as interesting electrical, piezoelectrical, magnetical, optical and chemical properties.[1] While up to temperatures of approximately 1200°C an amorphous structure of Si atoms bonded tetrahedrally to C, N, or O and containing nanoscale domains of carbon (graphene like turbostratic carbon) dominates, major crystal-line phases at higher temperatures are SiC, Si_3N_4, Si_2N_2O, SiO_2 and graphitic carbon or Si, Fig. 1.

Maximum values for Young´s modulus of 155 GPa, Vickers hardness of 26 GPa, fracture toughness of 3 $MPam^{1/2}$, and fracture strength of 1100 MPa can be found in literature.[3] A superior creep resistance at temperatures even exceeding 1500°C[4] was attributed to the evolution of a nanodomain network of graphene which was hypothesized to support stress even at very high temperatures.[5] These property values, however, often were measured on specimens of very small volume (a few mm^3) or low dimensionality (fibers, coatings) applying nano-techniques. Current applications are therefore mainly limited on low dimensional product shape such as high temperature resistant fibers,[6,7] coatings,[8] joints and seals,[9] micro- and macro-cellular foams,[10] sensor sheets[11] and micro electro-mechanical systems (MEMS).[12]

†Corresponding author : Peter Greil
E-mail : greil@ww.uni-erlangen.de
Tel : +49-9131-85-27543 Fax : +49-9131-85-28311

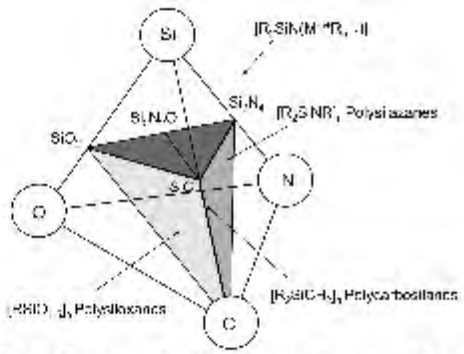

Fig. 1. Composition tetrahedra of major preceramic polymer derived Si-based ceramics (R = H, C_nH_{2n+1}, C_6H_5, CH_2=CH).

2. Polymer-Filler Reaction Pyrolysis

Enhancement of mechanical properties in bulk components of larger volume mainly faces two problems: i. control of the nano- and microstructure formation process under the constraints of limited transport of gaseous decomposition products and ii. retardation of strain relaxation upon polymer-to-ceramic conversion (e.g. visous to brittle elastic behaviour transition). Since polymer-to-ceramic conversion involves a pronounced increase in density by a factor of 2 – 3 and a volumetric shrinkage which may exceed 50 %, porosity and crack formation are difficult to avoid in bulk polymer derived ceramic products.[13] Reduction of residual porosity was achieved by application of stress-assisted consolidation techniques including pressure casting,[3] warm-pressing,[14] field assisted hot-pressing,[15] and hot-isostatic pressing.[16]

Journal of Advanced Ceramics
2012, 1(4): 249-267
DOI: 10.1007/s40145-012-0020-2 ISSN 2226-4108
Review

Generic principles of crack-healing ceramics

Peter GREIL*

Department of Materials Science (Glass and Ceramics), University of Erlangen-Nuernberg, Martensstr. 5, Erlangen 91058, Germany

Received: September 21, 2012; Revised: October 19, 2012; Accepted: October 20, 2012

Abstract: Ceramic materials able to heal manufacture or damage induced microstructure defects might trigger a change in paradigm for design and application of load bearing ceramics. This work reviews thermodynamic and kinetic aspects governing the regeneration of solid contact able to transfer stress between disrupted crack surfaces in ceramics. Major crack healing processes include perturbation of crack-like pores followed by sintering of isolated pores, as well as reaction with an environmental atmosphere and filling of the crack space with an oxidation product. Since thermally activated solid state reactions require elevated temperatures which may exceed 1000 ℃, processes able to trigger crack healing at lower temperatures are of particular interest for transferring into engineering applications. Generic principles of microstructure modifications able to facilitate crack repair at lower temperatures will be considered: (i) acceleration of material transport by grain boundary decoration and grain size reduction, and (ii) reduction of thermal activation barrier by repair filler activation. Examples demonstrating crack healing capability include oxidation reaction of low energy bonded intercalation metal from nano-laminate MAX phases and catalyzed surface nitridation of polymer derived ceramics containing repair fillers.

Key words: crack healing; microstructure modifications; oxidation healing; MAX phases; preceramic polymers

1 Introduction

Ceramic materials able to repair flaws and cracks and recover initial properties constitute a vital field of materials science that gained in significance recently [1-5]. Advanced engineering as well as functional (electrical, magnetic, chemical, nuclear, biomedical) ceramics are susceptible to damage cracks, which may form on the surface as well as deeply in the bulk caused by machining, overloading, creep, fatigue, or friction (Fig. 1). Many ceramic components are stressed mechanically or thermally with high cycle numbers (>10^6 to 10^9 per lifetime) — for instance piezoelectric-actors, components in piston engines and gas turbines including their temperature and corrosion protection systems, diesel particle filter systems, mounting and friction systems, also medical joint implants. Regardless of the application, once cracks have formed within ceramic materials, the integrity of the structure is significantly compromised. While

* Corresponding author.
E-mail: peter.greil@ww.uni-erlangen.de

Applied Surface Science 258 (2012) 2894–2900

Contents lists available at SciVerse ScienceDirect

Applied Surface Science

journal homepage: www.elsevier.com/locate/apsusc

The impact of substrate properties and thermal annealing on tantalum nitride thin films

M. Grosser[a,*], M. Münch[a], H. Seidel[a], C. Bienert[b], A. Roosen[b], U. Schmid[c]

[a] Chair of Micromechanics, Microfluidics/Microactuators, Saarland University, 66123 Saarbruecken, Germany
[b] Friedrich-Alexander-University Erlangen-Nuremberg, Martensstr. 5, D-91058 Erlangen, Germany
[c] Department for Microsystems Technology, Institute of Sensor and Actuator Systems, Vienna University of Technology, Floragasse 7, 1040 Vienna, Austria

ARTICLE INFO

Article history:
Received 31 January 2011
Received in revised form 31 October 2011
Accepted 1 November 2011
Available online 10 November 2011

Keywords:
Tantalum nitride
Thin films magnetron sputtering
Microstructure
Thermal annealing
LTCC
SiO_2
Resistivity

ABSTRACT

In this study film properties of sputter-deposited tantalum nitride (TaN_x) thin layers are investigated focusing on the impact of substrate properties, varying nitrogen content for film synthetization as well as post-deposition annealings in the temperature range up to 500 °C. For comparison, these investigations are done on low temperature co-fired ceramics and on silicon based substrates whereas the latter approach ensures defined and well-known surface properties. Furthermore, results on the phase evolution with high temperature annealings are presented showing a transformation of Ta_4N to Ta_2N in the temperature range between 350 °C and 500 °C. With increasing nitrogen content (i.e. nitrogen flow during film deposition) in the TaN_x layers the topography shows first an increase in surface roughness, next a range where a smoothing of the surface characteristics is observed, and finally buckling and the existence of grain agglomerates. All these analyses are further evaluated with electrical measurements on the film resistivity and on the oxidation behaviour to gain deeper insight into material parameters relevant for micromachined devices which are operated under harsh environmental conditions.

1. Introduction

Tantalum (Ta) and tantalum nitride-based thin films are known for their excellent properties in a wide range of applications, such as diffusion barriers for metallization systems made of copper in microelectronic devices [1], as high k dielectric in the form of Ta_2O_5 [2] or as top passivation layer for micromachined sensor elements [3]. Basically, the high chemical resistance of tantalum and its nitrides is based on the native tantalum oxide film developing surface near, even under normal conditions in air. Other interesting properties are their tunable film properties such as the hardness in dependence of structure and nitrogen content, showing values of 61.8 GPa for Ta_4N, 15.5 GPa for hexagonal $TaN_{0.8}$ and 49.9 GPa for cubic TaN [4] as well as the resistivity and the temperature coefficient of resistance (TCR) (i.e. 20 μΩ cm and 3200 ppm/K for α-Ta and up to -6×10^6 μΩ cm and −40,000 ppm/K for Ta_3N_5) [5]. Furthermore, tantalum nitride or oxynitride thin films are used as strain gauges in pressure sensors for operation temperatures ranging up to 300 °C [6–11] promising an enhanced performance compared to purely metallic strain gauges due to a gauge factor in the range 3.5–6.2 [10] and the possibility to realize a low TCR. When the strain-sensitive components are made of pure platinum a gauge factor of about 3.85 is determined at room temperature decreasing to about 2.4 at operation temperatures above 640 °C [12]. Furthermore, the TCR has a high value of 2600 ppm/K at room temperature and 2100 ppm/K at 850 °C.

For the realization of TaN_x thin films different methods like reactive sputtering, chemical vapour deposition (CVD) [5], atomic layer deposition (ALD) [13] and ion beam assisted deposition (IBAD) [14,15] are applied. Deposition techniques such as thermal evaporation play a minor role in film synthetization as the melting points of tantalum and tantalum nitrides are high (>2500 K up to a mole fraction of N over 0.6) [16] and a stoichiometric deposition from a TaN source is very challenging due to the large difference in melting points of N_2 (63 K) and Ta (2773 K) and hence, in vapour pressures. Therefore, reactive sputter deposition is favoured and provides the possibility to tailor the film properties in a wide range. Despite publications investigating the specific properties of tantalum nitride thin films as a function of sputter deposition parameters, such as the film thickness and the annealing temperatures [17–19], a systematic study focusing especially on the impact of substrate properties in combination with post-deposition annealings in the temperature range up to 500 °C on the film morphology, the surface-near chemical composition and resistivity of tantalum nitride thin films is not available in the literature to the best of the authors' knowledge.

Besides the need for robust and reliable strain sensitive elements when targeting the realization of micromachined pressure sensors for harsh environments (i.e. high temperatures, aggressive

* Corresponding author.
E-mail address: michaela_grosser@yahoo.de (M. Grosser).

0169-4332/$ – see front matter © 2011 Elsevier B.V. All rights reserved.
doi:10.1016/j.apsusc.2011.11.003

Slag Corrosion of Preceramic Paper Derived Multilayer Oxide Refractory

B. Gutbrod, N. Travitzky, A. Richter, M. Göbbels, P. Greil

Multilayer oxide ceramics of variable compositions were fabricated from preceramic paper to substitute carbon-bonded refractory. Alternating layers of ZrO_2, Al_2O_3–ZrO_2 and Al_2O_3–$MgAl_2O_4$ preceramic paper were bonded with a zirconia based interface adhesive layer and co-sintered at 1700 °C. The porous multilayer refractory structures were exposed to an industrial CaO–Fe_2O_3–SiO_2-slag melt at 1390 °C and the corrosion degradation mechanisms were analyzed. Progression of the corrosion zone is dominated by a layer-by-layer infiltration and dissolution reaction process. Zirconia laminates were found to exhibit superior corrosion resistance. Enhanced dissolution of interface layers was observed in the alumina-zirconia system. A pronounced volume expansion effect caused accelerated degradation in the alumina-spinel based system. ZrO_2 based interface bonding layers of lower porosity compared to the preceramic paper derived ceramic layers may improve corrosion resistance. Manufacturing of multilayer refractory structures from preceramic paper of various compositions offers high flexibility in stacking design optimization in order to adopt corrosion resistance to local environmental conditions.

1 Introduction

Refractories are used in a broad field of applications such as iron and non-iron metallurgy (70 %), glass-making, waste treatment and petrochemical refining [1]. During service they are generally exposed to elevated temperatures up to 2000 °C, thermal and/or mechanical stresses as well as corrosion attack by molten metal, silicate slags, salt fluxes and corrosive atmospheres [2–4]. The wide variety of desired functionalities lead to the development and application of a large variety of refractory compositions that are produced in numerous shapes and forms [1, 5]. Refractory components including for example shrouds, monoblock stoppers and submerged nozzles commonly consist of carbon-bonded materials, e.g. of MgO–C, Al_2O_3–C, ZrO_2–C, ZrO_2–CaO–C, Al_2O_3–SiO_2–SiC–C or Al_2O_3–SiO_2–C [6–10]. Fabrication often requires isostatic pressing of the oxide powder bonded by graphite loaded resin or pitch. Upon coking above 1000–1200 °C a carbon bond develops which increases the corrosion resistance in slag and metal melts, respectively. Furthermore, the carbon bond improves the thermo-mechanical properties, particularly the thermal shock resistance [6, 11].

Degradation of refractories is a complex phenomenon, which involves not only chemical wear (corrosion) but additional physical/mechanical wear (such as erosion/abrasion). When one of the phases involved is liquid, corrosion is often controlled by direct dissolution of the refractory with or without precipitation, by oxidation-reduction reactions between oxide and metallic elements or by complex reactions leading to the formation of new compounds [4]. In steel production, wear rate is often highest at the interface between slag and refractory lining. Most refractory materials have a certain amount of porosity which is not desired in terms of facilitated penetration of melt into the refractory microstructure. However, low porosity may increase susceptibility for thermal shock damage [3]. A certain amount of porosity, therefore, may improve refractory lifetime if penetration and corrosion are carefully controlled [2]. Theoretical aspects of chemical attack of solid refractories by liquid slags with emphasis on both penetration (simple permeation of liquid slag via open porosity) and reaction of the slag with the refractory phases are reviewed in [2]. Corrosion reactions during service of carbon-bonded refractories at elevated temperatures may involve the oxidation of the

Björn Gutbrod, Nahum Travitzky, Peter Greil
Department of Materials Science and Engineering (Glass and Ceramics) and Centre for Advanced Materials and Processes (ZMP)
University of Erlangen-Nürnberg
91058 Erlangen
Germany

Andreas Richter, Matthias Göbbels
Applied Mineralogy
GeoZentrum Nordbayern
University of Erlangen-Nürnberg
91054 Erlangen
Germany

Corresponding author: *Björn Gutbrod*
E-mail: bjoern.gutbrod@email.de

Keywords: preceramic paper, multi-layered refractories, slag corrosion

Received: 06.08.2012
Accepted: 14.08.2012

COMMUNICATION

ADVANCED ENGINEERING MATERIALS

DOI: 10.1002/adem.201100192

Manufacturing of Silicon Carbide Knit Fabrics**

By *Christian Heiss, Nahum Travitzky** and *Peter Greil*

Knit fabric textile structures are processed from silicon carbide multifilament fiber rovings. The minimum bending radius of the various single silicon carbide fibers is determined from loop tension test in order to derive boundary conditions for fiber bending in the knitting process. The processing conditions for knitting are modified in order to reduce buckling and friction acting on the silicon carbide fiber rovings. Fiber knit fabrics are fabricated with a modified 2 Tempi pattern chain which leads to high flexible manufacturing. Compared to woven silicon carbide fabric structures the knitted fiber perform offers a superior flexibility, wider range of pore size and a higher degree of drapability.

Silicon carbide fibers and textile structures made thereof have attracted increasing interest for manufacturing of fiber reinforced high temperature resistant ceramic matrix composites (CMC) materials.[1–4] The complexity of the fiber architecture in the textile structures increases with fiber orientation from one-dimensional (1D) to three-dimensional (3D) fiber orientation. One or multi-step textile manufacturing processes like braiding, weaving, warp, or weft knitting were applied to manufacture fiber performs with 1D, 2D, and 3D fiber orientation, respectively.[5] Depending on the fiber packing density and orientation the fabric structure the stiffness, deformation, and fracture behavior of the fabric structure may vary in a wide range.[6–13] Knitting is a common method of interlooping fibers for manufacturing of planar textile structures,[14] while interleaving vertical yarns with horizontal ones is characteristic for woven fabrics. In contrast to woven fabrics, which exhibit a low drapability and stretchability in different directions, warp-knitted fabrics are formed by creating loops which give rise for high flexibility and deformability. The potentials of using knitted fabrics for reinforcement of polymer matrix composites have been treated in many studies.[8–11,15–17]

A high Young's modulus ($E = 209$ GPa) and low a deformability ($\varepsilon = 1.4\%$) of Nicalon 607 silicon carbide ceramic fibers, however give rise for a large critical bending radius of 0.36 mm [18] which makes loop formation during knitting difficult.[19]

The critical bending radius is also affected by the friction which is caused by ribbing between fibers and the machine parts and by the friction between the fibers inside the roving. This causes that critical radius is increased due to occurrence of friction during manufacturing.

In the present study, the manufacturing of knitted fabrics made of silicon carbide fiber was demonstrated. Critical bending loads were derived from fiber knot and loop testing in order to optimize yarn pretension, working speed, and take up speed during knitting processing. The mechanical behavior of the knit fabric under tensional load was tested and examined.

1. Experimental Procedure

1.1. Fiber Materials

Three different silicon carbide fibers (NL 607, 202 and 200 Nicalon, Nippon Carbon Company, Japan) differing in surface sizing were applied for knitting processing (Table 1). All fibers are multi-filament 0.5 k zero-twisted rovings. The fibers are derived from polycarbosilane polymer precursors. Since the polymer precursors were cured in air the pyrolized fibers contain an appreciable amount of oxygen. These fibers typically consist of β-SiC (40 wt%, 1.6 nm crystal size), amorphous SiC_xO_y (55 wt%) and C (5 wt%). Due to oxidation and crystallite growth, the critical application temperature in air is approximately 1000 °C.[19,20]

1.2. Mechanical Fiber Testing

Knitting involves bending of fibers to produce loops to form stitches and additional inlay fibers to adapt the textile properties. The fibers were examined by loop tension and bending radius testing. Mean values were derived from the measurement.

Two 60 mm rovings were cut from the bobbin. Intertwining slings were formed which were fixed to clamps for tension loading (Fafegraph ME, Textechno Herbert Stein, Mönchengladbach, Germany). A clamping length of 10 mm, a strain rate of 1 mm · min^{-1} and a preload of 0.33 cN of the yarn were applied. Taking in the account the maximum tensile

[*] C. Heiss, Dr. N. Travitzky, Prof. P. Greil
Department of Materials Science, Glass and Ceramics Friedrich-Alexander-University Erlangen-Nuremberg, Martensstr. 5, 91058 Erlangen, Germany
E-mail: nahum.travitzky@ww.uni-erlangen.de

[**] Financial support from DFG project GR 967 (Graduate School 1229) is gratefully acknowledged.

ARTICLE IN PRESS
NOC-16244; No of Pages 8
Journal of Non-Crystalline Solids xxx (2012) xxx–xxx
Contents lists available at SciVerse ScienceDirect
Journal of Non-Crystalline Solids
journal homepage: www.elsevier.com/locate/jnoncrysol

Thermodynamic properties of vitreous electrodes in a Ni/NiP glass-crystal Galvanic cell

Nicolai Jordanov [a,*], Lothar Wondraczek [b], Ivan Gutzow [a]

[a] Institute of Physical Chemistry, Bulgarian Academy of Sciences, 1113 Sofia, Bulgaria
[b] Otto-Schott-Institute, University of Jena, 07745 Jena, Germany

ARTICLE INFO

Article history:
Received 16 August 2012
Received in revised form 18 October 2012
Available online xxxx

Keywords:
Metglasses;
EMF;
Thermodynamics of glasses;
Kinetics;
Electrodeposition

ABSTRACT

In the present paper, we present and discuss data on the thermodynamic properties of electrochemically deposited crystalline and vitreous metallic electrodes, focusing our attention on the model system of vitreous Ni/P alloys. Galvanic cells based on the glass→crystal transition are constructed and their electrochemical properties are analyzed as an alternative approach for the complete thermodynamic description of amorphous electron conductors. The EMF of the glass→crystal Ni/P–Ni battery when both crystalline Ni and the amorphous Ni/P layers electrodes placed in their native solution, gives $\Delta E(T)$ values from 0.120 to 0.140 V in the temperature range from 293 to 333 K. For the same system, we report a corrosion potential difference of $\Delta E = 0.100$ V (at 298 K, in a 1 M H_2SO_4 electrolyte) between the glassy and the crystalline electrodes. The kinetic considerations of the deposition process provide a new way for interpretation of the mechanism of formation of amorphous deposits during electrodeposition and electroless formation of amorphous Ni_3P layers based on a kinetic interpretation of Ostwald's Rule of Stages.

1. Introduction

The possibility of Galvanic cells or "physical" batteries based on the free energy differences between two physical states of matter of the same substance is known from many years in electrochemistry [1]. The electrochemical glass/crystal cell (GCC) present an interesting particular case of this problem which has been discussed in two of our previous publications [2,3]. Vitrification of one of the electrodes in a battery constituted of two crystalline electrodes with different composition should lead to an additional electromotive force (EMF) which is caused by the increased free energy of the respective glass. GCC batteries are not only of fundamental interest, but may possess also distinct technologically interesting properties (as, e.g., the "carbon" glass/graphite battery, [4] or amorphous lithium ferrophosphate electrodes [5,6]). For example, in the carbon GCC, incomplete "burning" of vitreous carbon glasses or other activated carbon materials to the respective crystalline phase (Graphite) should occur without the release of greenhouse gases (CO_2, CO): electrical energy could be generated due to the electrochemically induced "oxidation" process of the glassy electrode only via conversion of the potential energy difference between the vitreous and the crystalline states.

The theoretical problems connected with the glass/crystal cell have been examined in details in the above mentioned study [1], where we analyzed also the properties of three electron-conducting glass forming systems, relying mainly on existing literature data. These three cases considered were Carbon (vitreous C/Graphite), Antimony, Sb (amorphous "explosive" Sb/crystalline Sb) and several metallic alloy glasses. Here, we focus on the Ni/NiP GCC and provide experimental data on the electrochemical deposition and the electrochemical properties of this glass forming system. The mechanism of the electrochemical formation of vitreous Ni_3P studied is considered as an example for the electrochemical deposition of Ni/P glasses and of other metallic glasses in general.

2. Basic theoretical considerations

In order to determine the thermodynamic properties of conducting glasses we first employ classical thermodynamic considerations [1,3]. For temperatures sufficiently below the respective glass transition temperature, T_g (i.e. at $T << T_g$), the enthalpy difference, ΔH_g and entropy difference respectively, ΔS_g, between the vitreous and the crystalline state are connected according to these considerations in the following way

$$\Delta E_g(T) = \frac{1}{zF}\left[\Delta H_g - T\Delta S_g\right] = \frac{1}{zF}\Delta G(T) \quad (1)$$

with the EMF, $\Delta E_g(T)$ of the respective GCC.

Here z is the number of exchanged electrical charges, F is Faraday's constant ($F = 96485$ C mol^{-1}) and $\Delta G(T)$ is the molar free energy difference between glass and crystal at the same temperature, T. Based on this dependence, the thermodynamic functions of electron conducting glasses can be obtained by measuring the EMF in a electrochemical

* Corresponding author. Tel.: +359 2 9792552; fax: +359 2 9710688.
E-mail address: njordanov@ipc.bas.bg (N. Jordanov).

0022-3093/$ – see front matter © 2012 Elsevier B.V. All rights reserved.
http://dx.doi.org/10.1016/j.jnoncrysol.2012.10.028

Please cite this article as: N. Jordanov, et al., Thermodynamic properties of vitreous electrodes in a Ni/NiP glass-crystal Galvanic cell, Journal of Non-Crystalline Solids (2012), http://dx.doi.org/10.1016/j.jnoncrysol.2012.10.028

Journal of Non-Crystalline Solids 358 (2012) 1239–1256

Contents lists available at SciVerse ScienceDirect

Journal of Non-Crystalline Solids

journal homepage: www.elsevier.com/locate/jnoncrysol

Review

Thermodynamic properties of amorphous solids: The electrochemical approach

Nicolai Jordanov [a,*], Lothar Wondraczek [b], Ivan Gutzow [a]

[a] Institute of Physical Chemistry, Bulgarian Academy of Sciences, 1113 Sofia, Bulgaria
[b] Institute of Glass and Ceramics, Friedrich Alexander University Erlangen-Nürnberg, 91058 Erlangen, Germany

ARTICLE INFO

Article history:
Received 29 November 2011
Received in revised form 24 February 2012
Available online 27 March 2012

Keywords:
Glass/crystal cell;
Metglass;
Frozen-in entropy;
Electrochemistry of glasses

ABSTRACT

In the present contribution are critically analyzed and reexamined the possibilities to determine the thermodynamic properties of amorphous solids, of defect crystals and of glasses by means of electrochemical methods. After detailed theoretical considerations performed in the framework of the thermodynamics of irreversible processes it is demonstrated how the most significant thermodynamic parameters of amorphous systems with frozen-in structure—their configurational enthalpy and entropy ΔH_g and ΔS_g—can be electrochemically measured, when the systems under investigation are first order (electron) conductors, capable of forming the electrodes in a *glass → crystal* Galvanic cell. We refer here to existing classical experimental results with two such systems: vitreous Sb (so-called explosive antimony) and glassy carbon resins both used to demonstrate the applicability of the theoretical considerations developed. Results with several Metglass alloy systems (Ni/P, Fe, Ni/P, B, Co/B and Cu/Ti), obtained via corrosion potentio-dynamic electrochemical measurements are also summarized and used to estimate the thermodynamic properties of variously treated glass-forming systems. The electrochemical evidence analyzed clearly demonstrates in its integrity the particular, frozen-in nature of the basic thermodynamic parameters in the considered glass systems ($\Delta Hg \approx const > 0$, $\Delta Sg \approx const > 0$) as this is expected to be both from classical theory and from known calorimetric measurements. The contribution of direct glass/crystal Voltaic contacts to the thermodynamic properties of electrochemical cells with glassy or vitro-crystalline electrodes is also considered in details. Possible technical applications of Galvanic and Voltaic potentials, determined by glassy or vitro-crystalline electrode materials, including existing conventional battery systems and other horizons, opened to discussion by the present theoretical approach are also outlined.

1. Introduction

The thermodynamic properties of glasses, which are the most typical representatives of amorphous solids with frozen-in structure and properties, are generally determined from measurements of the specific heat differences $\Delta C_p(T)$ glass (liquid)/crystal. These measurements require the knowledge of the $\Delta C_p(T)$-course from the respective melting point, T_m, to temperatures far below the glass transition temperature, T_g. Classical measurements in this respect, determining the following developments of ideas for many years are given in refs. [1–3], in the discussion in the monograph [4], in the additional literature cited there and especially in Simon's paper [5]. All these measurements were performed down to temperatures, T, of only several degrees Kelvin, i.e. close to the absolute zero ($T = 0$ K). A necessary prerequisite in such determinations is also the exact knowledge of the enthalpy of melting, ΔH_m and thus (via $\Delta H_m = \Delta S_m T_m$) of the entropy of melting, ΔS_m.

The necessary thermodynamic formalism, connected with both the $\Delta C_p(T)$-measurements and the calculations of the thermodynamic functions of the respective glasses are also described in details in [4]. As far as glasses have to be considered as non-equilibrium, frozen-in systems these thermodynamic calculations include, when performed in the framework of classical thermodynamics, two substantial approximations introduced at the end of the 1920s by Simon [5,6]. These approximations governed for more than 80 years the development of the thermodynamics of glasses and gave, as we know now [7,8], a sound basis for many ideas formulated in glass science. Their exceptional merits, but also their limitations are critically reexamined by one of the present authors in two recent publications [7,8] in the current literature and in Chapter 8 of the monograph [9]. In these three publications the possible error limits introduced by Simon's approximations are calculated and it is found that the uncertainties introduced by them in fact could and can be safely neglected in most cases.

Nevertheless from the very beginning of the development of glass science there were also ways indicated to allow direct determinations of the glass/crystal differences, in the thermodynamic functions in which no $\Delta C_p(T)$ measurements are involved.

Here we have *first* to mention the possibility of determining the glass/crystal enthalpy difference, ΔH_g by measuring the respective

* Corresponding author. Tel.: +359 2 979 2552; fax: +359 2 9712688.
E-mail address: njordanov@ipc.bas.bg (N. Jordanov).

0022-3093/$ – see front matter © 2012 Elsevier B.V. All rights reserved.
doi:10.1016/j.jnoncrysol.2012.02.031

ADVANCED ENGINEERING MATERIALS

COMMUNICATION

DOI: 10.1002/adem.201100186

Synthesis of Ti_2SnC MAX Phase by Mechanical Activation and Melt Infiltration**

By *Young Jae Kang, Tobias Fey* and Peter Greil*

Ternary MAX phase Ti_2SnC was synthesized by Sn-melt infiltration into a porous preform of sub-stoichiometric titanium carbide $TiC_{0.5}$. Compared to synthesis starting from elemental Ti + C + Sn mixtures which require temperatures exceeding 1100 °C a significantly lower reaction temperature as low as 700 °C was observed in the $TiC_{0.5}$ + Sn system. This reduction in reaction temperature is rationalized in terms of accumulation of microstrain and decrease of crystallite size upon ball milling of the Ti + C powder mixture. Dense compacts of Ti_2SnC with only minor fractions of unreacted $TiC_{0.5}$ were obtained at 1025 °C. Thus reactive solid–liquid processing at lower temperatures might be of relevance for MAX phase systems containing low melting A-elements such as Sn, In, Ga, Pb, etc. which tend to become unstable at elevated temperatures.

Ternary $M_{n+1}AX_n$ phases of hexagonal crystal symmetry are distinguished by a unique alteration of metal bonded A-layers (A = A group element) and XM_6-octahedra layers (M = early transition metal and X = C, N) differing in stacking sequence e.g., n = 1, 2, or 3.[1] The mechanical properties of the MAX phases are highly reflected by the anisotropy in the crystal structure with a high compressibility in the [0001] direction dominated by A layer and lower compressibility perpendicular.[2] When deformed these materials are restricted to basal plane slip causing the dislocations generated to arrange themselves in arrays forming pile-ups.[3] Due to their nano-laminate structure MAX phase materials with M = Ti and A = Si, Al exhibit superior machinability, excellent thermal shock resistance as well as good thermal and electrical conductivity, respectively.[4] The electrical conduction mechanism proposed for the MAX phases is dominated by d-bands originating predominantly from the metal atoms located adjacent to the A-element atoms in the MAX phase crystal structure.[5]

MAX phases with A being a low melting metal (A = Ga, In) were recently reported to exhibit unusual physical phenomena. Thus, for example, Cr_2GaN was demonstrated to exhibit self-extrusion of pure Ga whiskers at room temperature.[6]

Low-temperature instability of Ti_2SnC was reported to cause depletion of Sn from the ternary carbide during cooling procedure which may yield Sn precipitation and substoichiometric $Ti_2Sn_{1-x}C$ confirmed by TEM, DSC, and X-ray analyses.[7] Though the driving force for the deintercalation of the A metal from the basal (0001) planes of M_2AC is still discussed controversly, the high mobility of the intercalating low melting metal indicates a low bonding energy state of the A metal layer which might be attractive for achieving novel properties and applications of MAX phases. For example, MAX phase based composite materials with low melting metals like Sn, In, or Pb on the A position might be of great interest for self healing materials requiring significantly lower activation energies (e.g., temperature) for triggering crack healing reactions compared to common engineering ceramic materials.[8]

The 211 MAX-phase Ti_2SnC (space group $P6_3/mmc$ with lattice parameters a = 0.3162 nm and c = 1.3678 nm[9]) was reported to be the only stable MAX phase in the Ti–Sn–C system.[10] Recent work, however, claimed the formation of Ti_2SnC_2 obtained by hot-isostatic pressing at 1315 °C under a pressure of 120 MPa.[11] Since Ti_2SnC synthesis reactions from mixtures of elemental Ti, Sn, and C powders required temperatures exceeding 1200 °C, uni-axial hot pressing,[12,13] hot-isostatic pressing[14] and self-propagation high temperature synthesis[15] were applied. Significantly lower synthesis temperatures of 650 °C were reported when mechanically alloyed Ti/Sn/C powders and Ti/Sn/MAed-C powders were applied in hot-pressing.[16] Formation of Ti_2SnC was observed as low as 650 °C and a large amount was found at 950 °C. The reduction of reaction temperature was attributed to a large grain boundary area and short diffusion pathway, which improve the sinterability.

[*] *Y. J. Kang, T. Fey, P. Greil*
Department of Materials Science (Glass and Ceramics), University of Erlangen-Nuernberg, Martensstr. 5, D-91058 Erlangen, (Germany)
E-mail: Tobias.Fey@uni-erlangen.de

[**] *Financial support from DFG Kosseleck program contract no. GR 961/32 is gratefully acknowledged.*

Journal of Non-Crystalline Solids 358 (2012) 1523–1529

Contents lists available at SciVerse ScienceDirect

Journal of Non-Crystalline Solids

journal homepage: www.elsevier.com/locate/jnoncrysol

Effect of Al_2O_3 addition on the formation of perovskite-type $NaNbO_3$ nanocrystals in silicate-based glasses

Keitaro Kioka [a], Tsuyoshi Honma [a], Keiichiro Oh-ishi [a], Sindy Reibstein [b], Ning Da [b], Lothar Wondraczek [b], Takayuki Komatsu [a,*]

[a] Department of Materials Science and Technology, Nagaoka University of Technology, 1603-1 Kamitomioka-cho, Nagaoka 940-2188, Japan
[b] Department of Materials Science, University of Erlangen-Nuremberg, Erlangen 91058, Germany

ARTICLE INFO

Article history:
Received 9 February 2012
Received in revised form 4 April 2012
Available online 5 May 2012

Keywords:
$NaNbO_3$;
Nanocrystals;
Aluminosilicate glass;
Transmission electron microscopy;
Laser patterning

ABSTRACT

The crystallization behavior of $30Na_2O$–$25Nb_2O_5$–$(45-x)$ SiO_2–$xAlO_{1.5}$ ($x=0$, 2.5, and 5) (mol%) glasses was examined and the effect of Al_2O_3 addition on the formation of perovskite-type $NaNbO_3$ crystals was clarified. It is found from X-ray diffraction analyses and transmission electron microscope observations that $NaNbO_3$ nanocrystals are formed in all glasses and the size of $NaNbO_3$ crystals decreases with the substitution of Al_2O_3 for SiO_2. A crystallized (heat-treated at 684 °C for 5 h) glass with $x=5$, which contains $NaNbO_3$ nanocrystals with an average size of 50 nm, shows good optical transparency in the wavelength region of 500–2000 nm and a small hysteresis loop in the polarization-electric field curve. The lines containing $NaNbO_3$ crystals were patterned on the surface of NiO-doped glass with $x=5$ by irradiations (power: 1.3–1.4 W, scanning speed: 10 μm/s) of Yb:YVO_4 fiber laser (wavelength: 1080 nm). The formation mechanism of $NaNbO_3$ nanocrystals in aluminosilicate glasses was also discussed.

1. Introduction

Nanostructures are the gateway into a new realm of physics, chemistry, biology, and materials science. Developing techniques for fabricating nanostructures inexpensively is an area that requires substantial effort. Crystallization of glass is a unique method for fabrication of transparent materials containing nanocrystals. Through the design of base glass composition and control of crystal nucleation and growth, it is possible to synthesize nanocrystals and to induce new active functions in glasses being usually available for passive usages like optical glass fibers. So far, many papers on the fabrication and characterization of crystallized glasses containing nanocrystals have been reported [1]. For instance, Yamazawa et al. [2] developed crystallized glasses containing ferroelectric $Sr_xBa_{1-x}Nb_2O_6$ nanocrystals and confirmed the appearance of electro-optic activity in such nanocomposites. Kanno et al. [3] succeeded in patterning lines consisting of Er^{3+}-doped CaF_2 nanocrystals on the surface of oxyfluoride glasses by laser irradiation and observed intense emissions.

Sodium niobate, $NaNbO_3$, has a perovskite-type structure (*Pbma*) with an orthorhombic unit cell at room temperature and exhibits anti-ferroelectric properties [4,5]. A small substitution of K^+ to Na^+ ion sites in $NaNbO_3$ produces ferroelectric properties [6–8], consequently providing good electro-optic coefficients, piezoelectricity, and electrical–mechanical coupling factors. (Na,K) NbO_3 crystals are also known to have photocatalytic activity [9]. It is, therefore, of extreme interest and importance to design and fabricate optically transparent composites, especially nanocomposites containing $NaNbO_3$ or (Na,K) NbO_3 nanocrystals. There have been several reports on the fabrication and characterization of crystallized glasses containing $NaNbO_3$ crystals, and some studies are summarized in Table 1 [10–23]. Because of high kinetic fragility and, hence, crystallization tendency, it is practically impossible to prepare bulk glasses of stoichiometric composition (i.e., $50Na_2O$–$50Nb_2O_5$ (mol%)) corresponding to $NaNbO_3$: the network-forming oxides such as SiO_2, B_2O_3, TeO_2, or GeO_2 have to be added into the binary system of Na_2O–Nb_2O_5. The kind and amount of these oxides change the coordination and connectivity states of NbO_6 polyhedra being present in a given glass [24], and consequently the formation behavior of $NaNbO_3$ nanocrystals varies depending on the glass system and composition. Indeed, as shown in Table 1, different glass systems and compositions have been examined for the synthesis of $NaNbO_3$ crystals. In other words, even at this moment, the design of glass composition providing the formation of $NaNbO_3$ nanocrystals has not been well established.

The purpose of this study is to fabricate transparent crystallized glasses with perovskite-type $NaNbO_3$ nanocrystals in Na_2O–Nb_2O_5–SiO_2–Al_2O_3 glasses and to clarify their formation mechanism, in particular, the effect of the SiO_2/Al_2O_3 ratio on the formation of $NaNbO_3$ nanocrystals. The laser patterning of lines containing $NaNbO_3$ crystals on the surface of glasses is also tried. Such lines would be regarded as

* Corresponding author. Tel.: +81 258 47 9313; fax: +81 258 47 9300.
E-mail address: komatsu@mst.nagaokaut.ac.jp (T. Komatsu).

0022-3093/$ – see front matter © 2012 Elsevier B.V. All rights reserved.
doi:10.1016/j.jnoncrysol.2012.04.011

Journal of
Ceramic Science
and Technology

J. Ceram. Sci. Tech., 03 [03] 111-118 (2012)
DOI: 10.4416/JCST2012-00008
available online at: http://www.ceramic-science.com

Processing, Microstructure and Properties of Paper-Derived Porous Al_2O_3 Substrates

C. Kluthe [*1], B. Dermeik [2], W. Kollenberg [1], P. Greil [2], N. Travitzky [2]

[1]Department of Natural Science, Bonn-Rhein-Sieg University of Applied Sciences, von-Liebig-Str. 20, 53359 Rheinbach, Germany
[2]Department of Materials Science and Engineering (Glass and Ceramics), University of Erlangen-Nuremberg, Martensstr. 5, 91058 Erlangen, Germany

received March 23, 2012; received in revised form June 20, 2012; accepted June 27, 2012

Abstract

In this work, preceramic papers containing 85 wt% Al_2O_3 were heat-treated at 1600 °C to obtain paper-derived ceramics. In order to increase the preceramic paper density prior to sintering, the papers were calendered at different roll temperatures and pressures. The influences of the calendering parameters on the microstructure and mechanical properties of the preceramic papers and the paper-derived ceramics were investigated. It was expected that especially the mechanical properties of the papers and derived ceramics would be improved by calendering.

The increase in the preceramic paper density led to an increase by ~ 85 % of the green tensile strength from ~ 20 MPa to ~ 37 MPa in cross direction (CD) and by ~ 91 %, from ~ 11 MPa to ~ 21 MPa in machining direction (MD). An increase in flexural strength by ~ 96 %, from ~ 138 MPa to ~ 270 MPa, was obtained for the paper-derived ceramics with an increase in density by ~ 25 %, from ~ 2.4 g/cm³ to ~ 3.0 g/cm³, and the shrinkage after sintering was reduced from ~ 15 % to ~ 12 % owing to the previous calendering of the preceramic paper.

Keywords: Preceramic paper, calendering, mechanical properties, sintering, porosity

1. Introduction

Over the past several years, preceramic papers and the resulting ceramics (paper-derived ceramics) have received research attention [1–3]. Preceramic papers can be shaped in different ways, such as by laser cutting or laminated object manufacturing (LOM) [4,5]. When these paper sheets are heated, finished ceramics in the preset shape are obtained. The cellulose fibers decompose during the heat treatment and any remaining organic content is removed from the paper (at 300 – 800 °C). The inorganic content is consolidated by sintering [2].

The fabrication of preceramic papers is similar to the production of common writing paper. Both papers consist of cellulose fibers and inorganic fillers. These fillers are powdered minerals (e.g. kaolin and talc) or synthetic powders (e.g. $CaCO_3$ or TiO_2). However, the content of inorganic filler is significantly increased for the production of preceramic paper. The differences in composition between conventional writing paper and preceramic paper are shown in Table 1.

Organic fibers and inorganic fillers are mixed into water for preparing the preceramic paper suspension. The inorganic filler is expected to have a particle size of below 30 µm to avoid powder sedimentation during the production process [6]. In addition to the main components, coagulation and flocculation agents are added to the preceramic paper suspension. The suspension is then fed into a paper machine, which produces a continuous sheet of preceramic paper by a dewatering process (see [2] for technical details).

Table 1: Compositions of different types of papers

	Common writing paper	Al_2O_3-filled pre-ceramic paper
Filler content /wt%	20 – 30	85
Mean particle size /µm	0.5 – 2	< 30
Sheet thickness /µm	110	750
Area density /g/m²	80	1000

The finished preceramic paper can be further processed in the calender. A calender applies a defined line load on the processed paper sheet by the pressure of its rolls. A defined calendering temperature is set by heating the calender rolls. The purpose of this work was to study the mechanical properties of the preceramic paper and of the paper-derived Al_2O_3-ceramic at different calendering temperatures and line loads. Also, the degree of material densification and surface smoothening was monitored for both materials.

* Corresponding author: christopher.kluthe@h-brs.de

J Mater Sci
DOI 10.1007/s10853-012-6919-8

Conceptional design of nano-particulate ITO inks for inkjet printing of electron devices

Nadja Kölpin · Moritz Wegener · Erik Teuber · Sebastian Polster · Lothar Frey · Andreas Roosen

Received: 18 June 2012 / Accepted: 22 September 2012

Abstract This manuscript presents the conceptional design of indium tin oxide inkjet inks for the manufacture of electron devices. For this purpose, the process window of the printer used is identified and the inks are conceived to meet the requirements. The nano-particles are effectively stabilized in different dispersion media. The rheological, the wetting and the drying behavior of the inks are adapted to the inkjet process and the substrates to be coated. To assemble a field effect transistor (FET), the most suitable ink is chosen and source and drain contacts are printed. In the device, a nano-particulate ZnO layer acts as semiconducting layer and the gate electrode as well as the dielectric layer is formed by a thermally oxidized silicon wafer. The electron device assembled shows the typical FET characteristic proving its functionality.

Introduction

Inkjet printing is an emerging technology with many potential applications in the field of electronics and biotechnology such as the assembly of organic electron devices, the direct printing of electronic bonds on circuits or the manufacture of "gene chips" [1–3]. Compared to more conventional printing methods like screen printing or offset printing, inkjet printing is more flexible as it is a direct printing technique and it is also contactless, which can be advantageous for sensitive substrates.

The inkjet printing technique was initially developed in the 1960s and 1970s using a continuous jet for industrial applications. Later on in the 1970s and 1980s the drop-on-demand printers using piezo or bubble jet technology were developed [4]; the printers with piezo heads are still very frequently used for research activities today because they can be applied to a broad variety of inks [5–8].

Fromm [9] made a contribution to the understanding of the printability of the inks by numerically calculating the fluid dynamics of drop-on-demand jets using Navier–Stokes equations. In order to describe the fluid properties, he used the Reynolds N_{Re} number and the Weber number N_{We} of the ink:

$$N_{Re} = \frac{va\rho}{\eta} \quad (1)$$

$$N_{We} = \frac{v^2 a\rho}{\sigma} \quad (2)$$

where v is the velocity, a is a characteristic dimension, i.e., the radius of the printing orifice, and ρ, η, and γ are the fluid density, viscosity and surface tension, respectively. These two parameters can be summarized to the so-called parameter Z, which is the inverse of the Ohnesorge number Oh [10, 11].

$$Z = Oh^{-1} = \frac{N_{Re}}{\sqrt{N_{We}}} = \frac{\sqrt{a \cdot \rho \cdot \gamma}}{\eta} \quad (3)$$

For inkjet inks, the Z-parameter should lie in between 1 and 14 [10, 11]. If the ink fulfills this condition, then a drop

N. Kölpin · M. Wegener · A. Roosen (✉)
Department of Materials Science, Glass and Ceramics, University of Erlangen-Nuremberg, Erlangen, Germany
e-mail: andreas.roosen@ww.uni-erlangen.de

M. Wegener
e-mail: moritz.wegener@ww.uni-erlangen.de

E. Teuber
Fraunhofer Institute for Integrated Systems and Device Technology, Erlangen, Germany

S. Polster · L. Frey
Department of Electrical, Electronic and Communication Engineering, University of Erlangen-Nuremberg, Erlangen, Germany

Published online: 10 October 2012

Thin Solid Films 520 (2012) 7130–7135

Contents lists available at SciVerse ScienceDirect

Thin Solid Films

journal homepage: www.elsevier.com/locate/tsf

Effect of thermal annealing on the mechanical properties of low-emissivity physical vapor deposited multilayer-coatings for architectural applications

Robert Meszaros [a], Benoit Merle [b], Michael Wild [c], Karsten Durst [b], Mathias Göken [b], Lothar Wondraczek [a,d,*]

[a] Institute of Glass and Ceramics, Department of Materials Science, University of Erlangen-Nuremberg, 91058 Erlangen, Germany
[b] Institute of General Materials Properties, Department of Materials Science, University of Erlangen-Nuremberg, 91058 Erlangen, Germany
[c] Interpane Glasgesellschaft mbH, 94447 Plattling, Germany
[d] Otto-Schott-Institute, University of Jena, 07743 Jena, Germany

ARTICLE INFO

Article history:
Received 10 November 2011
Received in revised form 17 July 2012
Accepted 19 July 2012
Available online 25 July 2012

Keywords:
Glass
Low-emissivity coatings
Nanomechanics
Annealing
Atomic force microscopy

ABSTRACT

Low-emissivity (low-E) coatings comprising a stack of multiple physical vapor deposited metallic and dielectric layers play an important role in energy management of modern buildings. The production process of such architectural glazings often requires that the coatings withstand a short-term thermal load of up to 700 °C. Here, we report on thermally-induced variations in the mechanical properties of representative large-area magnetron-sputtered low-E stacks on glass, developed specifically for high temperature stability. Coatings are investigated before and after heat treatment by bulge testing, curvature analyses using Stoney's equation, and nanoindentation. For as-deposited coatings, an in-plane residual compressive stress about 48 MPa and Young's modulus of 120 GPa are found, depending on the type of substrate. Short-term exposure to up to 700 °C converts this situation to in-plane residual tensile stress of > 400 MPa, while Young's modulus decreases to about 105 GPa. These changes in the residual stress state are explained on the basis of structural, topological and dimensional changes in the coating stack. They identified as one of the primary factors governing temperature-resistance of low-E coatings.

1. Introduction

Multilayer coatings with low infrared emissivity (low-E) are widely used to tailor spectral selectivity and solar transmission of architectural glazings ([1–4], see also Fig. 1). That is, low-E coatings are deposited on glasses for architectural applications for, e.g., high visible (VIS) transparency and, at the same time, high near-infrared (NIR) reflectivity to prevent energy loss from the building to the environment. Deposition is typically done by magnetron sputtering of layer stacks, generally comprising at least one conductive metallic layer (typically silver) with a thickness of about 10 nm. This metallic layer is embedded between various optically transparent dielectric layers such as oxides of zinc, tin, bismuth or titanium with a thickness below 40 nm and a refractive index of preferably more than 2 [5,6]. As a function of its plasmonic resonance frequency, the metallic layer is responsible for thermal/solar (IR) reflectivity. The dielectric layers may comprise antireflective functions in the visible spectral range and/or protect the metallic layer from chemical and mechanical damage. In addition, they act as adhesion layers, nucleation templates and diffusion barriers. Further components such as titanium, nickel and chromium alloys are applied as sacrificial layers with a thickness of < 5 nm to protect the metallic layer from oxidation during deposition of dielectric layers in oxygen-containing plasma. In practice, coatings are applied on soda lime silicate (SLS) float glass sheet with a typical size of approximately 20 m². For many architectural applications, these glasses undergo various secondary processing steps such as bending/vacuum forming and, most importantly, thermal toughening [7] where impact resistance is enhanced and specific fracture behavior is induced to avoid breakage into large and sharp fragments. Both processes require elevated temperature (i.e., up to 700 °C), and it is highly desirable or, in some applications, even required that coatings are applied prior to these process steps.

On the other hand, this demands that the coatings can withstand these high temperatures without trading-off functionality [3]. That is, at temperatures above 500 °C, due to enhanced diffusivity and melting point reduction, individual components of the stack (especially Ag) may tend to oxidize, to migrate through the coating, to form agglomerates, to recrystallize, to alloy, etc., and, hence, strongly alter optical properties [8,9]. In addition, delamination and/or dewetting phenomena may occur between coating layers due to the release of residual

* Corresponding author at: Department of Materials Science, Institute of Glass and Ceramics, University of Erlangen-Nuremberg, Martensstrasse 5, Erlangen D-91058, Germany. Tel.: +49 9131 85 27553; fax: +49 9131 85 28311.
E-mail address: lothar.wondraczek@www.uni-erlangen.de (L. Wondraczek).

0040-6090/$ – see front matter © 2012 Elsevier B.V. All rights reserved.
http://dx.doi.org/10.1016/j.tsf.2012.07.086

Hindawi Publishing Corporation
Advances in Materials Science and Engineering
Volume 2012, Article ID 525428, 8 pages
doi:10.1155/2012/525428

Research Article

Crystallisation Kinetics of a β-Spodumene-Based Glass Ceramic

Oscar Rubem Klegues Montedo,[1] Dachamir Hotza,[2] Antonio Pedro Novaes de Oliveira,[2] Robert Meszaros,[3] Nahum Travitzky,[3] and Peter Greil[3]

[1] *Unidade Acadêmica de Ciências, Engenharias e Tecnologias (UNACET), Universidade do Extremo Sul Catarinense (UNESC), 88806-000 Criciúma, SC, Brazil*
[2] *Group of Ceramic and Glass Materials (CERMAT), Department of Mechanical Engineering (EMC), Federal University of Santa Catarina (UFSC), 88040-900 Florianópolis, SC, Brazil*
[3] *Department of Materials Science, Institute of Glass and Ceramics, University of Erlangen-Nuremberg, 91058 Erlangen, Germany*

Correspondence should be addressed to Oscar Rubem Klegues Montedo, oscar.rkm@gmail.com

Received 25 February 2011; Revised 19 September 2011; Accepted 20 September 2011

Academic Editor: Joseph Lai

LZSA (Li_2O-ZrO_2-SiO_2-Al_2O_3) glass ceramic system has shown high potential to obtain LTCC laminate tapes at low sintering temperature (<1000°C) for several applications, such as screen-printed electronic components. Furthermore, LZSA glass ceramics offer interesting mechanical, chemical, and thermal properties, which make LZSA also a potential candidate for fabricating multilayered structures processed by Laminated Objects Manufacturing (LOM) technology. The crystallization kinetics of an LZSA glass ceramic with a composition of $16.9Li_2O \cdot 5.0ZrO_2 \cdot 65.1SiO_2 \cdot 8.6Al_2O_3$ was investigated using nonisothermal methods by differential thermal analysis and scanning electronic microscopy. Apparent activation energy for crystallization was found to be in the 274–292 $kJ \cdot mol^{-1}$ range, and an Avrami parameter n of 1 was obtained that is compared very favorably with SEM observations.

1. Introduction

A considerable effort has been spent to obtain high-performance glass ceramics for several potential applications in the medical, automotive, and telecommunication fields [1]. Low-temperature cofired ceramics (LTCCs) have created good perspectives for those applications, with special attention to the glass ceramic materials [2, 3]. LZSA glass ceramics (Li_2O-ZrO_2-SiO_2-Al_2O_3) have been studied because of their beneficial thermal, mechanical, and thermal properties [4], among other interesting features. Moreover, laminated LZSA bodies crystallized at 850°C/30 min have demonstrated to exhibit a low dielectric constant of 8.61 ± 0.84 at 1 MHz (room temperature) [5]. Furthermore, their relatively low temperatures of sintering [6] make β-spodumene-based glass ceramics (LZSA) a potential candidate for obtaining multilayered structures processed by LOM technology (Laminated Objects Manufacturing) [7]. However, the low sintering temperature is also accomplished by low crystallization temperature in this system, especially for very fine powders and low heating rates. In order to control thermal treatment for obtaining optimized properties, it is necessary to determine the kinetics parameters of crystallization for this glass ceramic system.

Isothermal crystallization kinetics of glass ceramic systems commonly refers to the following well-established Johnson-Mehl-Avrami equation [8]:

$$-\ln(1-x) = kt^n, \quad (1)$$

where x is the volume fraction crystallized at a given temperature and time t, n is the Avrami parameter related to the nucleation and crystal growth mechanisms, and k is the reaction rate constant related to the apparent activation energy for crystallization, E_c. Nonisothermal conditions have been more largely widespread in the crystallization studies

Journal of Non-Crystalline Solids 358 (2012) 3193–3199

Contents lists available at SciVerse ScienceDirect

Journal of Non-Crystalline Solids

journal homepage: www.elsevier.com/locate/jnoncrysol

Surface-luminescence from thermally reduced bismuth-doped sodium aluminosilicate glasses

Karsten H. Nielsen [a], Morten M. Smedskjaer [b], Mingyeng Peng [c], Yuanzheng Yue [b], Lothar Wondraczek [a,d,*]

[a] Department of Materials Science, Friedrich-Alexander University of Erlangen-Nuremberg, Germany
[b] Section of Chemistry, Department of Biotechnology, Chemistry and Environmental Engineering, Aalborg University, Denmark
[c] State Key Laboratory of Luminescent Materials and Devices and Institute of Optical Communication Materials, School of Materials Science and Engineering, South China University of Technology, Guangzhou, China
[d] Otto-Schott-Institute, University of Jena, Germany

ARTICLE INFO

Article history:
Received 9 July 2012
Received in revised form 11 September 2012
Available online 5 October 2012

Keywords:
Bismuth;
Aluminosilicate;
Luminescence;
Near-infrared;
Thermal reduction

ABSTRACT

We report on the effect of hydrogen annealing on the optical properties of bismuth-doped sodium aluminosilicate glasses. The redox state of bismuth in the as-melted glasses is governed by the composition, viz., NIR luminescence is observed only in the glasses with low optical basicity. Upon thermal reduction, visible emission from Bi^{3+} and, eventually, minor amounts of Bi^{2+} is significantly lowered, depending on heat-treatment time and temperature, and glass composition. Hydrogen treatment was also found to result in a decrease of the NIR emission intensity and, at the same time, formation of metallic bismuth particles in the surface region. Surface-tinting as well as the decrease of visible luminescence follow Arrhenian kinetics, suggesting that hydrogen permeation is the rate-governing process. Upon re-annealing in air, the effects of thermal reduction on the optical properties are reversible only to a limited extent.

1. Introduction

The optical properties of bismuth-doped oxide glasses have been arousing significant and renewed interest over the last few years. This has been motivated by various potential applications such as simple coloring [1], third order optical non-linearity (e.g. [2]), and surface conductivity (e.g. [3]) on the one side, and luminescence in the visible (VIS) and near-infrared (NIR) spectral range on the other side [4,5]. In particular, broadband NIR luminescence has been studied extensively for application in novel laser sources and optical amplifiers [5–8]. However, due to the large variety of redox states in which bismuth may be present in oxide glass matrices, the respective origin of luminescence and other optical properties remains debated [4]. It has therefore become important to be able to manipulate the redox state of bismuth in oxide glasses.

In silicate glasses, Bi^{3+} and metallic bismuth are traditionally regarded as the most prevalent species [9]. For instance, voltammetric studies on a soda lime silicate melt at 1250 °C have confirmed the presence of these two species (Bi^0 and Bi^{3+}), but also indicated the presence of a third species (presumably Bi^{5+}) [10]. The presence of bismuth in additional oxidation states (e.g., Bi^+, Bi^{2+} and Bi^{5+}) has also been suggested by, e.g., X-ray photoelectron spectroscopy [2,11], indicating that the redox chemistry of bismuth in glasses and glass-forming liquids is more complex than first assumed. Currently, this has prevented knowledge-based tools for exploiting ultrabroad NIR photoluminescence of bismuth-doped glasses, and even the nature of the NIR emitting center remains highly debated [5].

Luminescence from Bi^{3+} and Bi^{2+} occurs in the blue and red spectral ranges, respectively [11–13]. The origin of NIR luminescence has been ascribed to Bi^+ and subvalent species [4], and Bi ion clusters such as Bi_2^-, Bi_2^{2-} [14,15], or Bi_5^{3+} [16,17]. In addition, the highly oxidized valence state of bismuth, i.e., Bi^{5+} [15,18] has also been suggested as a source for NIR photoluminescence.

Several different approaches have been attempted to obtain and optimize NIR luminescence from bismuth-doped glasses by manipulating the oxidation state of bismuth. These approaches include controlling the optical basicity of the glass [19–21], controlling the melting atmosphere and temperature [22,23], adding oxidation [24] or reduction agents [23] to the batch, tempering the glass [23], crystallizing the glass [25], and irradiating the glass with femtosecond lasers, γ-rays, or high-energy electron rays [26–28]. Based on these previous efforts it can be stated that the occurrence of NIR-active Bi species is highly sensitive to numerous parameters [29] and that its optimization requires delicate tuning of all parameters which affect the oxidation state of bismuth [23].

Heat-treatment of a glass in a reducing atmosphere offers several levers for such tuning (i.e., gas type, partial pressure, temperature, and duration) [30]. It has been shown that the luminescence properties of rare earth-doped silicate [31], aluminosilicate [32], alkali borosilicate [33], and alkali aluminosilicate [33] glasses can be tuned through

* Corresponding author at: Otto-Schott-Institute, University of Jena, Fraunhoferstrasse 6, Jena D-07743, Germany. Tel.: +49 3641 9 48501; fax: +49 3641 9 48502.
E-mail address: lothar.wondraczek@uni-jena.de (L. Wondraczek).

0022-3093/$ – see front matter © 2012 Elsevier B.V. All rights reserved.
http://dx.doi.org/10.1016/j.jnoncrysol.2012.09.021

Journal of
Ceramic Science
and Technology

J. Ceram. Sci. Tech., 03 [04]181-188 (2012)
DOI: 10.4416/JCST2012-00018
available online at: http://www.ceramic-science.com

Surface Strengthening of Extrusion-Formed Polymer/Filler-Derived Ceramic Composites

L. Schlier*[1], N. Travitzky[1], J. Gegner[2], P. Greil[1]

[1]Department of Materials Science, (Glass and Ceramics), University of Erlangen-Nuernberg, Martensstr. 5, 91058 Erlangen, Germany
[2]Department of Material Physics, SKF GmbH, Gunnar-Wester-Str. 12, 97421 Schweinfurt, Germany

received June 4, 2012; accepted July 25, 2012

Abstract

Surface nitridation of extrusion-formed Fe-Si-Cr-filler-loaded polysiloxane polymer filaments was investigated. After the filaments were exposed to a nitrogen atmosphere at temperatures above 1000 °C, a gas-solid reaction caused the formation of a nitridation reaction layer covering the filament surface. Thermo-chemical calculations of equilibrium phase compositions at different nitrogen activity suggest the formation of Si_2N_2O and Si_3N_4 near the filament surface (high nitrogen content) whereas SiC and unreacted $CrSi_2$ and FeSi dominate in the core region (low nitrogen content), which was confirmed by means of XRD analyses. Compared to filaments annealed in an inert Ar atmosphere (no nitride reaction layer), specimens covered with a nitride surface layer of only 20 µm in thickness obtained a bending strength increment of + 35 % (mean fracture stress 400 MPa). The improved mechanical properties were attributed to a pronounced volume increase triggered by the nitride reaction, which gives rise to pore filling and crack healing. Since post-fabrication treatment in a reactive atmosphere is independent of the component shape and size, formation of a surface reaction zone with densified microstructure (reduced porosity and flaws) may offer a versatile route for improving the properties of bulk polymer-filler-derived ceramic components.

Keywords: Polymer derived ceramics, surface strengthening, reaction surface zone

I. Introduction

Polymer-derived ceramics (PDCs) were developed from a number of organo-silicon and organo-silicon-boron polymer precursors which upon thermal decomposition in an inert atmosphere (pyrolysis) yield ceramics in the systems Si-C-N-B-O [1]. PDCs with variable composition and an amorphous or crystalline microstructure were reported to offer excellent thermal stability [2] as well as interesting electric, piezoelectric, magnetic, optical and chemical properties [1]. The mechanical and tribological properties of PDCs and PDC-based composites may vary in a wide range. Maximum values for Young's modulus of 155 GPa, Vickers hardness of 26 GPa, fracture toughness of 3 $MPam^{1/2}$, and fracture strength of 1100 MPa can be found in the literature [3]. A superior creep resistance at temperatures even exceeding 1500 °C observed in Si-(B)-C-N-based PDCs [4] was attributed to the evolution of a nanodomain network of graphene that was hypothesized to support stress even at very high temperatures [5]. These property values, however, were often measured on specimens with a very small volume (a few mm^3) or low dimensionality (fibres, layers with thickness < 1 mm) with the application of nanotechniques. Current applications are therefore mainly limited to low-dimensional product shapes such as high-temperature-resistant fibres [6,7], coatings [8], joints and seals [9], micro- and macrocellular foams [10], sensor sheets [11] and micro electro-mechanical systems (MEMS) [12].

Enhancement of mechanical properties in bulk components with larger volume is hampered mainly by the problem of controlling the nano- and microstructure formation process under the constraints of limited transport of gaseous decomposition products and retardation of strain relaxation upon polymer-to-ceramic conversion. Since polymer-to-ceramic conversion involves a pronounced increase in density by a factor of 2–3 and a volumetric shrinkage that may exceed 50 %, porosity and crack formation are difficult to avoid in bulk-polymer-derived ceramic products [13]. Introducing non-reactive and reactive fillers that are able to compensate for the volume dilatation of the polymer phase with an appropriate expansion of a filler reaction phase successfully demonstrated near-net shape processing of complex-shaped polymer-derived functional components [14]. Loading of the polymeric precursor with solid filler powder (particles or fibres), however, may give rise to an increase in viscosity, which is likely to retard densification based on viscous flow (e.g. < 600 – 700 °C) and sintering (> 600 – 700 °C) required to achieve elimination of transient porosity upon polymer-to-ceramic conversion [15]. Reduction of residual porosity was achieved by application of stress-assisted consolidation techniques including pressure casting [3], warm-

* Corresponding author: lorenz.schlier@ww.uni-erlangen.de

Journal of
Ceramic Science
and Technology

J. Ceram. Sci. Tech., 03 [02] 81-88 (2012)
DOI: 10.4416/JCST2012-00003
available online at: http://www.ceramic-science.com

Robocasting of Alumina Lattice Truss Structures

T. Schlordt*, F. Keppner, N. Travitzky, P. Greil

Department of Materials Science, Glass and Ceramics, Friedrich-Alexander-University Erlangen-Nuernberg, Martensstr. 5, 91058 Erlangen, Germany

received January 20, 2012; received in revised form February 8, 2012; accepted February 25, 2012

Abstract

Robocasting of aqueous colloidal α-Al_2O_3 gels for manufacturing cellular ceramics with periodical lattice truss structures was investigated. Coagulation of gels loaded with 48 vol% α-Al_2O_3 was induced by adding CH_3COONH_4. The gels exhibit shear-thinning behavior, shear elastic moduli ranging from 6.7 to 390 kPa and yield-stresses from 25 to 570 Pa. Continuous filaments with a diameter of 0.5 mm were extruded with a deposition speed of up to 35 mm/s on a high-precision six-axis robotic system equipped with a single-screw micro-extruder. The lattice structures consist of alternating layers formed by a linear array of circular rods aligned parallel with a distance of 1 mm and an angle of 90° between alternating layers. After being dried for 12 h, the robocast grids were sintered in air at 1650 °C for 2 h resulting in a fractional strut density > 0.95, a mean filament diameter of 400 µm, a volume filling fraction of 0.49 (sealed walls) and 0.35 (meshed walls), and macro-cells in the deposition plane of quadratic shape with a mean area of 0.136 $mm^2 \pm$ 0.017 mm^2 Based on gravitation-driven viscous flow, model conditions for attaining free spanning ligaments were discussed.

Keywords: Robocasting, alumina gel, lattice truss structures

I. Introduction

Moldless robocasting of ceramics is a solid freeform technique working on the principle of continuous writing of a filament and layer-by-layer build-up of a three-dimensional filamentary preform [1,2]. Aqueous colloidal gels and colloid-loaded thermoplastic polymers were applied to demonstrate the capability of robocasting technology to manufacture three-dimensional preforms with excellent shape variability including high aspect walls as well as unsupported spanning structures [3]. While robocasting in air was successfully performed applying nozzles with diameters exceeding 500 µm, decoupling the deposition kinetics from the drying process by extrusion into a non-wetting oil bath allowed the generation of filament diameters smaller than 100 µm [4]. The dried extruded preform can be sintered without a separate debinding process as only a low organic content (< 3 wt%) is required. Applications include manufacturing of grid and lattice structures for composites, bone restoration and meshes for filters. Ceramic gels based on silica [1], alumina [5–7], mullite [8], lead-zirconate-titanate [9], tricalciumphosphate [10], hydroxyapatite [11], lead-magnesium-niobate (PMN) [12], porcelain [13] and barium-titanate [14] were applied to robocasting. Gelation was induced by lowering the pH-value, increasing the ionic strength or adding a polymeric flocculant. In order to prevent sedimentation and syneresis, cellulose derivatives were added which may give rise to appreciable yield-stress of the particle suspension [15]. Depending on the extrusion speed and rheological behavior, flow of a colloidal gel through the extrusion nozzle may cause a pronounced shear-rate gradient over the filament diameter. Plug-flow with an unyielded core and a surface region depleted of particles (slip-plane) was reported [4]. The opportunities and challenges of robocasting e.g. direct filament writing were surveyed in an excellent review by Lewis *et al.* [1].

In this work, a novel six-axis robot system was coupled to a single-screw micro-extruder to provide high geometrical precision and line control flexibility for continuous filament writing. Regular grids of alumina were manufactured with an aqueous-based alumina gel feedstock. The rheological behavior of the colloidal alumina gel was systematically varied by adding CH_3COONH_4 (NH_4Ac). Yield stress, shear elastic modulus and relaxation kinetics of the gel filaments were analyzed to select optimum parameters for control of shape and dimensional stability. Three-dimensional lattice truss structures of alumina were manufactured, and the potential of robot-assisted continuous filament deposition was demonstrated.

II Experimental Procedure

(1) *Preparation of the colloidal alumina gel*

An aqueous slurry containing 52 vol% (81 wt%) of a submicron α-Al_2O_3 powder (CT3000 SG, Almatis GmbH, Ludwigshafen, Germany, d_{50} = 0.35 µm, S_V = 8.3 m^2/g) was prepared in a tumbling mixer (Turbula T2F, Willi A. Bachofen AG, Muttenz, Switzerland) using ZrO_2 milling balls. The slurry contained 1.6 wt% NH_4-polymethacrylate dispersant (Darvan C-N, R.T. Van-

* Corresponding author: tobias.schlordt@www.uni-erlangen.de

nature COMMUNICATIONS

OPEN

ARTICLE

Received 18 May 2012 | Accepted 3 Sep 2012 | Published 9 Oct 2012

DOI: 10.1038/ncomms2109

Hybrid nanoparticle–microcavity-based plasmonic nanosensors with improved detection resolution and extended remote-sensing ability

Markus A. Schmidt[1,*], Dang Yuan Lei[1,*], Lothar Wondraczek[2], Virginie Nazabal[3] & Stefan A. Maier[1]

Optical nanosensors based on plasmonic nanoparticles have great potential for chemical and biological sensing applications, but their spectral detection resolution is severely constrained by their broad resonance linewidth, and their spatial sensing depth is limited to several tens of nanometres. Here we demonstrate that coupling a strong dipolar plasmonic resonance of a single metallic nanoparticle to the narrow bandwidth resonances of an optical microcavity creates a hybrid mode and discretizes the broad localized resonance, boosting the sensing figure-of-merit by up to 36 times. This cavity-nanoparticle system effectively combines the advantages of Fabry-Perot microresonators with those of plasmonic nanoparticles, providing interesting features such as remote-sensing ability, incident-angle independent resonances, strong polarization dependence, lateral ultra small sensing volume and strongly improved detection resolution. Such a hybrid system can be used not only to locally monitor specific dynamic processes in biosensing, but also to remotely sense important film parameters in thin-film nanometrology.

[1] The Blackett Laboratory, Department of Physics, Imperial College London, London SW7 2AZ, UK. [2] Otto-Schott-Institute, University of Jena, 07745 Jena, Germany. [3] Institute of Chemical Sciences of Rennes, Glass and Ceramics team, University of Rennes, Rennes, France. * These authors contributed equally to this work. Correspondence and requests for materials should be addressed to M.A.S. (email: m.schmidt@imperial.ac.uk).

International Journal of Applied Glass Science 3 [1] 44–52 (2012)
DOI:10.1111/j.2041-1294.2011.00076.x

INTERNATIONAL JOURNAL OF
Applied Glass
SCIENCE

Chemical Stability of $ZnO–Na_2O–SO_3–P_2O_5$ Glasses

Sergey Sirotkin, Robert Meszaros, and Lothar Wondraczek[*,†]

Department of Materials Science, University of Erlangen-Nuremberg, 91058, Erlangen, Germany

We report on chemical stability and corrosion behavior of highly depolymerized sulfophosphate glasses from the system $ZnO–Na_2O–SO_3–P_2O_5$ in aqueous solution, providing data on weight loss, ion release rates, and modifications of surface topology as a function of time, temperature and pH value. Observations seem consistent with the previously developed structural model of chemical heterogeneity, where cations Na^+ and Zn^{2+} cluster selectively in the vicinity of sulfate and phosphate anions, respectively.

Introduction

Sulfophosphate (SP) melts of the type $SO_3–P_2O_5–ZnO–Na_2O$ enable fabrication of surprisingly stable ionic glasses with glass transformation temperature T_g well below 400°C.[1] Partly based on phenomenological observations of apparently increasing chemical stability of pyrophosphate glasses when adding sulfate, such low-melting SP glasses have been proposed for, for example, waste vitrification,[2] photonic applications[3] or as reinforcing phase in structural glass-polymer composites. Although each of these applications relies on significant corrosion stability, neither quantitative nor semi-quantitative data are presently available. On the other hand, also low corrosion stability (viz., high or tunable dissolution rates) could be of interest for other types of applications, for example, in biomedicine.

As has recently been demonstrated by nuclear magnetic resonance spectroscopy, Raman spectroscopy, and small angle X-ray scattering, SP glasses represent an interesting class of glasses where short- and mid-range structures are largely determined by fluctuations in chemistry and density (G. G. S. Reibstein, J.-P. Simon, and L. Wondraczek, unpublished data).[4] Depending on composition, the glass lattice may be understood as a pyrophosphate-type network of highly depolymerized $[POO_{3/2}O_2]^{2-}$ (Q^1), $[POO_{0/2}O_3]^{3-}$ (Q^0) and $[SO_4]^{2-}$-groups where cations locate selectively around either the sulfate or a phosphate species. By controlled thermal treatment, this chemical heterogeneity may then evolve to microscopic separation of sulfate and phosphate-rich phases and subsequent crystallization (G. G. S. Reibstein, J.-P. Simon, and L. Wondraczek, unpublished data). In this setting, also the dissolution behavior in aqueous solution should, on the one side, resemble dissolution of phosphate glasses but, on the other side, exhibit pronounced consequences of structural heterogeneity. The role of $[SO_4]^{2-}$ is not obvious, particularly regarding its apparent stabilizing effect.

Mechanisms of corrosion and dissolution of phosphate glasses are now well established.[5–7] The uniform

*Member, The American Ceramic Society.
†lothar.wondraczek@fmw.uni-erlangen.de

journal

J. Am. Ceram. Soc., 95 [2] 684–689 (2012)
DOI: 10.1111/j.1551-2916.2011.04836.x

Tape Casting of ITO Green Tapes for Flexible Electroluminescent Lamps

Nadja Straue, Martin Rauscher, Martina Dressler, and Andreas Roosen[†,*]

Department of Materials Science, Glass and Ceramics, University of Erlangen-Nuremberg, Erlangen, Germany

Indium tin oxide (ITO) is a widely applied optoelectronic material. However, conventionally, it is deposited via cost- and energy-intensive physical vapor deposition processes (PVD) like sputtering, resulting in rather brittle layers. In this report, the tape casting process is presented as an alternative processing route for the manufacture of transparent, conductive ITO layers. Tape casting is a particle-based technique, thus ITO nano-particles are first dispersed and stabilized in organic solvents. Subsequently, slurries are prepared using polyvinyl butyral binder and benzyl phthalate plasticizer. The rheological behavior of the slurries is analyzed and adapted to the tape casting process. After tape casting, the ITO green tapes are characterized concerning their electrical and optical behavior. Optical transmission up to 75% and electrical resistances down to 2 Ω·cm are reached without any further treatment. The ITO layers which exhibit such values are already suitable for applications in certain electronic devices. In this study, the applicability of the ITO green tapes is demonstrated by the assembly of functional, fully flexible electroluminescent lamps, which are laminated using the ITO green tapes as well as other functional green tapes in the as-deposited state.

I. Introduction

TRANSPARENT, conductive oxides (TCOs) are important materials for many electronic applications, such as touch panels, solar cells, and display applications.[1,2] One of the most prominent members in the group of TCOs is tin-doped indium oxide (indium tin oxide, ITO), which exhibits excellent transparency in the visible regime with transmission values above 85% and specific electrical resistances down to 10^{-4} Ω·cm for sputtered layers.[1,3,4] Conventionally, ITO is deposited via physical vapor deposition (PVD) processes like sputtering or pulsed-laser deposition.[5] These processes have two major drawbacks: first, cost- and energy-intensive vacuum technology is needed; second, the obtained layers are very brittle.[6] These drawbacks can be overcome by printing ITO nano-particle/polymer composites. Printing processes in ambient conditions are highly economical. Furthermore, in the composite, the ITO particles provide electrical conductivity, whereas the polymer matrix yields flexibility, that is, the specific properties of both materials are combined. Furthermore, this provides the opportunity to realize new, innovative electronic devices, such as flexible displays and bendable electroluminescent lamps. To date, only few publications about the processing of conductive ITO polymer composites exist.[7,8] Most of the articles report innovations in nano-particle synthesis[9,10] or printing of sol–gel precursors.[11,12]

In this report, the tape casting process, which is widely applied for the manufacture of multilayer devices, is used to manufacture ITO green tapes. The tape casting process is highly economical and can be easily scaled up.[13–15] The functionality of the ITO tapes will be proven by the assembly of electroluminescent (EL) lamps, which can be understood as "luminescent capacitors."[16,17] A schematic drawing of an EL lamp is shown in Fig. 1, in which the materials used in this work and their function in the EL lamp are denoted.

II. Experimental Procedure

(1) Manufacture and Characterization of ITO Slurries

For the manufacture of flexible ITO tapes, spherically shaped ITO particles from Evonik Degussa GmbH were used (VP ITO TC 8; Evonik Degussa GmbH, Hanau, Germany). The powder exhibited a specific surface area of 47.6 m^2/g, which was determined by BET (ASAP 2000; Micromeritics Instrument Corp., Norcross, GA). This corresponds to a diameter of 19 nm. As reported earlier,[18,19] these particles can be stabilized and dispersed in ethanol with the carboxylic acid 2-[2-(2-methoxyethoxy)ethoxy] acetic acid (Sigma Aldrich, Milwaukee, WI), also called 3,6,9-trioxadecanoic acid or TODA. Thus, ethanol-based dispersions with varied solids content in the range of 3.0–10.9 vol% and 0.18 vol% TODA with respect to the solids content were prepared in PE bottles with yttrium-stabilized zirconia milling balls ($d \sim 1.5$ mm). The dispersions were de-agglomerated in a tumbling mixer (Turbula, Willy A. Bachofen AG, Basel, Switzerland) for 24 h. After this treatment, the dispersions exhibited agglomerate sizes $d_{50,vol}$ in the range of 80–120 nm, which were determined by dynamic light scattering measurements (Ultra Fine Particle Analyzer UPA150; Microtrac, North Largo, FL). Subsequently, polyvinyl butyral binder (PVB, Butvar B-98; Solutia Inc., St. Louis, MO) and benzyl phthalate plasticizer (Santicizer 261A; Ferro Corp., Cleveland, OH) were added. The PVB binder exhibited a molecular weight of 40 000–70 000 g/mol and ~80 wt% polyvinyl butyral. The slurries were homogenized in the tumbling mixer with milling balls for 24 h. Subsequently, the milling balls were separated from the slurries using steel screens. Slurries were degassed in a rotary evaporator (Rotavapor EL, Büchi Laboratoriums-Technik GmbH, Essen, Germany) at 200 mbar for 30 min. The compositions of the prepared slurries and the resulting green tapes are shown in Table I. Slurries are denominated according to their binder to ITO ratio, for example, the slurry with 8.8 vol% PVB and 8.8 vol% ITO is denominated as S1.00.

The rheological behavior of the ITO slurries was characterized using a rheometer in a cone plate arrangement with a cone diameter d_{cone} of 50 mm and a cone angle of

Fig. 1. Schematic diagram of an electroluminescent lamp.

R. Moreno—contributing editor

Manuscript No. 29678. Received May 03, 2011; approved August 05, 2011.
*Member, The American Ceramic Society.
†Author to whom correspondence should be addressed. e-mail: andreas.roosen@ww.uni-erlangen.de

Journal of Non-Crystalline Solids 358 (2012) 1032–1037

Contents lists available at SciVerse ScienceDirect

Journal of Non-Crystalline Solids

journal homepage: www.elsevier.com/locate/jnoncrysol

Micromechanical properties of (Na,Zn)-sulfophosphate glasses

Simon Striepe [a], Ning Da [b], Joachim Deubener [a,*], Lothar Wondraczek [b]

[a] Institute of Non-Metallic Materials, Clausthal University of Technology, Zehnternstraße 2a, 38678 Clausthal-Zellerfeld, Germany
[b] Department of Material Science, Friedrich-Alexander-University of Erlangen-Nuremberg, Martensstraße 5, 91058 Erlangen, Germany

ARTICLE INFO

Article history:
Received 19 December 2011
Received in revised form 23 January 2012
Available online 20 February 2012

Keywords:
Sulfophosphate glasses;
Elastic constants;
Hardness;
Crack resistance;
Brittleness

ABSTRACT

Elastic constants, hardness and crack initiation resistance of sulfur-bearing sodium-zinc-phosphate glasses were determined by ultrasonic echography and Vickers indentation experiments. Incorporation of up to 35 mol% of sulfur into the glass structure resulted in a decrease in molar volume of 23% and an increase of Poisson's ratio up to a value of ~0.32. Resistance against permanent deformation and cracking decreased with compaction of the glass structure, i.e. a more brittle character of softer sulfophosphate glasses was observed when tested under normal atmosphere. Under flowing N_2 gas only a weak compositional dependence of the crack-to-indent size ratio was evident, which indicates that surface reactions dominate micromechanical crack initiation in sulfophosphate glasses.

1. Introduction

Glass formation in the alkali-zinc-sulfophosphate system has been pioneered by Mamoshin and colleagues in the 1980s, e.g. as potential materials for the vitrification of sulfatic wastes [1–3]. Later, low-melting sulfophosphate glasses (T_g <400 °C) received considerable attention as lead-free candidate for sealing applications, polymer co-forming [4–6] and recently for infiltration of various types of preforms [7,8]. Sulfur is mainly incorporated into sulfophosphate glasses as isolated SO_4^{2-} groups [9], whereby replacing P_2O_5 with SO_3 results in a progressive depolymerization of the phosphate network, i.e. increase of the ionic character. In this way, the glass forming region was extended to compositions with an average number of non-bridging oxygen per phosphate anion of more than 3.5 [10]. To control the hot forming processes connected with these potential applications a detailed study on melt rheology ($T>T_g$) was carried out, which show that the shift from PO_4^{3-} to SO_4^{2-} structural units decreases the kinetic fragility of the melts and results in gradually decreasing glass transition and softening point [10]. At the same time a sub-T_g relaxation phenomena was evident and correlated to sulfate structural units decoupled from the phosphate network [11]. Further, a stabilizing influence of sulfate structural units (reduced humidity attack at room temperature) was reported in sulfophosphate glasses [11,12] although the accompanying depolymerization of the phosphate network structure is known to result in poor chemical resistance. This specific behavior was related to topological heterogeneity and early-stage phase separation [13]. For the preferred use of sulfophosphates as seals and solders, practical strength, i.e. flaw tolerance, and therefore brittleness are of fundamental interest since mechanical loading of the glasses during preparation and service has to be considered. For their specific structural compartment, sulfophosphate glasses, beyond concrete applicability, further appear as an interesting reference material for examining the topological origin of mechanical properties [14].

However, to our best knowledge, the influence of the sulfate solubility in phosphate glasses on micromechanical properties has so far not been investigated.

To fill this gap we report in the present study on elastic constants such as Young's modulus and Poisson's ratio and on the resistance against plastic deformation and cracking of a series of glasses in the system ZnO–Na_2O–SO_3–P_2O_5 using ultrasonic echography and Vickers indentation experiments.

2. Experimental

2.1. Glass preparation

Glasses of the pseudo-ternary glass forming system $Zn_2P_2O_7$–$Na_2ZnP_2O_7$–$ZnSO_4$ (Fig. 1) were prepared from mixtures of Na_2CO_3, ZnO, $ZnSO_4 \cdot 7H_2O$ and $NH_4H_2PO_4$ (p.a., Fluka Analytical). The glass series S0–S70 was fabricated, starting from the eutectic pyrophosphate $0.58Na_2O \cdot 1.42ZnO \cdot P_2O_5$ at S0 and stepwise adding $ZnSO_4$ (Table 1). Each glass batch (ca. 100 g, 90Pt-10Rh crucible) was heated in an electrical resistance furnace in air up to 573 K at 10 K min^{-1}, dwelled for 3 h and then heated at 3 K min^{-1} to the melting temperature of 1073 K (S0–S40) and 1173 K (S50–S70), respectively. After melting for 1 h the liquefied material was poured into a pre-heated graphite mould and subsequently annealed in a muffle at 573 K for 1 h before shutting down the power supply to allow cooling (approx.

* Corresponding author. Tel.: +49 5323 722463; fax: +49 5323 723710.
E-mail address: joachim.deubener@tu-clausthal.de (J. Deubener).

0022-3093/$ – see front matter © 2012 Elsevier B.V. All rights reserved.
doi:10.1016/j.jnoncrysol.2012.01.045

JOURNAL OF TISSUE ENGINEERING AND REGENERATIVE MEDICINE
J Tissue Eng Regen Med (2012)
Published online in Wiley Online Library (wileyonlinelibrary.com) DOI: 10.1002/term.1511

RESEARCH ARTICLE

Induction of bone formation in biphasic calcium phosphate scaffolds by bone morphogenetic protein-2 and primary osteoblasts

LA Strobel[1], SN Rath[1], AK Maier[2], JP Beier[1], A Arkudas[1], P Greil[2], RE Horch[1] and U Kneser[1]*
[1]*Department of Plastic and Hand Surgery, University of Erlangen Medical Center, Friedrich-Alexander-University of Erlangen-Nürnberg, Germany*
[2]*Department of Materials Science and Engineering, Friedrich-Alexander-University of Erlangen-Nürnberg, Germany*

Abstract

Bone tissue engineering strategies mainly depend on porous scaffold materials. In this study, novel biphasic calcium phosphate (BCP) matrices were generated by 3D-printing. High porosity was achieved by starch consolidation. This study aimed to characterise the porous BCP-scaffold properties and interactions of osteogenic cells and growth factors under *in vivo* conditions. Five differently treated constructs were implanted subcutaneously in syngeneic rats: plain BCP constructs (group A), constructs pre-treated with BMP-2 (group B; 1.6 μg BMP-2 per scaffold), seeded with primary osteoblasts (OB) (group C), seeded with OB and BMP-2 (group D) and constructs seeded with OB and pre-cultivated in a flow bioreactor for 6 weeks (group E). After 2, 4 and 6 weeks, specimens were explanted and subjected to histological and molecular biological analyses. Explanted scaffolds were invaded by fibrovascular tissue without significant foreign body reactions. Morphometric analysis demonstrated significantly increased bone formation in samples from group D (OB + BMP-2) compared to all other groups. Samples from groups B-E displayed significant mRNA expression of bone-specific genes after 6 weeks. Pre-cultivation in the flow bioreactor (group E) induced bone formation comparable with group B. In this study, differences in bone distribution between samples with BMP-2 or osteoblasts could be observed. In conclusion, combination of osteoblasts and BMP-2 synergistically enhanced bone formation in novel ceramic scaffolds. These results provide the basis for further experiments in orthotopic defect models with a focus on future applications in orthopaedic and reconstructive surgery. Copyright © 2012 John Wiley & Sons, Ltd.

Received 16 September 2011; Revised 28 January 2012; Accepted 4 February 2012

Keywords **biphasic calcium phosphate; bioreactor; BMP-2; bone morphogenetic protein; flow perfusion; osteoblasts; scaffolds**

1. Introduction

Since the late 1980s, tissue engineering has been one of the key technologies in regenerative medicine. With regard to bone tissue, an approach based on a patient's own cells, suitable growth factors and 3D scaffolds has been proposed (Bruder and Fox, 1999; Pneumaticos *et al.*, 2010). For this purpose, scaffolds were used as carriers for cells and growth factors. Scaffold material properties and porosity must allow cell adhesion, migration, proliferation and differentiation.

Biphasic calcium phosphate (BCP) ceramics consist of a mixture of hydroxyapatite (HA) and beta-tricalcium phosphate (β-TCP). HA and β-TCP play an important role in hard tissue repair because of their similarity to the minerals in human bone and their outstanding bioactivity (Pilliar *et al.*, 2001; Eyckmans *et al.* 2010). Combining the reactivity of β-TCP and the stability of HA enhances bioactivity with retained degradability (Hutmacher *et al.*, 2007). To realise complex and controllable internal structures, 3D-printing as a manufacturing technique is widely used in biomaterial fabrication (Seitz *et al.*, 2005).

Correspondence to: Ulrich Kneser, M. D., Department of Plastic and Hand Surgery, University of Erlangen Medical Center, Friedrich-Alexander-University of Erlangen-Nürnberg, Krankenhausstrasse 12, D-91054 Erlangen, Germany. E-mail: ulrich.kneser@uk-erlangen.de

REVIEW/CRITICAL ASSESSMENT

Processing of ceramic–metal composites

N. Travitzky*

Design and development of advanced materials for high performance applications and bringing these materials into use are the most challenging tasks of modern engineering. Ceramic–metal composites are natural candidates for these demanding applications due to their very attractive properties. Various processing techniques have been used to fabricate ceramic–metal composites. Melt infiltration is one of the preferred techniques to fabricate ceramic–metal composites. Ceramic–metal composites have been fabricated using non-reactive and reactive pressureless and pressure assisted processing techniques. Owing to the inability of current processing technology to fabricate complex shaped ceramic–metal parts with desired microstructures and properties, additive manufacturing is becoming an increasingly important processing approach. Additive manufacturing in combination with infiltration methods was used for the fabrication ceramic–metal composites with a complex geometry.

Keywords: Ceramic–metal composites, Processing, Reactive processing, Melt infiltration, Additive manufacturing

This paper is part of a special issue on Novel Advanced Ceramic and Coating Processing

Introduction

Advanced ceramics for high performance applications

Design and development of advanced ceramics for high performance applications ranging from automotive to aerospace and defense oriented applications are the most challenging tasks of modern engineering. Examples of current and future applications of advanced ceramics are summarised in Table 1.[1,2] It is an incontrovertible fact that the need for advanced ceramics primarily depends on the growth of end-use markets. On the other hand, technological innovations have continuously contributed to performance and productivity improvements that stimulated extension of the use of advanced ceramics in key sectors. Advanced ceramic materials offer a high potential for high performance applications due to their exceptional mechanical properties (such as high hardness and wear resistance), high Young's modulus and strength/weight ratio, high creep resistance, chemical stability from ambient to peek operation temperatures and radiation resistance. The electrical, optical and thermal properties may be tailored in a wide range by control of microstructure variations. Depending on the composition, the advanced ceramic materials can be classified into oxides, carbides, nitrides, borides and silicides of metals such as aluminium, silicon, titanium, zirconium or a combination thereof. Depending on the kind of application, advanced ceramics can be categorised into functional and structural materials (Table 1). In the last two decades, diversification of functional ceramics has shown remarkable development, while applications of structural ceramics have experienced a steady growth.[2]

An increase in the functionality of structural ceramics has become important in terms of development strategy. In spite of the outstanding properties, the wide use of ceramics in modern mechanical engineering is limited because of their low toughness compared to metals and limited experience in design with brittle materials, particularly in metal oriented industries. In addition, the current restrictions of today's structural ceramics to niche products for pump components or textile machinery, for example, result from high manufacturing expenditure and limited shaping freedom, particularly for complex near net shape three-dimensional (3D) parts. The one last mentioned is of great importance because the post-hard machining of ceramics is time consuming and an expensive process, which commonly requires diamond tools and thus incurs in many cases up to 80% of the overall manufacturing costs of a ceramic product.

The above mentioned remarks clearly demonstrate the necessity for new ceramic based materials and processes that give better combination of properties for excellent performance. The key advantages of advanced processing of these materials should include low cost manufacturing, flexibility in composition and morphology of the final microstructures, near net shape capability, potential to fabricate graded composites and avoiding health hazards associated with fine particles.

Ceramic–metal composites: properties and applications

In contrast to metals, which are able to exhibit plastic deformation before fracture due to the high mobility of dislocations, ceramics do not show plasticity at ambient temperatures. Owing to plastic deformation, the fracture process in metals involves extensive energy dissipation. The absence of such energy dissipating phenomenon in

University of Erlangen-Nuremberg, Erlangen, Bavaria, Germany

*Corresponding author, email nahum.travitzky@ww.uni-erlangen.de

Published by Maney on behalf of the Institute
Received 14 November 2011; accepted 7 December 2011
DOI 10.1179/1743676111Y.0000000073

journal

J. Am. Ceram. Soc., 95 [11] 3387–3393 (2012)
DOI: 10.1111/j.1551-2916.2012.05368.x

Sintering of 3D-Printed Glass/HAp Composites

Alexander Winkel,[‡] Robert Meszaros,[‡] Stefan Reinsch,[§] Ralf Müller,[§] Nahum Travitzky,[‡] Tobias Fey,[‡] Peter Greil,[‡] and Lothar Wondraczek[‡,†]

[‡]Chair of Glass and Ceramics, Department of Materials Science and Engineering, University of Erlangen-Nuremberg, Erlangen 91058, Germany

[§]BAM Federal Institute for Materials Research and Testing, Berlin 12484, Germany

We report the sintering of 3D-printed composites of 13-93 bioactive glass and hydroxyapatite (HAp) powders. The sintering process is characterized on conventionally produced powder compacts with varying HAp content. A numeric approximation of the densification kinetics is then obtained on the basis of Frenkel, Mackenzie–Shuttleworth, and Einstein–Roscoe models, and optimized sintering conditions for 3D-printed structures are derived. Fully isotropic sintering of complex cellular composites is obtained by continuous heating to 750°C at a rate of 2 K/min for a HAp content of 40 wt%. The approach can readily be generalized for printing and sintering of similar glass-ceramic composites.

I. Introduction

BIOACTIVE glasses and glass-ceramic composites are receiving continuous attention for bone and tissue replacement in unloaded conditions.[1–3] Depending on composition, they may exhibit different kinds of bioactivity such as, e.g., supporting growth and proliferation of various cell types.[4–7] Most of today's processing routes for the preparation of bioactive glass bodies rely on sintering powder-derived green bodies. Such green bodies may be prepared in various geometries and degrees of porosity by, e.g., replica forming,[8,9] tape casting,[10,11] gel casting,[12] or additive manufacture.[13,14] Sintering inherently requires high processing temperature, what may lead to recrystallization of the employed glass. Although the effect of crystallization on bioactivity is still debated (e.g., 15 and 16), processes and glass compositions are typically sought to avoid crystallization.[7,17–23] As one example, glasses of the type (wt%) $6Na_2O$–$12K_2O$–5MgO–20CaO–4 P_2O_5–$53SiO_2$ ("13-93", Refs. 24 and 25) have been developed to provide a broad working range. Crystallization-free sintering of this glass can be performed within the process window of about 650°C–730°C.[14]

Sintering of glass powders inherently relies on viscous flow. Depending on the initial green body density, this is typically associated with high and anisotropic shrinkage. Especially larger or complex parts may deform significantly as a result of gravity, surface tension, intrinsic strain or temperature and density gradients. This complicates congruent or net-shape processing of such parts by, e.g., three-dimensional (3D) printing.[14] On the other side, such 3D manufacturing processes are almost always motivated by qualitative reproduction of specific, often complex target geometries. To overcome this problem, glass-ceramic composite structures may be considered, where the glass fraction and, hence, the extent of viscous sintering is reduced and a secondary, stiff phase is used to geometrically stabilize the green body during sintering, to reduce overall shrinkage, and to improve fracture toughness and strength of the final part. For this purpose, the present report focuses on compoundation of bioactive glass type 13-93 and crystalline hydroxyl apatite (HAp) powder to produce 3D scaffolds by printing and subsequent sintering. Besides particle fraction and HAp content, the impact of various processing parameters such as type and content of binder, and isothermal and non-isothermal sintering conditions are considered. On the basis of Frenkel,[26] Mackenzie–Shuttleworth,[27] and Einstein–Roscoe[28] models, a previously developed approximation[29,30] is used to predict sintering kinetics and to optimize sintering conditions.

II. Experimental Procedure

(1) Glass Synthesis and Compoundation

By melting a batch of 300 g of reagent grade raw materials for 1 h at 1400°C 13-93 type bioactive glass was synthesized (see also Ref. 14). Glass frit was produced by quenching in water. An additional slab of bulk glass was produced to prepare samples for dilatometry and 3-point bending viscometry by casting the melt into a carbon mold and subsequent annealing at 600°C for 1 h. Glass viscosity was measured using beam bending viscometry (VIS 401; Baehr, Huellhorst, Germany) in the regime of ~10^{12}–10^{9} dPa·s and concentric cylinder rotational viscometry (VT550; Haake, Erlangen, Germany) in the regime of <10^{6} dPa·s. The glass transition temperature T_g = 600°C and the thermal expansion coefficient $CTE_{60°C–550°C} = 13.5 \times 10^{-6}$ K^{-1} were measured using differential scanning calorimetry (DSC, 404 F1 Pegasus; Netzsch, Selb, Germany, Pt crucibles) and horizontal dilatometry (DIL 402 C; Netzsch), respectively. The viscosity–temperature dependence η (T) of the employed glass was interpolated by the VFT-equation, $\log [\eta/\text{Pa·s}] = -2.25 + 3797°C/(T-335°C)$ (note that a more accurate VFT-fit was obtained as compared to Ref. 14 because of the inclusion of high-temperature data). Glass density ρ_G = 2.66 g/cm^3 ±0.001 g/cm^3 was determined on bulk glass samples via the Archimedes method (AG 204; Mettler-Toledo, Gießen, Germany). The frit was crushed to a size of about 2 mm in a jaw crusher (Pulverisette 1; Fritsch, Idar-Oberstein, Germany) and subsequently ball-milled in a porcelain containment using alumina balls (diameter of 10 mm). The final milling step was carried out in an agate swing mill (TS 100A; Siebtechnik GmbH, Mülheim-Ruhr, Germany). Powder batches of three different particle size distributions were produced by milling for different time periods, i.e., d_{50} = 3, 8, and 14 μm, respectively (Mastersizer 2000; Malvern Instruments, Malvern, Great Britain, see inset of Fig. 1). Reference glass powder compacts of cylindrical shape were produced from a molding paste by position-controlled uniaxial pressing of a constant mass of powder (60 MPa, Ø = 5 mm,

H.-E. Kim—contributing editor

Manuscript No. 30507. Received October 24, 2011; approved June 14, 2012.
[†]Author to whom correspondence should be addressed. e-mail: lothar.wondraczek@uni-jena.de

Luminescence from bismuth-germanate glasses and its manipulation through oxidants

A. Winterstein,[1] S. Manning,[2] H. Ebendorff-Heidepriem,[2] and L. Wondraczek[1,3,*]

[1]*Department Material Science, University of Erlangen-Nuremberg, 91058 Erlangen, Germany*
[2]*Institute for Photonics & Advanced Sensing, The University of Adelaide, Adelaide, SA 5005, Australia*
[3]*Otto-Schott-Institute, University of Jena, 07745 Jena, Germany*
*lothar.wondraczek@uni-jena.de

Abstract: We report on the luminescence properties of bismuth-germanate glasses in which the speciation of bismuth is controlled via addition of CeO_2 as an oxidant. A glass system with the composition $(70.5\text{-}x)GeO_2$ – $24.5Bi_2O_3$ – $5WO_3$: $xCeO_2$, with $x = 0...2.0$, is analyzed in terms of optical properties and redox states of bismuth and cerium. We show that optical transmission and luminescence in the visible to near-infrared (NIR) spectral range can be adjusted by the ratio of bismuth and cerium. Specifically, ultra-broad NIR luminescence spanning the range of 1000 – 1600 nm can be obtained for $x \leq 0.1$. This is of particular interest for application of this type of glass in fiber-optical amplifiers where no additional dopants would be required.

OCIS codes: (160.2750) Glass and other amorphous materials; (160.2540) Fluorescent and luminescent materials; (140.4480) Optical amplifiers; (060.4510) Optical communications.

References and links

1. K. Richardson, D. Krol, and K. Hirao, "Glasses for photonic applications," Int. J. Appl. Glass Sci. 1(1), 74–86 (2010).
2. M. Peng, C. Zollfrank, and L. Wondraczek, "Origin of broad NIR photoluminescence in bismuthate glass and Bi-doped glasses at room temperature," J. Phys. Condens. Matter 21(28), 285106 (2009).
3. J. Lucas, "Infrared fibers," Infrared Phys. 25(1-2), 277–281 (1985).
4. W. H. Dumbaugh and J. C. Lapp, "Heavy metal oxide glasses," J. Am. Ceram. Soc. 75(9), 2315–2326 (1992).
5. D. L. Wood, K. Nassau, and D. L. Chadwick, "Optical properties of new oxide glasses with potential for long-wavelength optical fibers," Appl. Opt. 21(23), 4276–4279 (1982).
6. S. S. Rojas, J. E. De Souza, M. R. B. Andreeta, and A. C. Hernandes, "Influence of ceria addition on thermal properties and local structure of bismuth germanate glasses," J. Non-Cryst. Solids 356(52-54), 2942–2946 (2010).
7. M. Peng, N. Da, S. Krolikowski, A. Stiegelschmitt, and L. Wondraczek, "Luminescence from Bi^{2+}-activated alkali earth borophosphates for white LEDs," Opt. Express 17(23), 21169–21178 (2009).
8. M. Peng and L. Wondraczek, "Photoluminescence of $Sr_2P_2O_7$:Bi^{2+} as a red phosphor for additive light generation," Opt. Lett. 35(15), 2544–2546 (2010).
9. M. Peng and L. Wondraczek, "Bi^{2+}-doped strontium borates for white-light-emitting diodes," Opt. Lett. 34(19), 2885–2887 (2009).
10. Y. Fujimoto and M. Nakatsuka, "Infrared luminescence from bismuth-doped silica glass," Jpn. J. Appl. Phys. 40(Part 2, No. 3B), L279–L281 (2001).
11. R. Cao, M. Peng, L. Wondraczek, and J. Qiu, "Superbroad near-to-mid-infrared luminescence from Bi_5^{3+} in $Bi_5(AlCl_4)_3$," Opt. Express 20(3), 2562–2571 (2012).
12. S. Khonthon, S. Morimoto, Y. Arai, and Y. Ohishi, "Luminescence characteristics of Te- and Bi-doped glasses and glass-ceramics," J. Ceram. Soc. Jpn. 115(1340), 259–263 (2007).
13. V. O. Sokolov, V. G. Plotnichenko, and E. M. Dianov, "Origin of broadband near-infrared luminescence in bismuth-doped glasses," Opt. Lett. 33(13), 1488–1490 (2008).
14. K. H. Nielsen, M. M. Smedskjaer, M. Peng, Y. Z. Yue, L. Wondraczek, communicated to J. Non-Cryst. Solids (2012).
15. W. A. Weyl, *Coloured Glasses*, 5th ed. (Sheffield: Society of Glass Technology, 1999).
16. M. Peng, B. Sprenger, M. A. Schmidt, H. G. Schwefel, and L. Wondraczek, "Broadband NIR photoluminescence from Bi-doped $Ba_2P_2O_7$ crystals: insights into the nature of NIR-emitting bismuth centers," Opt. Express 18(12), 12852–12863 (2010).

#172414 - $15.00 USD Received 11 Jul 2012; revised 13 Aug 2012; accepted 14 Aug 2012; published 31 Aug 2012

COMMUNICATION

ADVANCED ENGINEERING MATERIALS

DOI: 10.1002/adem.201100351

Extrusion Foaming of a Preceramic Silicone Resin with a Variety of Profiles and Morphologies**

By *Friedrich Wolff, Bruno Ceron Nicolat, Tobias Fey, Peter Greil* and *Helmut Münstedt**

Preceramic foams with a variety of profiles and morphologies were fabricated by a continuous foam extrusion process based on a single-screw extruder. A methyl silicone resin was used as the preceramic polymer and carbon dioxide as the foaming agent. Variations of the foam morphology were achieved by changing the key process parameters carbon dioxide content, foaming pressure, and foaming temperature. Samples of different porosities, cell densities, pore sizes, and pore size gradients were obtained. From these results, conditions for the fabrication of particular foam structures can be derived. Various foam profiles as rods, tapes, and tubes were extruded and pyrolysed into ceramic foams.

In case of ceramic foams the general properties of bulk ceramics such as high stiffness, strength, temperature stability, and chemical resistance can be combined with a low density, large surface area, and low thermal conductivity. Hence, ceramic foams have a great potential in high temperature thermal insulation, lightweight construction, filtering, and catalysis. Depending on the desired application, different foam geometries and morphologies are necessary since they strongly influence many properties. In literature there are reports on a variety of processing methods for ceramic foams leading to diverse foam morphologies (e.g. ref.[1–3]). The most important production routes are the replica method, the template method, and direct foaming. To obtain certain properties such as a hierarchical foam structure,[4] an open cell morphology,[5,6] or a bimodal cell size distribution[7] these methods can also be combined.

Many fabrication routes to ceramic foams are based on preceramic polymers since these materials enable a large degree of freedom in processing and design. The direct foaming of preceramic polymers is based on its thermoplastic behavior in the uncrosslinked state. Therefore, experience available on the foaming of conventional organic thermoplastics can be used.

Direct foaming is classified in physical foaming,[8–12] chemical foaming,[13–18] and a combination of both by co-blowing the preceramic polymer together with polyurethane.[17,19–24] In chemical foaming, either degradation products of an added blowing agent or volatile condensation products such as water or ethanol resulting from the crosslinking process are used for foaming. In both cases the generation of the gaseous foaming agent is strongly related to the crosslinking of the material due to the high temperatures that are necessary. Therefore, such processes are difficult to control. In physical foaming, however, process parameters like temperature, pressure, and amount of foaming agent can be varied in a wide range independently. Physical foaming of preceramic polymers was first investigated in a batch process.[8–11] The samples are saturated with carbon dioxide under high pressure in an autoclave. The foaming is initiated by a rapid pressure drop leading to a thermodynamic instability. This method is well suited to fundamentally assess the foaming properties of polymers,[11] however, it is only applicable on a laboratory scale.

In order to physically foam preceramic polymers on a technical scale, foam extrusion well known from organic thermoplastics (e.g. ref.[25–30]) was applied. Apart from a linear shrinkage of about 20% the ceramic foam obtained after pyrolysis was distinguished by maintaining the same morphology as the foamed polymer precursor.[12]

In this paper the versatility of this process is demonstrated. The foam morphology was varied by changing process

[*] *Prof. H. Münstedt, F. Wolff*
Institute of Polymer Materials,
University Erlangen-Nürnberg,
Martensstr. 7, D-91058 Erlangen, Germany
E-mail: helmut.muenstedt@ww.uni-erlangen.de
B. Ceron Nicolat, Dr. T. Fey, Prof. P. Greil
Institute of Glass and Ceramics,
University Erlangen-Nürnberg,
Martensstr. 5, D-91058 Erlangen, Germany

[**] *The authors acknowledge the financial support from the German Research Foundation (DFG) within the Cluster of Excellence "Engineering of Advanced Materials" at the University Erlangen-Nürnberg.*

APPLIED PHYSICS LETTERS **100**, 191911 (2012)

Sequential three-step three-photon near-infrared quantum splitting in β-$NaYF_4$:Tm^{3+}

D. C. Yu,[1] S. Ye,[1] M. Y. Peng,[1] Q. Y. Zhang,[1,a)] and L. Wondraczek[2]
[1]*State Key Laboratory of Luminescent Materials and Devices, and Institute of Optical Communication Materials, South China University of Technology, Guangzhou 510641, People's Republic of China*
[2]*Department of Materials Science, University of Erlangen-Nuremberg, 91058 Erlangen, Germany*

(Received 3 February 2012; accepted 24 April 2012; published online 10 May 2012)

We report on sequential three-step three-photon near-infrared (NIR) quantum splitting in Tm^{3+}-doped β-$NaYF_4$, where an incident blue photon around 470 nm is split into three NIR photons (1165, 1466, and 1800 nm). The underlying mechanism is analyzed by means of static and dynamic photoemission spectroscopy. Here, an experimental total quantum yield of ~32% is obtained. When quenching due to residual hydroxyl groups and other defect species can be overcome, numerical analyses indicate a theoretical maximum quantum yield of 158%, suggesting application in efficient spectral converters.
 [http://dx.doi.org/10.1063/1.4714505]

Efficient phosphor materials are key requisites for modern lighting and display devices.[1] Typically, they rely on optical down-conversion of incident high-energy radiation to photons of lower energy. Since the energy of a vacuum ultraviolet (VUV) photon is more than twice that of a visible photon, it is theoretically possible to split such a VUV photon into two visible photons, yielding a hypothetic quantum yield (QY) of up to 200%. Such two-(or more) photon luminescence phenomena have been referred to as quantum splitting (QS) or photon cascade emission (PCE).[2] Since the first demonstration of QS for deep-blue emission of Pr^{3+}-doped fluorides,[3–5] numerous studies have been conducted on this area with the specific focus on VUV-excited QS phosphors activated by rare-earth (RE) ions.[6–10] Similar to VUV-VIS QS, an UV-to-blue photon could be split into three or more near-infrared (NIR) photons.[2,11–18] If such a conversion process can be conducted efficiently, ideally for splitting one visible photon into three NIR photons, this could pave the way to ultra-efficient spectral converters, e.g., for photovoltaic applications, sensing, etc. Despite the importance of this issue, suitable pairs of activator and matrix material are presently not available.

In the present letter, we discuss the concept of sequential three-step three-photon NIR QS in Tm^{3+} singly doped β-$NaYF_4$. We demonstrate how upon excitation with a blue photon, three NIR photons can be obtained. Further development of an efficient triply splitting NIR phosphor might open a path towards ultra-efficient low-bandgap solar cells thermo-photovoltaic energy converters.[19–21]

Powder samples of $NaYF_4$:1%Tm^{3+} and $NaYF_4$:1%Tm^{3+}, 1%Yb^{3+} were synthesized through a facile hydrothermal procedure.[22] The crystal structure and habitus of the obtained products were characterized by means of x-ray powder diffractometry (XRD, Philips Model PW1830, Cu $K\alpha$) and scanning electron microscopy (SEM, JEOL JEM-1010). Luminescence spectra were determined on a high-resolution spectrofluorometer (Edinburgh FLS920) equipped with a static and a microsecond-pulse xenon (Xe) lamp as excitation sources. For time-correlated single photon counting (TCSPC), visible- and NIR-sensitive photomultiplier tubes (PMTs, Hamamatsu R928 and R5509-72) were employed. In addition and for reference, static mid-infrared (MIR) emission spectra were recorded with a PbSe photoconductive detector on a Horiba Jobin-Yvon Triax320 spectrofluorometer (450 W Xe lamp and 976 nm laser diode, LD, respectively, as the excitation sources). For measurement of the absolute QY, a barium sulfate coated integrating sphere with an inner diameter of 120 mm was mounted on the FLS920 system with the standard Xe lamp for excitation.

XRD patterns of the as-prepared samples generally confirmed the presence of $NaYF_4$ (JCPDS card no. 16-0334) as sole crystalline phase. As observed by SEM, crystals are present in the form of hexagonal micorods with a mean size of 1 μm in diameter and several microns in length. In Fig. 1, NIR photoluminescence (PL) spectra of $NaYF_4$:1%Tm^{3+} and $NaYF_4$:1%Tm^{3+}, 1%Yb^{3+} are shown. For $NaYF_4$:Tm^{3+} excited at 470 nm, typical emission bands of Tm^{3+} occur at 646 ($^1G_4 \rightarrow {}^3F_4$) and 804 nm ($^3H_4 \rightarrow {}^3H_6$) (inset of Fig. 1(a), see also Ref. 13). Intense NIR PL occurs in three bands at 1165, 1466, and 1800 nm. These bands are assigned to the electronic transitions of $^1G_4 \rightarrow {}^3H_4$, $^3H_4 \rightarrow {}^3F_4$ and $^3F_4 \rightarrow {}^3H_6$ in Tm^{3+},[13,22,23] respectively. For a rigorous investigation on the NIR emission process, additional PL spectra were recorded for excitation at 798 nm (monochromator) and 976 nm (LD). When the $NaYF_4$:Tm^{3+} sample is excited at 798 nm (Fig. 1(b)), only the bands at 1466 and 1800 nm can be observed ($^3H_4 \rightarrow {}^3F_4$ and $^3F_4 \rightarrow {}^3H_6$). In comparison, as shown in Fig. 1(c), in the co-doped sample, only the transition of $^3F_4 \rightarrow {}^3H_6$ (Tm^{3+}, 1800 nm) is obtained as a result of Stokes energy transfer (ET) from Yb^{3+} when exciting at 976 nm LD.[24,25] Noteworthy, the spectral response of the detectors which, for the NIR R5509-72 PMT, decreases sharply beyond the range of 1600 nm must be taken into account for data interpretation. For comparison, spectra were recorded also with an PbSe photoconductor with optimal spectral response in this wavelength regime (Fig. 1(c)).[22,23]

a)Author to whom correspondence should be addressed. Electronic mail: qyzhang@scut.edu.cn.

Journal of Alloys and Compounds 541 (2012) 323–327

Contents lists available at SciVerse ScienceDirect

Journal of Alloys and Compounds

journal homepage: www.elsevier.com/locate/jalcom

Enhanced NIR emission from nanocrystalline LaF_3:Ho^{3+} germanate glass ceramics for E-band optical amplification

W.J. Zhang [a,b], Q.J. Chen [a], J.P. Zhang [a], Q. Qian [a], Q.Y. Zhang [a,*], L. Wondraczek [b]

[a] State Key Lab of Luminescent Materials and Devices and Institute of Optical Communication Materials, South China University of Technology, Guangzhou 510641, PR China
[b] Department of Materials Science, University of Erlangen-Nuremberg, Erlangen 91058, Germany

ARTICLE INFO

Article history:
Received 2 May 2012
Received in revised form 10 June 2012
Accepted 18 June 2012
Available online 6 July 2012

Keywords:
Oxyfluoride glass ceramic
Ho^{3+} ions
Optical amplifiers
Infrared

ABSTRACT

Nanocrystalline LaF_3 germanate glass ceramics were prepared and used as host for optically active Ho^{3+} ions. LaF_3 crystallites precipitate by internal nucleation with sizes in the range of 7–17 nm. During crystallization, Ho^{3+} is incorporated into the fluoride lattice on La^{3+} sites, leading to reduced probability of multiphonon relaxation and, hence, significantly enhanced emissions within 1300–1440 and 1400–1550 nm wavelength range. Excited state absorption spectra, stimulated emission spectra and spectral gain coefficients of the ($^5S_2$, $^5F_4$) → $^5I_5$ transition indicate suitability of the material for E-band optical amplification.

1. Introduction

Continuously increasing demand for data transmission capacity of optical communication systems has been stimulating an ongoing search for fiber optical amplifiers which operate within the low-loss transmission window of OH-free silica fiber (1.2–1.7 μm) [1]. Ideally, this would be achieved by a material with broadband luminescence in the relevant spectral range, which has been demonstrated for doping with various transition and heavy metal ions such as Ni^{2+} [2,3] and various Bi-species [4]. At present, however, despite their much lower emission bandwidth, rare earth ions remain the dopant-of-choice because of superior emission cross-section and/or lifetime. Pr^{3+}-doped fiber amplifiers (PDFA, 1.3 μm) and Tm^{3+}-doped fiber amplifiers (TDFA, 1.4 μm) have been developed as additions to the commercially available Er^{3+}-doped fiber amplifier (EDFA, C-(1530–1565 nm) and L-(1565–1625 nm) bands) [5,6]. For complete exploitation of the silica transmission window, however, also the E-(1360–1460 nm) and U-(1625–1675 nm) bands must be covered. For this purpose, Ho^{3+} has been considered as a promising active ion for its ($^5S_2$, $^5F_4$) → $^5I_5$ and $^5I_5$ → $^5I_7$ radiative transitions [7–9]. Owing to the narrow gap between the fluorescing level and the next lower-lying level, these emissions can only be achieved in hosts with low phonon energy such as fluoride, selenide and chalcohalide glass systems [7,8]. From the point of view of real-world applicability, however, the poor chemical and mechanical properties of these matrix candidates remain a critical issue. So far, only oxyfluoride glass ceramics (GC) [10–13] which combine the low phonon energy of a crystalline fluoride lattice with the high chemical and mechanical stability of oxide glasses appear to overcome this problem. Recently, transparent Ho^{3+}-doped oxyfluoride GC have been reported as potential material for optical amplifiers operating at 0.75 and 1.2 μm [14,15].

In the present paper, we are considering precipitation of LaF_3 nanocrystallites which act as host for Ho^{3+} dopant in a matrix of germanate glass. Compared to silicate GC, gallate or bismuthate matrices, this provides even lower phonon energy [16,17] as well as lower melting temperature of the glass and, hence, more easy processing. The spectroscopic properties of the Ho^{3+} center are examined with particular attention to the emission bands and gain coefficients at 1.37 and 1.45 μm.

2. Experiments

GC samples were prepared by thermal precipitation of LaF_3 crystallites from precursor glasses (PG) with nominal molar composition of $(50-x)GeO_2$–$22Al_2O_3$–$13LaF_3$–$15LiF$–$xHoF_3$ (denoted as PGHx) (x = 0, 0.05, 0.1, 0.2, 0.4, and 0.8). For that, batched of properly mixed raw materials (analytical grade) were melted in covered corundum crucibles at 1350 °C for 1 h. The melts were then quenched on a preheated stainless steel plate and subsequently annealed at 450 °C for 2 h to remove residual stress. Transformation into visually transparent GC was conducted via a heat-treatment at 560 °C for 8 h (samples denoted as GCHx). Differential scanning calorimetry (DSC) was carried out on ground glass (PGH0.8) at a heating rate of 10 K/min to evaluate the characteristic temperatures of glass transformation and crystallization onset. For microstructural analyses, X-ray powder diffractometer (X' Pert PROX, Cu Kα) and transmission electron microscopy (TEM, JEM-2010) were employed. The density (ρ = 4.07 g/cm^3) of GCH0.4 was measured by the Archimedes method. The refractive index was obtained using a Metricon 2010 prism cou-

* Corresponding author. Tel.: +86 20 87113681.
E-mail address: qyzhang@scut.edu.cn (Q.Y. Zhang).

0925-8388/$ – see front matter © 2012 Elsevier B.V. All rights reserved.
http://dx.doi.org/10.1016/j.jallcom.2012.06.092

Proceedings

U. Deisinger, T. Fey, A. Roosen

Realisation of Large Cavities in Multilayer Ceramics by Cold Low Pressure Lamination and Their Characterisation by µCT

In: Proceedings 8th International Conference and Exhibition on Ceramic Interconnect and Ceramic Microsystems Technologies, 16th-19th April 2012, Erfurt, Germany. Ed.: IMAPS, Washington, D.C., USA, 2012, 263-268

Books

A. Roosen

Tape Casting

In: Ceramics Science and Technology: Synthesis and Processing. R. Riedel, I.W. Chen (eds.), Wiley-VCH Verlag GmbH, Weinheim, Germany, 2012, 39-62

4. CONFERENCES, WORKSHOPS, LECTURES, AWARDS

Conferences and Workshops Organised by Members of the Institute

A. Roosen

5th Advanced Training Course on „Tape Casting and Ceramic Multilayer Technology", University of Erlangen-Nuremberg, Germany, 14 February 2012

A. Roosen

Member of the Program Committee and Session Chair, Annual Meeting of the Deutsche Keramische Gesellschaft and Symposium of Advanced Ceramics Symposium, Nuremberg, Germany, 5-7 March 2012

A. Roosen

Session Chair, 8th International Conference and Exhibition on Ceramic Interconnect and Ceramic Microsystems Technologies, Erfurt, Germany, 16-19 April 2012

A. Roosen

General Chair of the DKG-Symposium „Joining of Ceramics", Erlangen, Germany, 4-5 December 2012

N. Travitzky

2nd meeting of the working group „Generative Manufacturing of Ceramic Components", Erlangen, Germany, 8 March 2012

N. Travitzky

Symposium Organiser: Materials Science & Technology Conference & Exhibition, Symposium: “Advanced Materials, Processes and Applications for Additive Manufacturing, Pittsburgh, Pennsylvania, USA, 07-11 October 2012

Annual glass week: Mr. Peter Reinhardt teaches Dr. Sergey Sirotkin in glass blowing

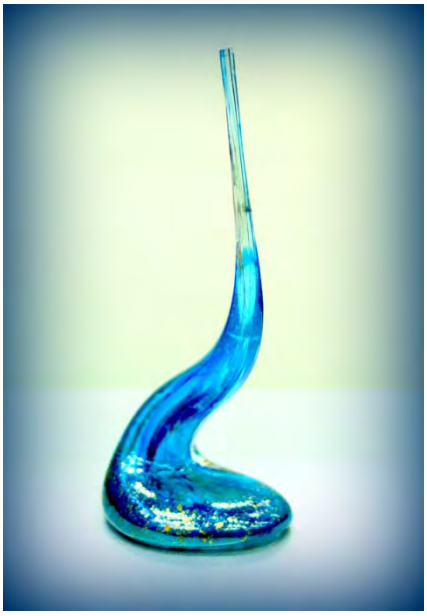

Some beautiful results of our homemade glass ware

Invited Lectures

U. Deisinger, A. Roosen

Manufacturing of multilayer LTCC ceramics

Annual Meeting of the "Deutsche Keramische Gesellschaft", Nuremberg, Germany, 5-7 March 2012

U. Deisinger, A. Roosen, A. Heunisch, T. Rabe

Processing of multilayer ceramics applying thermocompression

DKG-Symposium „Joining of Ceramics", Erlangen, Germany 4-5 December 2012

N. Travitzky, T. Schlordt, L. Schlier, J. Cypris, M. Weclas, **T. Fey**, R. Kaiser, P. Greil

Additive manufacturing of macro-cellular ceramic structures

36th International Conference and Exposition on Advanced Ceramics and Composites, Daytona Beach Florida, USA, 22-27 January 2012

T. Fey

Cellular ceramics

2nd International Symposium on Ceramics Nanotune Technology for Young Researchers, NITECh, Nagoya, Japan, 7-9 March 2012

T. Fey, B. Ceron-Nicolat, P. Greil

Ceramic foams from preceramic polymers

Ceramitec, Munich, Germany, 23 May 2012

T. Fey, N. Travitzky, A. Khosravani, P. Greil

Cellular ceramics by generative processing: microstructure and simulation,

MS&T 2012, Pittsburgh, PA, USA, 7-12 October 2012

P. Greil

Advancements in Polymer-Filler Derived Ceramics

ISASC 2012, Seoul, South Korea, 25-28 March 2012

P. Greil

Cellular Ceramics

Cellmat 2012, Dresden, Germany, 7-9 November 2012

P. Greil

Crack Healing Ceramics

Northwestern Polytechnical University Xi'an, China, December 2012

A. Roosen

Multilayer processing of 3D-structures

3rd Innovation Workshop "Energy Storage and Future Applications", Wittenberg, Germany 4-6 July 2012

A. Roosen

Processing of Miniaturized Planar Ceramic Structures

5th International Symposium on Designing, Processing and Properties of Advanced Engineering Materials ISAEM-2012, Toyohashi, Japan, 5-8 November 2012

A. Roosen

Manufacture of Novel Multilayered Refractories via Tape casting

Materials Science Colloquium, Nagoya Institute of Technology, Nagoya, Japan, 9 November 2012

N. Travitzky

Additive Manufacturing of complex-shaped ceramic structures

36th International Conference on Advanced Ceramics and Composites (ICACC), Daytona Beach, Florida, 22-27 January 2012

Awards

K. Hattori (V), M. Beck, K. Kakimoto, A. Roosen:

Effect of Lamination Methods on Transparent Spinel Ceramics

Best Student Poster Award, 5th International Symposium on Designing, Processing and Properties of Advanced Engineering Materials ISAEM-2012, Toyohashi, Japan, 5-8 November 2012

Impressions of our year-end meeting in December

5. Address and Map

Department of Materials Science - Glass and Ceramics

Friedrich-Alexander University of Erlangen-Nuremberg

Martensstr. 5

91058 Erlangen, GERMANY

Phone: ++49-(0) 9131-852-7543 (Secretary)

Fax: ++49-(0) 9131-852-8311

E-mail: ww3@ww.uni-erlangen.de

Internet: http://www.glass-ceramics.uni-erlangen.de/

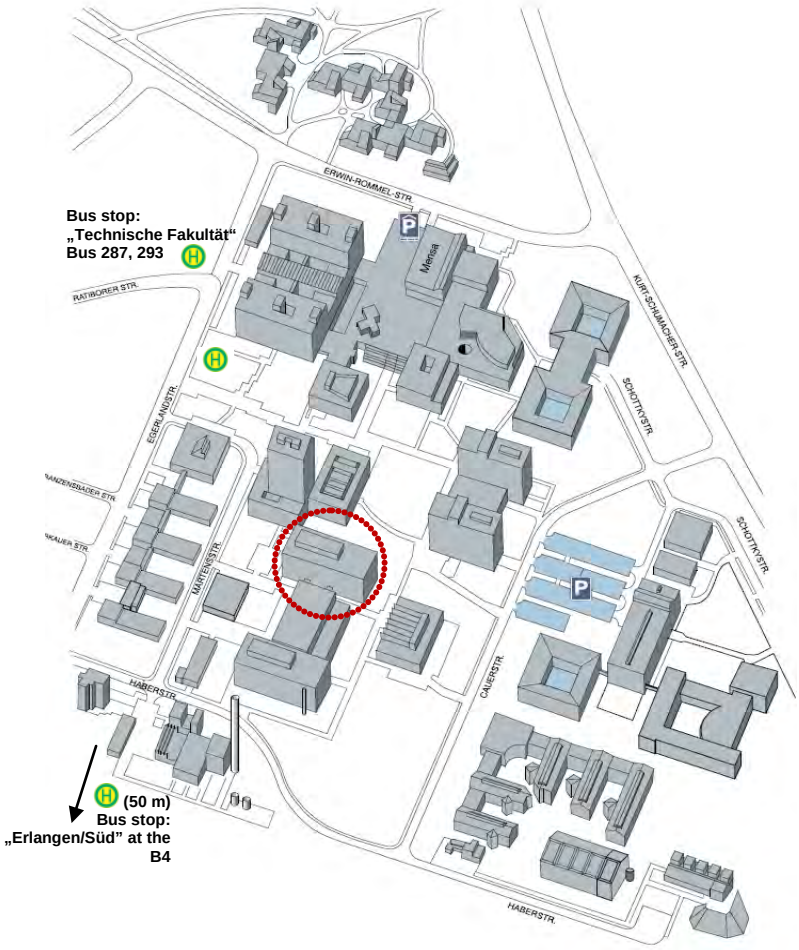

By car:

Highway A3 exit **Tennenlohe**; direction to Erlangen (B4).

Follow the signs **„Universität Südgelände“**.

After junction „**Technische Fakultät**“ please follow the map.

By train:

Railway station **Erlangen**.

Bus line No. 287 direction „**Sebaldussiedlung**“.

Bus Stop „**Technische Fakultät**“.

50 meters to a layout plan; search for „**Department Werkstoff-wissenschaften**“.

http://www.glass-ceramics.uni-erlangen.de/Home/contact.htm

Institute of Advanced Materials and Processes (ZMP)

Dr.-Mack-Strasse 81

Technikum, Ebene 3

90762 Fürth, GERMANY

Tel.: ++49-(0) 911-950918-10

Fax: ++49-(0) 911-950918-15

Internet: http://www.zmp.uni-erlangen.de/

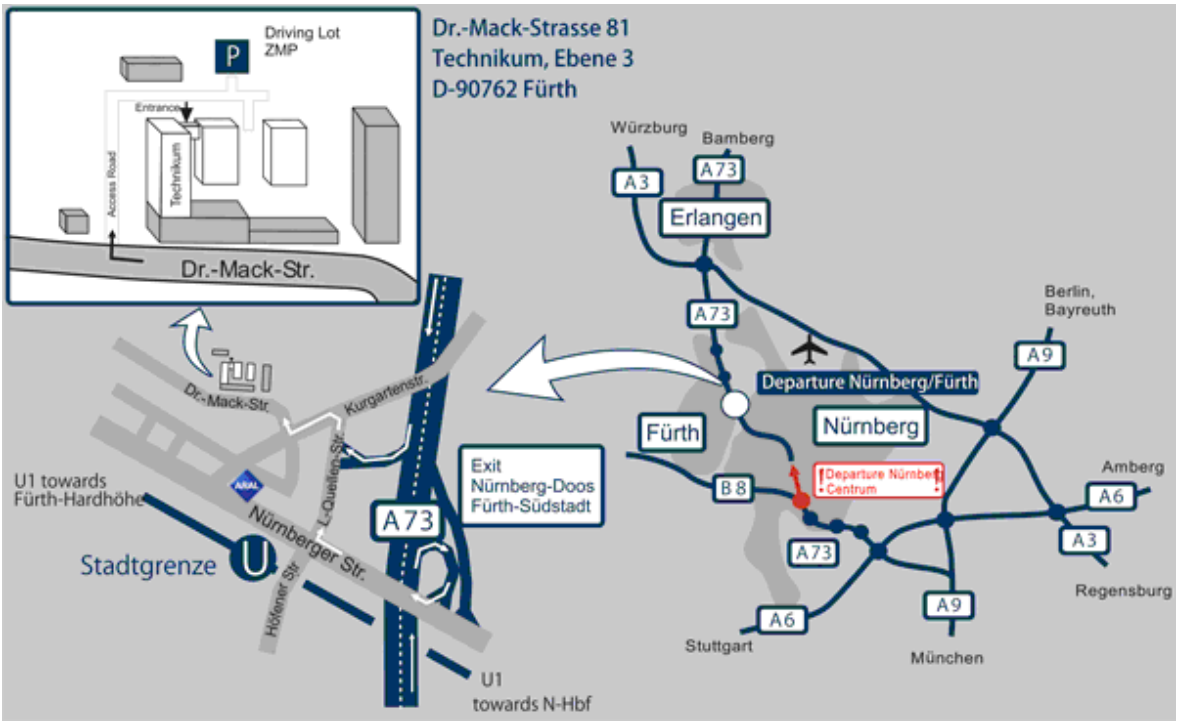

http://www.zmp.uni-erlangen.de/anfahrt/

Pratum Fürth

Friedrich-Alexander University of Erlangen-Nuremberg

Dr. Mack Str. 77

90762 Fürth, GERMANY

6. IMPRESSUM

Prof. Dr. Peter Greil

Dr. Andrea Dakkouri-Baldauf

Department of Materials Science – Institute of Glass and Ceramics

Martensstraße 5

91058 Erlangen, GERMANY